Montgomery Michael (Orcid ID: 0000-0001-5383-4648)
Smith Roger (Orcid ID: 0000-0002-3668-1608)

R. K. Smith, M. T. Montgomery and G. KilroyKinetic energy in tropical cyclones

a Meteorological Institute, Ludwig Maximilians University of Munich, Munich, Germany
b Dept. of Meteorology, Naval Postgraduate School, Monterey, CA
Prof. Roger K. Smith, Meteorological Institute, Ludwig-Maximilians University of Munich, Theresienstr. 37, 80333 Munich, Germany. E-mail: roger.smith@lmu.de

Many previous diagnoses of the global kinetic energy for a tropical cyclone have given prominence to a global integral of a pressure-work term in the generation of kinetic energy. However, in his erudite textbook of atmospheric and oceanic dynamics, Gill (1982) derives a form of the kinetic energy equation in which there is no such explicit source term. In this paper we revisit the interpretations of the generation of kinetic energy given previously in the light of Gill's analysis and compare the various interpretations, which are non-unique.

Further, even though global energetics provide a constraint on the flow evolution, in the context of the kinetic energy equation, they conceal important aspects of energy generation and consumption, a finding that highlights the limitations of a global kinetic energy budget in revealing the underlying dynamics of tropical cyclones.

Tropical cyclone, hurricane, typhoon, spin-up, energetics Mon Jun 25 11:40:19 2018

The generation of kinetic energy in tropical cyclones revisited

Roger K. Smitha, Michael T. Montgomeryb and Gerard Kilroya

Mon Jun 25 11:40:18 2018

1 Introduction

In a classical review paper, Anthes (1974, section DI) summarized the global energetics

of tropical cyclones, based in part on the work of Palmén and Jordan (1955) and Palmén and Riehl (1957). In this review he argues that the kinetic energy is dominated by the horizontal velocity components and he derives an expression for the rate-of-generation of kinetic energy, showing that "The important source of kinetic energy production in the hurricane is the radial flow toward lower pressure in the inflow layer, represented by $u\,\partial p/\partial r$." (Here u is the radial velocity component, r is the radius and p is the pressure). In a similar vein, Palmén and Riehl *op. cit.* note that "the generation depends on the vertical correlation between radial flow component and pressure gradient which, for production of kinetic energy, must be positive, i.e., the strongest inflow must occur at the strongest inward directed pressure gradient. They conclude that "kinetic energy production within the cyclone can take place only if the cyclone is of the warm core type." Anthes goes on to argue that "This inflow is a result of surface friction, which reduces the tangential wind speed and thereby destroys the gradient balance, so that the inward pressure gradient force exceeds the Coriolis and centripetal forces. In the warm core low the maximum pressure gradient ($\partial p/\partial r < 0$)[1] occurs just above the surface layer, at which the inflow ($u < 0$) is maximum in magnitude. In the outflow layer, where the radial flow is reversed, the pressure gradient is much weaker. The result is a net production of kinetic energy, dominated by the contribution from the inflow region."

The foregoing interpretations seem at odds with the kinetic energy equation in flux form presented by Gill (1982) in which the term $-u\,\partial p/\partial r$ does not appear. Nevertheless, in the context of tropical cyclones, subsequent work has built on the formulation by Palmén and Riehl as reviewed by Anthes (e.g. Kurihara 1975, Tuleya and Kurihara 1975, Frank 1977, DiMego and Bosart 1982, Hogsett and Zhang 2009, Wang *et al.* 2016). The generation of kinetic energy in the context of the global climate is discussed by Peixoto and Oort (1992, section 13.2).

The purpose of this paper is to reconcile the different interpretations of kinetic energy generation and to calculate the various terms in the kinetic energy budget from an idealized high-resolution numerical simulation of a tropical cyclone.

2 Kinetic energy equations

In its most basic form, the momentum equation may be written as

$$\frac{\partial \mathbf{u}}{\partial t} + \mathbf{u}\cdot\nabla\mathbf{u} + \mathbf{f}\wedge\mathbf{u} = -\frac{1}{\rho}\nabla p - g\mathbf{k} - \mathbf{F} \qquad (1)$$

where $\mathbf{u}$ is the three dimensional velocity vector, p is the pressure, ρ is the density, $\mathbf{F}$ is the frictional force opposing the motion, $\mathbf{f} = f\mathbf{k}$, f is the Coriolis parameter ($2\Omega\sin\phi$, where ϕ is latitude and Ω is the earth's rotation rate), g is the acceleration due to gravity, and $\mathbf{k}$ is the unit vector in the vertical direction (here and below, all vector quantities are in bold type). For simplicity, an f-plane is assumed (f = constant) and the Coriolis terms proportional to the cosine

[1] Presumably Anthes meant $\partial p/\partial r > 0$

of the latitude have been neglected as is customary for geophysical flow analyses off of the equator (e.g., McWilliams 2011).

The kinetic energy equation is obtained by taking the scalar product Equation (1) with $\mathbf{u}$ using the identity $\mathbf{u}\cdot\nabla\mathbf{u} = \nabla(\frac{1}{2}\mathbf{u}^2) + \omega\wedge\mathbf{u}$, where $\omega = \nabla\wedge\mathbf{u}$ is the vorticity vector. This procedure gives:

$$\frac{\partial}{\partial t}(\tfrac{1}{2}\mathbf{u}^2) + \mathbf{u}\cdot\nabla(\tfrac{1}{2}\mathbf{u}^2) = -\tfrac{1}{\rho}\mathbf{u}\cdot\nabla p - gw - \mathbf{u}\cdot\mathbf{F}, \quad (2)$$

where $w = \mathbf{k}\cdot\mathbf{u}$ is the vertical component of velocity. Note that the Coriolis force ($-\mathbf{f}\wedge\mathbf{u}$) does not appear in the energy equation because it is orthogonal to $\mathbf{u}$.

An alternative form of the energy equation is obtained by removing some hydrostatically-balanced reference pressure, $p_{ref}(z)$, from (1), where $dp_{ref}/dz = -g\rho_{ref}$ defines a reference density, ρ_{ref}, that is a function of altitude z. Then, with the substitution $p = p_{ref}(z) + p'$ and $\rho = \rho_{ref}(z) + \rho'$, the first two terms on the right-hand-side of Equation (1), $-(1/\rho)\nabla p - g\mathbf{k}$, become $-(1/\rho)\nabla p' + b\mathbf{k}$, where $b = -g(\rho - \rho_{ref})/\rho$ is the buoyancy force of an air parcel per unit mass. Then, Equation (2) becomes

$$\frac{\partial}{\partial t}(\tfrac{1}{2}\mathbf{u}^2) + \mathbf{u}\cdot\nabla(\tfrac{1}{2}\mathbf{u}^2) = -\tfrac{1}{\rho}\mathbf{u_h}\cdot\nabla_h p' + Pw - \mathbf{u}\cdot\mathbf{F}, \quad (3)$$

where $\mathbf{u_h}$ is the horizontal velocity vector, ∇_h is the horizontal gradient operator and

$$P = -\tfrac{1}{\rho}\frac{\partial p}{\partial z} - g = -\tfrac{1}{\rho}\frac{\partial p'}{\partial z} + b \quad (4)$$

is the net vertical perturbation gradient force per unit mass. Despite the explicit appearance of p' in the first term on the right-hand-side, all the terms in Equation (3) are independent of the reference pressure $p_{ref}(z)$, since, in particular, $\mathbf{u_h}\cdot\nabla_h p_{ref}(z) = 0$. For simplicity, we take $p_{ref}(z)$ and $\rho_{ref}(z)$ to be the ambient pressure and density, respectively, assuming that these are in hydrostatic equilibrium. Then p' vanishes at large distances from the vortex axis.

We examine now the different forms of Equation (3) derived by Anthes (1974), Gill (1982), and others beginning with a slight modification of Gill's formulation.

2.1 Modified Gill's formulation

In essence, Gill's formulation of the kinetic energy equation is as follows. Using the result that for any scalar field, γ,

$$\rho\frac{D\gamma}{Dt} = \frac{\partial}{\partial t}(\rho\gamma) + \nabla\cdot(\rho\gamma\mathbf{u}), \quad (5)$$

where $D/Dt = \partial/\partial t + \mathbf{u}\cdot\nabla$ is the material derivative (see Gill 1982, Equation 4.3.6)[2], the material form of Equation (3) times ρ may be written in flux form as

[2] If the density refers to that of a moist air parcel consisting of dry air, water vapour and liquid water, the density is conserved only if the liquid water component is suspended in the parcel. In the presence of precipitation, there will be a small source or sink of density associated with the flux divergence of falling precipitation. In what follows, we will ignore the effects of this source/sink term in the kinetic energy budget.

$$\frac{\partial}{\partial t}\left(\frac{1}{2}\rho\mathbf{u}^2\right)+\nabla\cdot\mathbf{F}_{\mathbf{KE}}=p'\nabla_h\cdot\mathbf{u}_\mathbf{h}+\rho Pw+\frac{\partial(p'w)}{\partial z}-\rho\mathbf{u}\cdot\mathbf{F}, \quad (6)$$

where

$$\mathbf{F}_{\mathbf{KE}}=\left(p'+\frac{1}{2}\rho\mathbf{u}^2\right)\mathbf{u}, \quad (7)$$

is the *mechanical energy flux density vector* (Gill, 1982, cf. Equation 4.6.4).

The global kinetic energy budget can be obtained by integrating Equation (6) over a cylindrical volume of space, V, of radius R and height H centred on the storm and using the boundary conditions that $u=0$ at $r=0$, and $w=0$ at $z=0$ and $z=H$. Here, we use a cylindrical coordinate system (r,λ,z) centred on the vortex, where r is the radius, λ is the azimuth and z is the height. We denote an integral of the quantity χ over the volume V by

$$\overline{[\chi]}=\frac{1}{\pi R^2 H}\int_0^R r\,dr\int_0^{2\pi}d\lambda\int_0^H \chi\,dz$$

Then (6) becomes MODIFIED GILL'S FORM

$$\frac{d}{dt}\overline{\left[\frac{1}{2}\rho\mathbf{u}^2\right]}=\overline{[p'\nabla_h\cdot\mathbf{u}_\mathbf{h}]}+\overline{[\rho Pw]}-F_{KEG}-D, \quad (8)$$

where

$$F_{KEG}=\frac{1}{\pi R^2 H}\int_0^{2\pi}d\lambda\int_0^H\left[u\left(p'+\frac{1}{2}\rho\mathbf{u}^2\right)\right]_{r=R}dz, \quad (9)$$

is the *flux of mechanical energy* through the side boundary $r=R$, and for a Newtonian fluid with dynamic viscosity coefficient μ,

$$D=\overline{[\mu\Phi_v]}, \quad (10)$$

where, in cylindrical coordinates,

$$\Phi_v=2\left[\left(\frac{\partial u}{\partial r}\right)^2+\left(\frac{1}{r}\frac{\partial v}{\partial\lambda}+\frac{u}{r}\right)^2+\left(\frac{\partial w}{\partial z}\right)^2\right]+\left[r\frac{\partial}{\partial r}\left(\frac{v}{r}\right)+\frac{1}{r}\frac{\partial u}{\partial\lambda}\right]^2+\left[\frac{1}{r}\frac{\partial w}{\partial\lambda}+\frac{\partial v}{\partial z}\right]^2+\left[\frac{\partial u}{\partial z}+\frac{\partial w}{\partial r}\right]^2-\frac{2}{3}(\nabla\cdot\mathbf{u})^2 \quad (11)$$

is the dissipation function[3]. Here, v is the tangential wind component.

Since $\nabla_h\cdot\mathbf{u}_\mathbf{h}$ is the fractional change in the horizontal area of an air parcel per unit time, the first term on the right-hand-side of Equation (8) is the cumulative effect of the kinetic

[3] Equation (8) is, in essence, the kinetic energy equation for the Reynolds averaged flow in which the quantity μ is a turbulent eddy counterpart. In this case, we are presuming that a K-theory closure is adequate so that the Reynolds averaged equations look essentially like the Newtonian fluid formulation. Further, in the mechanical energy flux through the side boundary in Equation (9) we have neglected the eddy diffusive radial flux of kinetic energy. Relative to the advective flux of kinetic energy, the diffusive flux scales as the inverse Reynolds number of the flow, which is always small compared to unity outside of the surface layer. This conclusion is based on recently obtained estimates of the turbulent eddy diffusivity observed in major hurricanes on the order of $50-100\,\mathrm{m^2\,s^{-1}}$ (Zhang *et al*. 2011).

energy generated locally when an air parcel with positive perturbation pressure expands in the horizontal or one with a negative perturbation pressure contracts in the horizontal. The second term on the right-hand-side of this equation represents the rate of kinetic energy production by air rising in the presence of a positive net vertical perturbation pressure gradient force ($P > 0$) and air sinking in the presence of a negative net vertical perturbation pressure gradient force ($P < 0$). In Gill's original formulation, the net vertical perturbation pressure gradient force term in Equation (8) is replaced by a buoyancy force, which, by itself, is a non-unique force, and the second term on the right-hand-side is replaced by $\nabla \cdot \mathbf{u}$, which is the fractional change in volume of an air parcel. Note that, in Gill's formulation, there is no term corresponding with $u\,\partial p/\partial r$ (or equivalently $u\,\partial p'/\partial r$) in Anthes' formulation of the problem, which a number of authors have argued is the key term in generating kinetic energy.

2.2 Generalized Anthes' formulation

As noted above, Anthes reasonably supposes that the vertical velocity makes only a small contribution to the global kinetic energy and his derivation of the kinetic energy equation is based on the horizontal momentum equations only and the neglect of the contribution from $\frac{1}{2}w^2$ in the kinetic energy. Nevertheless, Anthes retains the vertical velocity component in the advection term $\mathbf{u} \cdot \nabla \mathbf{u}$ in Equation (1) and $\mathbf{u} \cdot \nabla(\frac{1}{2}\mathbf{u}^2)$ in Equation (2). A slightly generalized form of Anthes' equation follows directly from ρ times Equation (3), which in flux form analogous to (6) is

$$\frac{\partial}{\partial t}(\frac{1}{2}\rho\mathbf{u}^2) + \nabla \cdot \mathbf{F}_{\mathbf{KEA}} = -\mathbf{u}_\mathbf{h} \cdot \nabla_h p' + \rho P w - \rho \mathbf{u} \cdot \mathbf{F}, \quad (12)$$

where

$$\mathbf{F}_{\mathbf{KEA}} = (\frac{1}{2}\rho\mathbf{u}^2)\mathbf{u}. \quad (13)$$

Again integrating over the cylinder, Equation (12) becomes GENERALIZED ANTHES' FORM

$$\frac{d}{dt}\overline{\left[\frac{1}{2}\rho\mathbf{u}^2\right]} = -\overline{[\mathbf{u}_\mathbf{h} \cdot \nabla_h p']} + \overline{[\rho P w]} - F_{KEA} - D, \quad (14)$$

where

$$F_{KEA} = \frac{1}{\pi R^2 H}\int_0^{2\pi} d\lambda \int_0^H \left[u(\frac{1}{2}\rho\mathbf{u}^2)\right]_{r=R} dz. \quad (15)$$

Equation (14) is a generalization of Anthes' formulation to include the three-dimensional wind vector in the definition of kinetic energy and the rate of working of the net vertical perturbation gradient force per unit volume, $\overline{[\rho P w]}$, which is a non-hydrostatic effect. As in Anthes' original form, the pressure-work term, $-\overline{[\mathbf{u}_\mathbf{h} \cdot \nabla_h p']}$, appears explicitly in the global form of the kinetic energy equation. For an axisymmetric flow, this term is simply $\overline{[-u\,\partial p$â€™$/\partial r]}$ and, at first

sight, one might question its prominence as a source of kinetic energy, since ∂pâ€™/ ∂r is *not* the only radial force acting on fluid parcels en route to the storm core. Above the frictional boundary layer, the radial pressure gradient is closely balanced by the sum of the centrifugal force and the radial component of the Coriolis force. Moreover, this source term does not appear in Gill's formulation (cf. Eq. (8)), although it is replaced by the term $\overline{[p'\nabla_h \cdot \mathbf{u_h}]}$ and the boundary flux terms are different. Even so, one should bear in mind that even in the axisymmetric case, $\overline{[-u\,\partial p$â€™/ $\partial r]}$ is generating *not only a radial contribution to the kinetic energy, but also an azimuthal contribution* through the action of the generalized Coriolis force $(f + v/r)u$. The generation of this azimuthal contribution is implicit in the kinetic energy equation as the generalized Coriolis force does no work, but it does convert radial momentum to tangential momentum.

3 Kinetic energy budget for an idealized simulation

We examine now the generation terms in the two forms of the kinetic energy equation for the case of an idealized tropical cyclone simulation. We begin with a brief description of the numerical model and go on to present the results.

3.1 The numerical model

The numerical model used for this study is Bryan's three-dimensional, nondydrostatic cloud model (CM1), version 16 (Bryan and Fritsch, 2002). The simulations relate to the prototype problem for tropical cyclone intensification, which considers the evolution of an initially axisymmetric, cloud-free, warm-cored, baroclinic vortex in a quiescent environment on an f-plane. The initial vortex is in thermal wind balance. A latitude of 20 ^{o}N and a constant sea surface temperature of 28 ^{o}C are assumed. The model configuration is more or less the same as described in section 2 of C̄rnivec *et al.* (2016). The differences are that, following the work of Mapes and Zuidema (1996), a more realistic time scale for Newtonian relaxation to the temperature field (10 days) is applied here instead of the previous default value in CM1 (12 h). Further, an open boundary condition is taken at lateral boundaries instead of rigid walls and the Dunion moist tropical sounding is used as the environmental sounding (Dunion 2011).

The initial tangential wind speed has a maximum of 15 m s $^{-1}$ at the surface at a radius of 100 km. The tangential wind speed decreases sinusoidally with height, becoming zero at a height of 20 km. Above this height, up to 25 km, the tangential wind is set to zero. The balanced pressure, density and temperature fields consistent with this prescribed tangential wind distribution are obtained using the method described by Smith (2006). The calculations are carried out for a period of 4 days with data output every 15 min.

(a)
(b)
(c)

Figure 1: Time series of (a) maximum azimuthally-averaged tangential wind speed (V_{max}). Panel (b) shows the radius R_{vmax} at which the maximum tangential wind speed occurs (V_{max}). Panel (c) shows the radius at which gale force winds occurs (R_{gales}), where R_{gales} calculated at a height of 1 km, and corresponds to the radius of 17 m s $^{-1}$ total winds outside the eyewall.

3.2 A few details of the simulation

Figure 1 summarizes the vortex evolution in the simulation. Panel (a) shows time series of the maximum azimuthally-averaged tangential wind speed, V_{max}, and panel (b) shows the radius R_{vmax} at which V_{max} occurs. Typically, V_{max} is located a few hundred meters above the surface, within a shallow inflow layer. The evolution is broadly similar to that described in Kilroy *et al.* (2016), who used a different numerical model and a much coarser horizontal resolution (horizontal grid spacing 5 km compared with 1 km used here). In brief, after a gestation for about a day during which deep convection becomes established inside R_{vmax}, the vortex undergoes a rapid intensification phase lasting about 36 h, before reaching a quasi-steady state. Initially R_{vmax} is located at a radius of 100 km, but contracts to a little more than 20 km after about $2\frac{1}{4}$ days. The most rapid contraction occurs during the rapid intensification phase as absolute angular momentum surfaces are drawn inwards quickly within and above the boundary layer.

Figure 1(c) shows the outermost radius of gale-force winds, R_{gales}, defined here as the radius of 17 m s $^{-1}$ azimuthally-averaged tangential winds at a height of 1 km, which is approximately at the top of the frictional boundary layer. Shown also is R_{galesF}, defined as the (outer) radius at which the total wind speed at any grid point at a height of 10 m is 17 m s $^{-1}$. Both quantities serve as a measure of the vortex size, R_{galesF} being closest to the quantity used by forecasters[4], but R_{gales} being a preferred measure from a theoretical viewpoint (Kilroy *et al.* 2016). The evolution of storm size based on R_{galesF} is similar to that based on R_{gales}, although R_{gales} always exceeds the value of R_{galesF}. After 4 days, R_{gales} exceeds R_{galesF} by about 80 km.

Figure 3.2 shows vertical cross sections of the azimuthally-averaged, 3 h time averaged, radial and tangential velocity components, the vertical velocity component, and the M-surfaces

[4] Based on the wind speed in a particular sector and not azimuthally averaged.

during the intensification phase of the vortex. The time averages are centred on 36 h during the period of rapid intensification and at 60 h near the end of this period. The basic features of the flow are qualitatively similar at both times, but all three velocity components strengthen over the period, the M-surfaces moving inwards in the lower troposphere and outwards in the upper troposphere. The flow structure is similar to that which has been described in many previous studies (see e.g. the recent review by Montgomery and Smith 2017a and refs.) with a layer of strong shallow inflow marking the frictional boundary layer, a layer of weaker inflow in the lower troposphere, a region of strong outflow in the upper troposphere and a layer of enhanced inflow below the outflow. The maximum tangential wind speed occurs within, but near the top of the frictional boundary layer[5]. Much of the ascent occurs in an annular region on the order of 50-60 km in radius. The region inside this annulus shows mostly descent.

(a) (b)

(c) (d)

Left panels: Vertical cross sections of the azimuthally-averaged, 3 hour time averaged tangential velocity component (blue contours) centred at 36 h and 60 h. Superimposed are contours and shading of the averaged vertical velocity. Contour intervals are as follows. Tangential velocity: blue contours every 5 m s $^{-1}$, with a thick black contour highlighting the 17 m s $^{-1}$ contour. Vertical velocity: thin red contours every 0.05 m s $^{-1}$ to 0.2 m s $^{-1}$, thick red contour interval 0.5 m s $^{-1}$, thin dashed red contours indicate subsidence at intervals of 0.02 m s $^{-1}$. Right Panels: Vertical cross sections of the azimuthally-averaged, 3 hour time averaged radial velocity component together with the averaged vertical velocity centred at the same times. Contour intervals are as follows. Radial velocity: thick blue contours 4 m s $^{-1}$, dashed negative, thin blue dashed contours every 0.5 m s $^{-1}$ down to -3.5 m s $^{-1}$. Absolute angular momentum: thick black contours every 2×10^5 m ^{2} s $^{-1}$, with the 6×10^5 m ^{2} s $^{-1}$ contour highlighted in yellow.

3.3 Kinetic energy evolution

Figure 2 shows time series of the domain-averaged kinetic energy per unit mass, $\overline{\left[\frac{1}{2}\rho\mathbf{u}^2\right]}$, for domain radii 300 km and 500 km and a domain height of 20 km. As anticipated by Anthes (1974), this quantity is dominated by the horizontal velocity components: in fact, the curves for $\overline{\left[\frac{1}{2}\rho\mathbf{u}^2\right]}$ and $\overline{\left[\frac{1}{2}\rho\mathbf{u}_\mathbf{h}^2\right]}$ essentially overlap. It follows that the contribution of the vertical

[5] At 60 h, the tangential wind field exhibits a second local maximum in the eyewall. This is a transient feature that is presumably associated with a centrifugal wave near the base of the eyewall (e.g. Montgomery and Smith 2017, p550) excited by an elevated pulse of boundary layer outflow shortly before. This feature is not seen at 48 h or 72 h and its presence doesn't alter the findings concerning the kinetic energy budget.

velocity to the global kinetic energy is negligible. Notable features of the curves for both domain sizes are the slight decrease during the first 12 h on account of surface friction, followed by a rapid increase as the vortex intensifies. As time proceeds, the rate of increase progressively declines.

3.4 Kinetic energy generation: Anthes' formulation

Figure 3 shows time series of the principal terms in the generalized Anthes formulation (the right-hand-side of Equation (14)), excluding only the global dissipation term since the focus of the paper is on kinetic energy generation. For both domain radii, 300 km (Fig. 4(a)) and 500 km (Fig. 4(a)), both the terms $\overline{[-\mathbf{u_h} \cdot \nabla_h p']}$ and $\overline{[\rho P w]}$ are positive, but, perhaps surprisingly, the former term is not appreciably larger than the latter, even beyond 2 days when the differences are largest. The boundary flux term F_{KEA} is virtually zero throughout the calculation. For the larger domain size (R = 500 km), the temporal behaviour of the various terms is similar, but, as expected, the magnitudes of the respective terms are appreciably smaller (Fig. 4(b)), since the largest contributions to the averages are from well inside a 300 km radius (note the different scales on the ordinate in Figs. 4(a) and 4(b)).

The finding that the two terms $\overline{[-\mathbf{u_h} \cdot \nabla_h p']}$ and $\overline{[\rho P w]}$ are not appreciably different in magnitude is at first sight surprising since, as shown in Figure 2, the contribution of the vertical velocity to the total kinetic energy is negligible. Moreover, the $\overline{[\rho P w]}$ term does not appear in Anthes' original formulation because the formulation was based on the horizontal momentum equations only. An explanation of this result is suggested by an examination of the radial-height structure of the azimuthally-averaged generation term before completing the columnar average, i.e. $< -\mathbf{u_h} \cdot \nabla_h p' >$, where the angle brackets denote an azimuthal average. The structure of this average together with those of the other generation term, $< \rho P w >$, at 36 h and 60 h, is shown in Figure 4. At both times, the Anthes generation term $< -\mathbf{u_h} \cdot \nabla_h p' >$ shows coherent regions of large kinetic energy generation and of large kinetic energy destruction. The main region of generation in panels (a) and (b) is at low levels, below about 2 km, where the strongest inflow occurs and where the inward directed radial pressure gradient force is particularly strong (panels (c) and (d) of Figure 4). There is a second region of generation in an annular column, mostly on the outer side of the eyewall updraught below about 9 km at 36 h and below about 12 km at 60 h. The generation terms in panels (a) and (b) are similar in structure and magnitude to that shown by Kurihara (1975, Figure 42, upper right) for a lower resolution axisymmetric simuulation.

Figure 2: Time series of the left-hand-side of Equation 14, $\overline{\left[\frac{1}{2}\rho \mathbf{u}^2\right]}$ (curves labelled uvw)

compared to $\overline{\left[\frac{1}{2}\rho\mathbf{u_h^2}\right]}$ (curves labelled uv) for cylinders of 300 km and 500 km. The curves for each cylinder size lie essentially on top of each other so that only a single curve is evident. The curves for the 500 km domain are labelled with a '5'.

(a) (b)

Figure 3: Time series of the kinetic energy tendency terms on the right-hand-side of Equation (14), the Anthes' formulation, averaged over a cylinder of size (a) 300 km and (b) 500 km. Units on the ordinate are 10^{-3} W m $^{-3}$. The dissipation term is not shown. A1 stands for $\overline{[-\mathbf{u_h}\cdot\nabla_h p']}$, FK for F_{KEA} and PW for $\overline{[\rho P w]}$. A1+ and A1- stand for the contributions to A1 from regions where the argument $-\mathbf{u_h}\cdot\nabla_h p'$ is positive and negative, respectively.

(a) (b)
(c) (d)
(e) (f)

Figure 4: Radius-height cross sections of azimuthally-averaged quantities in Equation (14), before performing the columnar average: $<-\mathbf{u_h}\cdot\nabla_h p'>$ (panels (a), (b)); and $<\rho P w>$ (panels (e), (f)), at 36 h (left panels) and 60 h (right panels). Panels (c) and (d) show similar cross sections of $<\partial p'/\partial r>$ at these times. Contour intervals are as follows. Panels (a), (b), (e) and (f): thick contours 5×10^{-2} W m $^{-3}$: thin contours 1×10^{-2} W m $^{-3}$. Solid red contours positive, dashed blue contours negative. Panels (c) and (d): thin contours 0.2×10^{-2} Pa m $^{-1}$ to 0.8×10^{-2} Pa m $^{-1}$; medium thick contours 1.0×10^{-2} Pa m $^{-1}$ to 5.0×10^{-2} Pa m $^{-1}$; thick contours every 5.0×10^{-2} Pa m $^{-1}$. Numbers indicated on the side bar should be multiplied by 10^{-2}.

(a) (b)
(c) (d)

Figure 5: Time series of the kinetic energy tendency terms: $\overline{[p'\nabla_h\cdot\mathbf{u_h}]}$ (denoted by G1); $\overline{[\rho P w]}$ (denoted PW) and F_{KEG} (denoted FK) in the modified Gill formulation [Equation (8) averaged over a cylinder of size (a) 300 km and (b) 500 km. Units on the ordinate are 10^{-3} W m $^{-3}$. Panels (c) and (d) show the azimuthally averaged terms $<p'\nabla_h\cdot\mathbf{u_h}>$ in Equation (8) at 36 h and 60 h, respectively. Contour intervals are: thick contours 5×10^{-2} W m $^{-3}$: thin contours 1×10^{-2} W m $^{-3}$. Solid red contours positive, dashed blue contours negative. Numbers indicated on the side bar should be multiplied by 10^{-2}.

Since the radial pressure gradient is positive at all heights [panels (c) and (d) of Figure 4],

these generation regions must be ones in which there is generally inflow[6]. For the same reason, where there is outflow, there is kinetic energy removal as seen in the two principal coherent regions in panels (a) and (b) where $< -\mathbf{u_h} \cdot \nabla_h p' >< 0$. It follows that the computed value of $\overline{[-\mathbf{u_h} \cdot \nabla_h p']}$ is the remainder resulting from the cancellation of two comparatively large contributions from $< \mathbf{u_h} \cdot \nabla_h p' >$ of opposite sign, namely $< -\mathbf{u_h} \cdot \nabla_h p' >_+$ and $< -\mathbf{u_h} \cdot \nabla_h p' >_-$, the former being the sum of all positive values of $-\mathbf{u_h} \cdot \nabla_h p'$ and the latter $< -\mathbf{u_h} \cdot \nabla_h p' >_-$ to be the sum of all negative values. This large cancellation is evident in the time series shown in Figure 3.

In summary, a substantial fraction of the kinetic energy that is generated is removed in regions where there is outflow and the residual is relatively small, comparable, indeed, with the kinetic energy generated by the rate-of-working of the net vertical perturbation pressure gradient force (buoyancy plus perturbation pressure gradient), principally in the region of diabatically-forced ascent. The structure of the net vertical perturbation pressure gradient force at 36 h and 60 h is shown in panels (e) and (f) of Figure 4. As expected, this force is concentrated in an annular region overlapping the region of diabatic heating.

3.5 Kinetic energy generation (Gill's formulation)

Figure 5 shows time series of the principal terms in the modified Gill formulation (the right-hand-side of Equation (8)), excluding again the global dissipation term. In this formulation, the term $\overline{[p' \nabla_h \cdot \mathbf{u_h}]}$ is positive with mean amplitude and fluctuations about this mean increasing with time during the 4 day calculation [Fig. 5(b)]. For the first day, the term is a little less than the $\overline{[\rho P w]}$ term, but thereafter becomes progressively larger. The increasing energy source represented by the sum of the two foregoing terms is opposed, in part, by the net outward flux of mechanical energy through the radial boundary, F_{KEG}.

Panels (c) and (d) of Figure 5 show the structure of the term $< p' \nabla_h \cdot \mathbf{u_h} >$, again 36 h and 60 h. The radial and vertical integral of this term form the cylindrical average $\overline{[p' \nabla_h \cdot \mathbf{u_h}]}$ in the modified Gill's formulation of the energy equation. The qualitative radius-height structure of $< p' \nabla_h \cdot \mathbf{u_h} >$ at the two times shown is less easy to infer from the solutions in Figure 3.2. Moreover, as shown in Figure 5, there is significant cancellation between the term $\overline{[p' \nabla_h \cdot \mathbf{u_h}]}$ and the boundary flux term in Gill's formulation [Equation (8)]. For this reason, the Anthes' formulation of the energy equation would seem to be preferable to Gill's formulation, even though both formulations are correct and give the same tendency of kinetic energy over the control volume of integration (see next subsection).

[6] Note that eddy effects are included in all generation terms.

Figure 6: Sum of the terms for Gill's and Anthes' formulation excluding the dissipation term for cylinders of radius $R = 300$ km and 500 km. Values on the ordinate have been multiplied by 10^3 for plotting purposes. The two curves for each value of R lie essentially on top of each other.

3.6 Total kinetic energy generation

A check on the foregoing calculations is provided by calculating the total tendency of kinetic energy generation, which is the sum of all the terms on the right-hand-side of Equations (8) or (14). This sum should be the same for each formulation. That this is the case is verified in Figure 6, which shows the sum for each domain size. As expected, the curves for the two formulations are coincident.

4 Discussion

Anthes' statement noted in the Introduction that "the important source of kinetic energy production in the hurricane is the radial flow toward lower pressure in the inflow layer, represented by $-u\,\partial p/\partial r$" may seem at first sight problematic because, above the boundary layer, the radial pressure gradient is very closely in balance with sum of centrifugal and Coriolis forces. Thus the energy source associated with $-u\,\partial p/\partial r$ might appear, at least at first sight, to be a gross overestimate. However, the kinetic energy equation doesn't recognize the balance constraint and, in this equation, the radial pressure gradient acts to generate not only kinetic energy of radial motion, but also that of tangential motion through the action of the generalized Coriolis force $(f + v/r)u$, a term that appears in the tangential momentum equation in cylindrical coordinates. This is despite the fact that the generalized Coriolis force does not appear explicitly in the kinetic energy equation.

As noted also in the Introduction, Anthes recognized that much of the inflow into the storm is " ... a result of surface friction, which reduces the tangential wind speed and thereby destroys the gradient balance, so that the inward pressure gradient force exceeds the Coriolis and centripetal[7] forces" and he pointed out that "In the warm core low the maximum pressure gradient ($-\partial p/\partial r < 0$ [sign corrected: our insertion]) occurs at the lowest level, at which the inflow ($u < 0$) is maximum. In the outflow layer, where the radial flow is reversed, the pressure gradient is much weaker. The result is a net production of kinetic energy, dominated by the contribution from the inflow region". While this view is broadly supported by the calculations presented herein, the calculations provide a sharper view of the *net* production of kinetic

[7] Presumably, Anthes means the centrifugal force.

energy indicating a region of significant kinetic energy generation accompanying inflow *throughout* the lower troposphere above the boundary layer as well as significant regions where kinetic energy is consumed as air flows outwards, against the radial pressure gradient, above the boundary layer. Indeed, the generation above the boundary layer is a manifestation of spin up by the classical mechanism articulated by Ooyama (1969), while the generation within the boundary layer, highlighted by Anthes, is a manifestation of the nonlinear boundary layer spin up mechanism articulated by Smith and Vogl (2008), Smith *et al.* (2009), Smith and Montgomery (2016) and Montgomery and Smith (2017b).

Anthes argues that the boundary layer " ... must be responsible for a net gain of kinetic energy" even though "a substantial dissipation of kinetic energy in the hurricane occurs in the boundary layer through turbulent diffusion and ultimate loss of energy to the sea surface". As a result, he is led to the paradox that "surface friction is responsible for a net increase in kinetic energy and without friction the hurricane could not exist." The resolution of this paradox would appear to be Anthes' de-emphasis of the role of the classical mechanism for spin up in the kinetic energy budget.

The results of our study, especially the noted cancellation of relatively large generation and consumption contributions to the term $\overline{[-\mathbf{u_h} \cdot \nabla_h p']}$ points to limitations in the utility of a global kinetic energy budget in revealing the underlying dynamics of tropical cyclone intensification. An alternative approach would be to examine the energetics of individual air parcels as they move around some hypothetical circuit (see Emanuel (2004) and references), but this approach relies on assumptions about the circuits traversed, circuits that may or may not be realizable in reality.

5 Conclusions

We have re-examined the traditional theory for kinetic energy generation in a tropical cyclone used by Palmén and Jordan (1955), Palmén and Riehl (1957), Frank (1977), Hogsett and Zhang (2009) and succinctly summarized in the review article by Anthes (1974). We have compared this with an alternative interpretation of global kinetic energy generation in geophysical flows inspired by Gill (1982), noting that such interpretations are non-unique.

We have shown that the *net* rate of production of kinetic energy is a comparatively small difference between the generation in regions of inflow and the magnitude of the consumption in regions of outflow, so much so, that this difference is comparable in magnitude with the rate of generation by the net vertical perturbation pressure gradient force. The latter effect was not contained in Anthes' original formulation, which was based only on the horizontal momentum equations.

We pointed out that the kinetic energy generation term in Anthes' formulation involving the radial pressure gradient does not appear in Gill's formulation of the kinetic energy equation

or our modification thereof. It is replaced by a term comprising the global integral of the rate of working by perturbation pressure ($\overline{[p'\nabla_h \cdot \mathbf{u_h}]}$) as the flow expands in the horizontal. However, this generation term is largely compensated in the modified Gill formulation by the boundary flux of mechanical energy (F_{KEG}). The fact that the boundary flux of kinetic energy in the Anthes formulation (F_{KEA}) is typically negligible, as well as the difficulty in anticipating the structure of the term $\overline{[p'\nabla_h \cdot \mathbf{u_h}]}$ in a tropical cyclone are factors weighing in favour of using Anthes' formulation when applied to the generation of kinetic energy in a tropical cyclone. However, in the light of the large cancellation of positive and negative values in the radial pressure-work term, the contribution from the rate of working of the net vertical force is non-negligible in comparison and should be included in any global kinetic energy budget.

While global energetics provide a constraint on flow evolution, we have shown in the context of the kinetic energy equation that they conceal important aspects of energy generation and consumption. This finding highlights the limitations of a global kinetic energy budget in revealing the underlying dynamics of tropical cyclones.

6 Acknowledgements

We thank Drs. Chris Landsea, Anastassia Makarieva and an anonymous reviewer for their perceptive comments on the original manuscript. GK and RKS acknowledge financial support for tropical cyclone research from the Office of Naval Research Global under Grant No. N62909-15-1-N021. MTM acknowledges the support of NSF grant AGS-1313948, NOAA HFIP grant N0017315WR00048, NASA grant NNG11PK021, ONR grant N0001417WX00336, and the U. S. Naval Postgraduate School.

7 Appendix: Calculation of the net vertical force, P

The net vertical force per unit mass, P, defined in Equation (4) and used to construct Figures 4(e) and 4(f) was first calculated on the stretched model grid at the levels where thermodynamic quantities are defined. The vertical perturbation pressure gradient was determined by fitting a quadratic function to three successive levels z_{i-1}, z_i and z_{i+1} at which the perturbation pressure has values p'_{i-1}, p'_i and p'_{i+1}, respectively. Then

$$\left(\frac{\partial p'}{\partial z}\right)_i = \frac{(p'_{i+1}-p'_i)dz_i^2-(p'_{i-1}-p'_i)dz_{i+1}^2}{dz_{i+1}dz_i(z_{i+1}-z_{i-1})} \quad (16)$$

where $dz_i = z_i - z_{i-1}$.

8 References

Anthes RA. 1974. The dynamics and energetics of mature tropical cyclones. *Rev. Geophys. Space Phys*, **12**: 495-522

Bryan GH, Fritsch JM. 2002. A benchmark simulation for moist nonhydrostatic numerical models. *Mon. Weather Rev.*, bf 130: 2917â€“2928.

Č rnivec N, Smith RK, Kilroy G. 2016. Dependence of tropical cyclone intensification rate on sea surface temperature. *Q. J. R. Meteorol. Soc.*, **142**: 1618-1627.

DiMego GJ, Bosart LF. 1982. The transformation of tropical storm Agnes into an extratropical cyclone. Part II: Moisture, vorticity and kinetic energy budgets. *Mon. Weather Rev.*, bf 110: 412-433.

Dunion JP. 2011. Rewriting the climatology of the tropical North Atlantic and Carribean sea atmosphere. *J. Clim*, **24**: 893â€“908.

Emanuel K. 2004. Tropical cyclone energetics and structure. In *Atmospheric turbulence and mesoscale meteorology*, E. Fedorovich, R. Rotunno and B. Stevens, editors, Cambridge University Press, pp280.

Frank WM. 1977. The structure and energetics of the tropical cyclone ll. Dynamics and energetics. *Mon. Weather Rev.*, **105**: 1136-1160.

Gill AE. 1982. *Atmosphere-Ocean Dynamics*. New York: Academic. 4th ed., 662pp

Hogsett W, Zhang D-L. 2009. Numerical simulation of Hurricane Bonnie (1998). Part III: Energetics. *J. Atmos. Sci.*, **66**: 2678-2696.

Kilroy G, Smith RK, Montgomery MT. 2016. Why do model tropical cyclones grow progressively in size and decay in intensity after reaching maturity? *J. Atmos. Sci.*, **73**: 487-503.

Kurihara Y. 1975. 1975: Budget analysis of a tropical cyclone simulated in an axisymmetric numerical model. *J. Atmos. Sci.*, , **32**: 25-59.

McWilliams JC. 2011. *Fundamentals of geophysical fluid dynamics*. Cambridge University Press, 283pp.

Mapes BE, Zuidema P. 1996: Radiative-dynamical consequences of dry tongues in the tropical troposphere. *J. Atmos. Sci.*, **53**: 620-638.

Montgomery MT, Smith RK. 2017a: Recent developments in the fluid dynamics of tropical cyclones. *Annu. Rev. Fluid Mech*., **49**: 1-33, doi:10.1146/annurev-fluid-010816-060022.

Montgomery MT, Smith RK. 2017b: On the applicability of linear, axisymmetric dynamics in intensifying and mature tropical cyclones. *Fluids*, **2**: 69. doi:10.3390/fluids2040069.

Ooyama K. 1969: Numerical simulation of the life-cycle of tropical cyclones. *J. Atmos. Sci.*, **26**: 3-40.

Palmén E, Jordan CL. 1955. Note on the release of kinetic energy in tropical cyclones. *Tellus*, **7**: 186-189.

Palmén E, Riehl H. 1957. Budget of angular momentum and energy in tropical storms. *J. Meteor.*, **14**: 150-159.

Peixoto JP, Oort AH. 1992 *Physics of climate*. American Institute of Physics, New York, p 520.

Smith RK. 2006. Accurate determination of a balanced axisymmetric vortex. *Tellus*, **58A**: 98-103.

Smith RK, Vogl S, 2008: A simple model of the hurricane boundary layer revisited. *Q. J. R. Meteorol. Soc*., **134**: 337-351.

Smith RK, Montgomery MT, 2016: The efficiency of diabatic heating and tropical cyclone intensification. *Q. J. R. Meteorol. Soc.*, **142**: 2081-2086.

Smith RK Montgomery MT Nguyen SV. 2009: Tropical cyclone spin up revisited. *Q. J. R. Meteorol. Soc*., **135**: 1321-1335.

Tuleya RE, Kurihra Y. 1975. The energy and angular momentum budgets of a three-dimensional tropical cyclone model. *J. Atmos. Sci.*, **32**: 287-301.

Wang Y, Cui X, Li, X, Zhang W, Huang Y. 2016. Kinetic energy budget during the genesis period of Tropical Cyclone Durian (2001) in the South China Sea. *Mon. Weather Rev.*, **144**: 2831-854.

Zhang JA Rogers RF Nolan DS and Marks FD 2011: On the characteristic height scales of the hurricane boundary layer. *Mon. Weather Rev.*, **139**: 2523-2535.

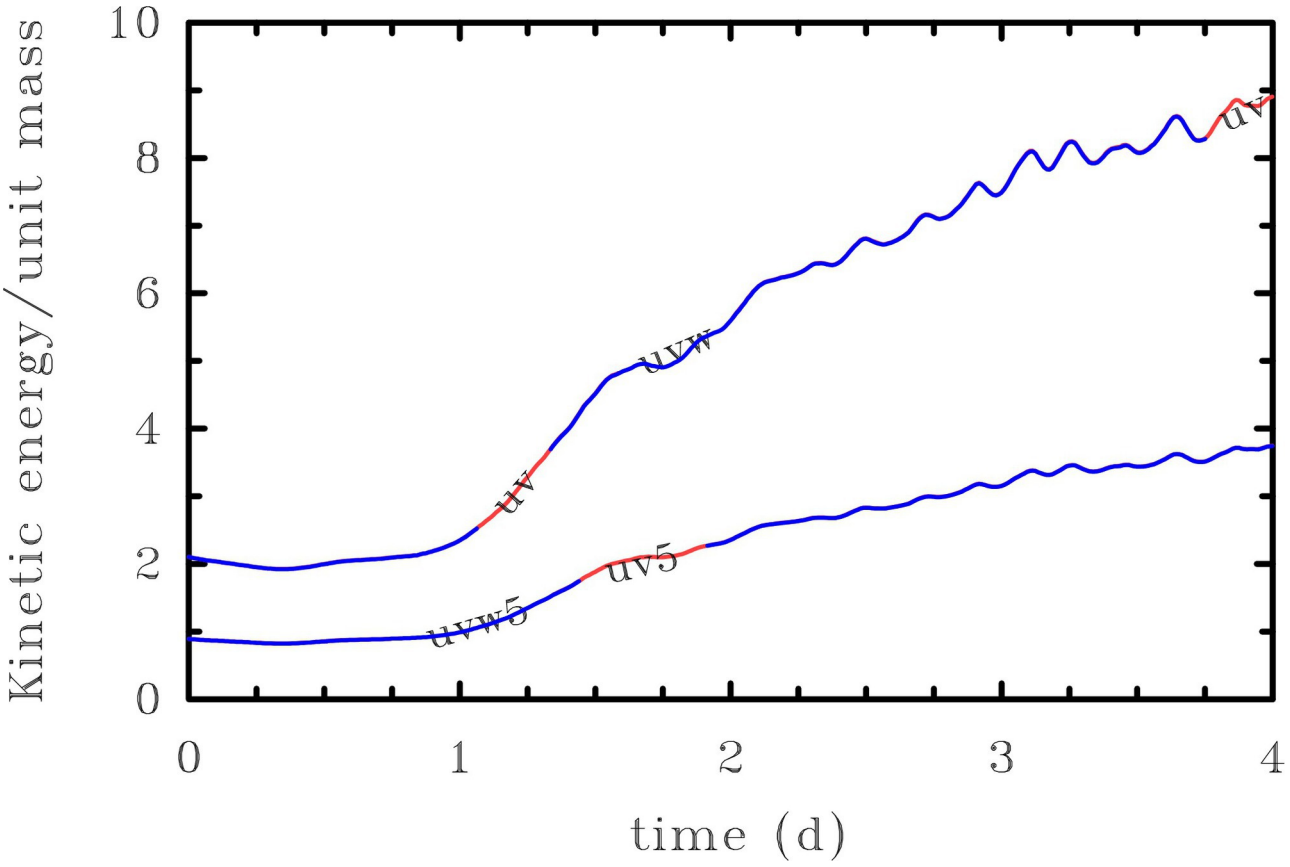

fig3.eps

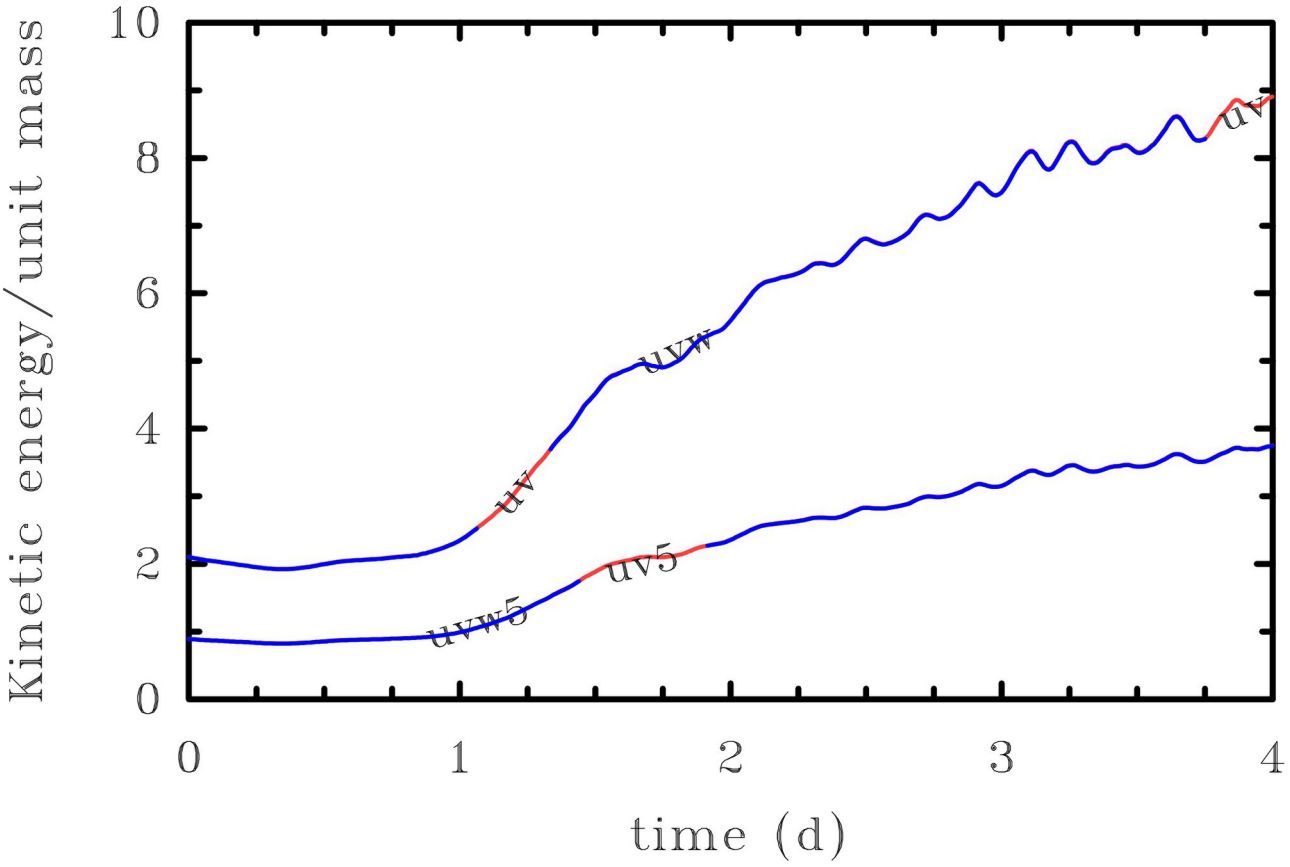

fig3.eps

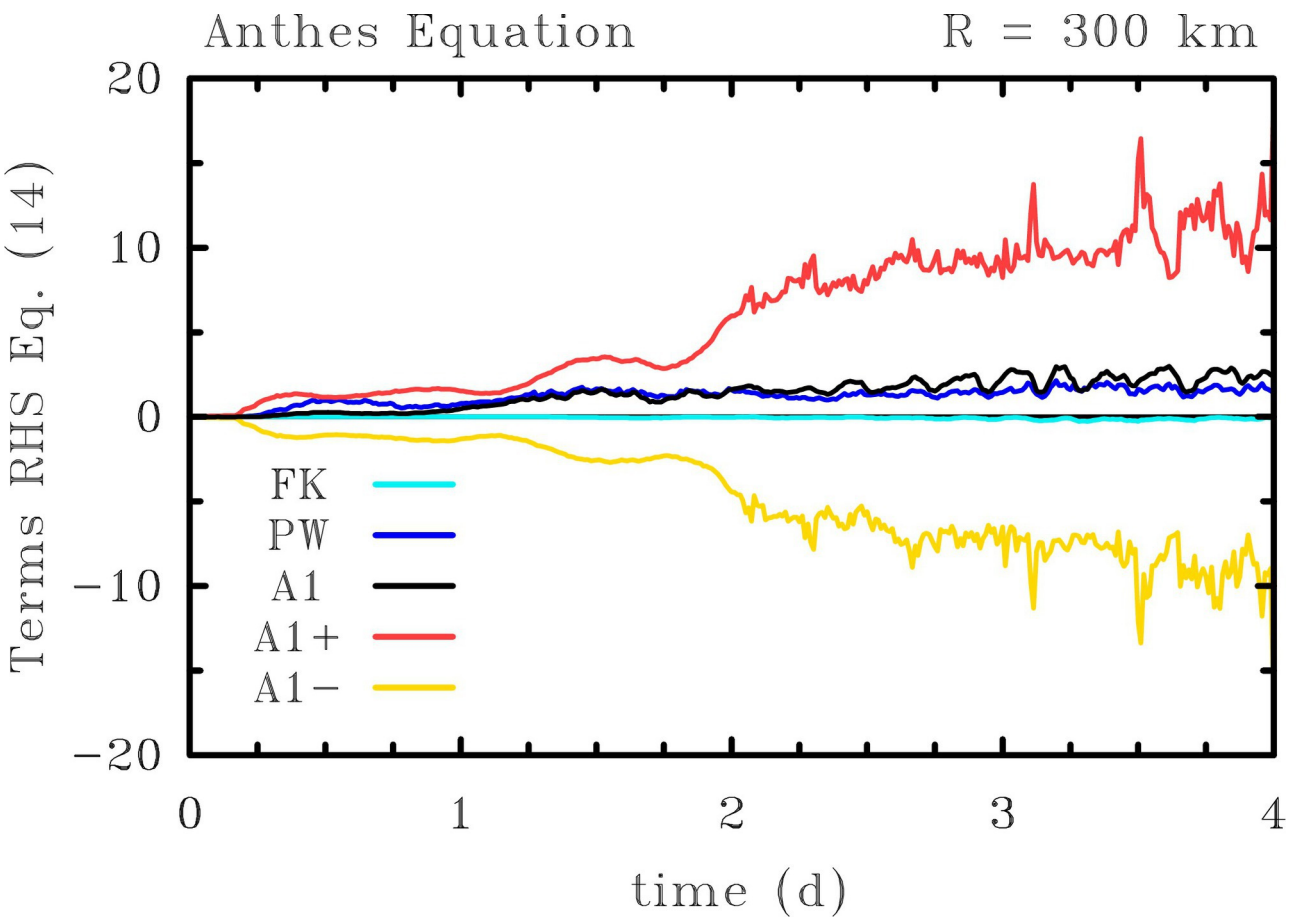

fig4a.eps

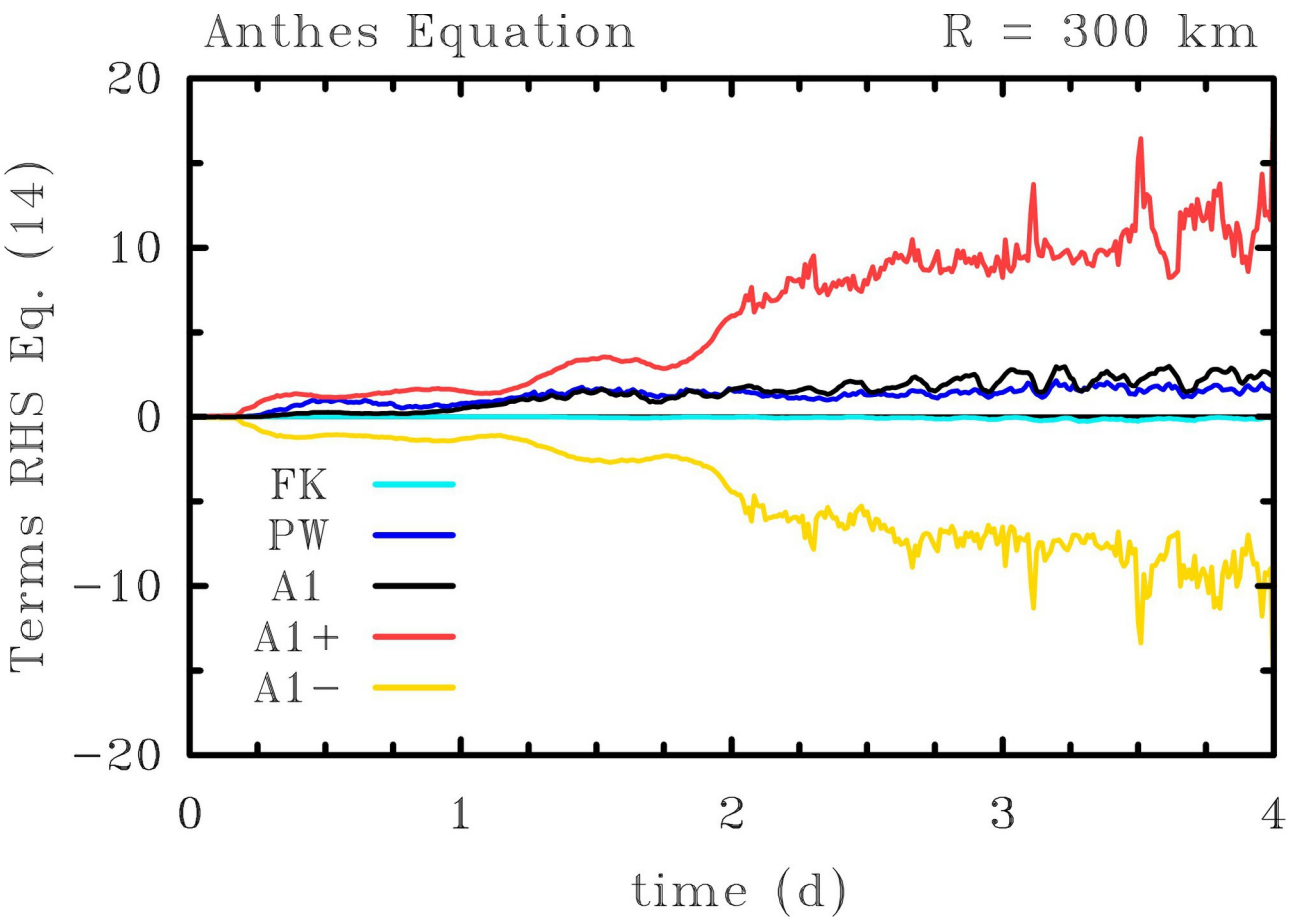

fig4a.eps

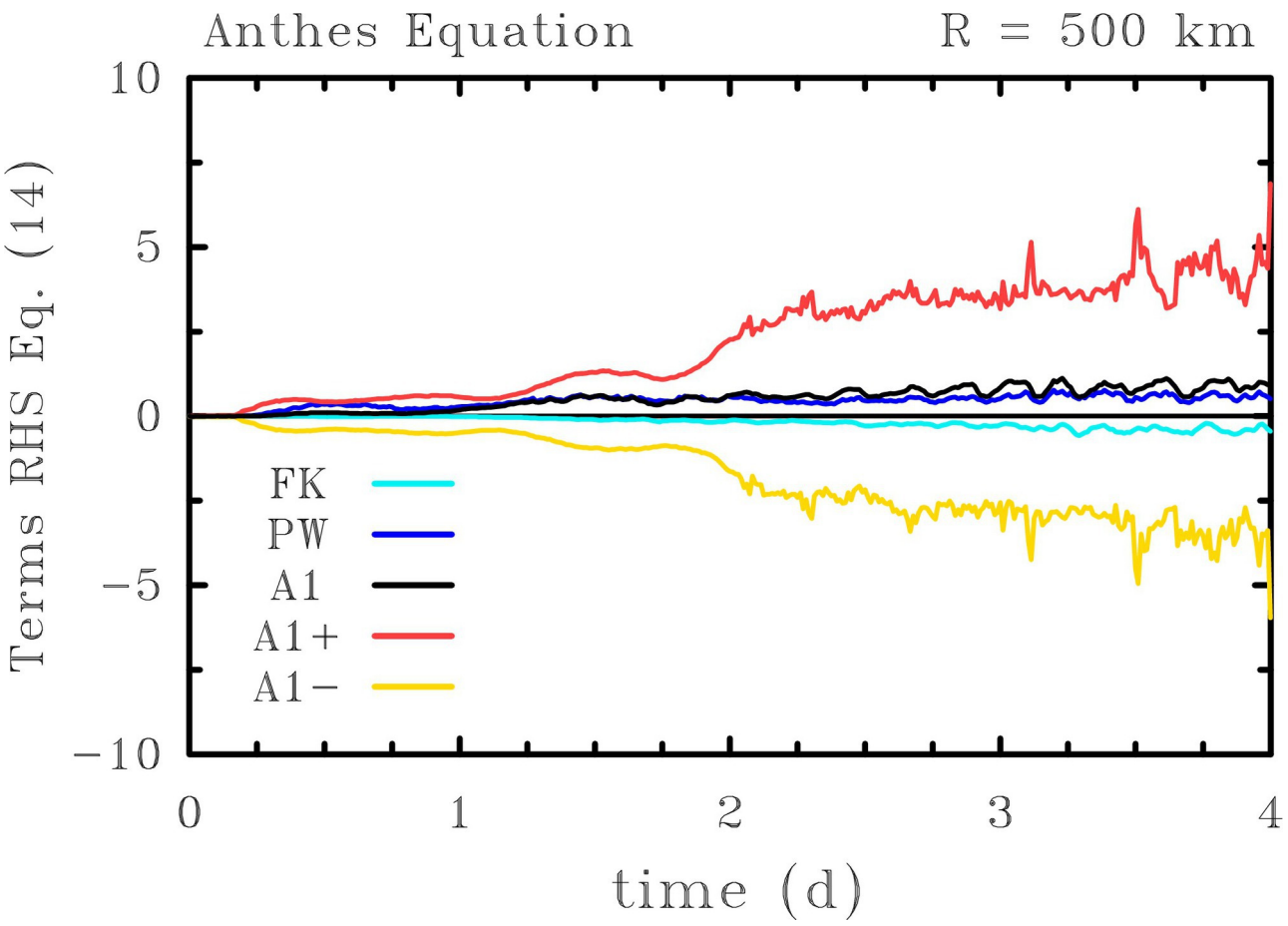

fig4b.eps

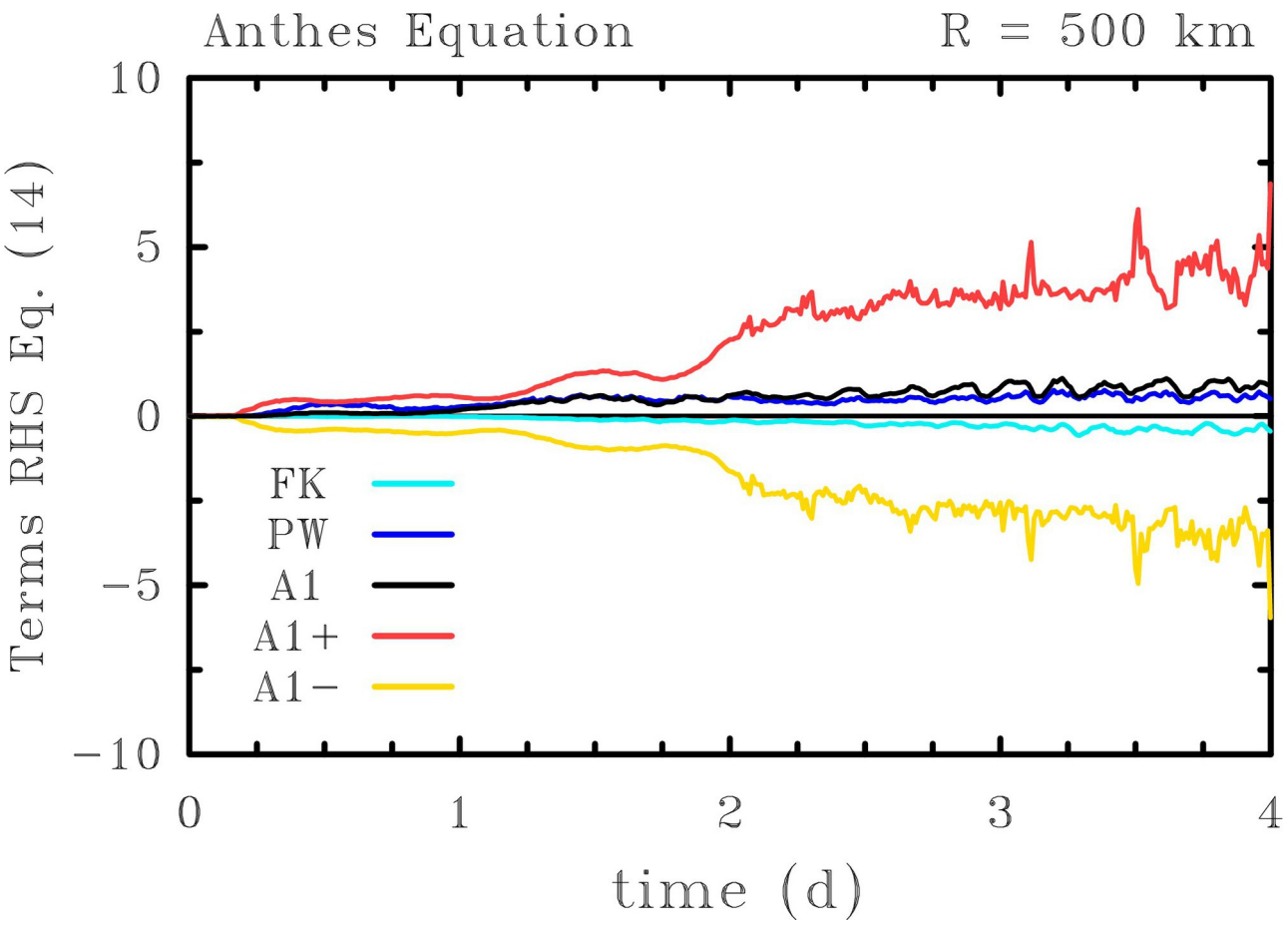

fig4b.eps

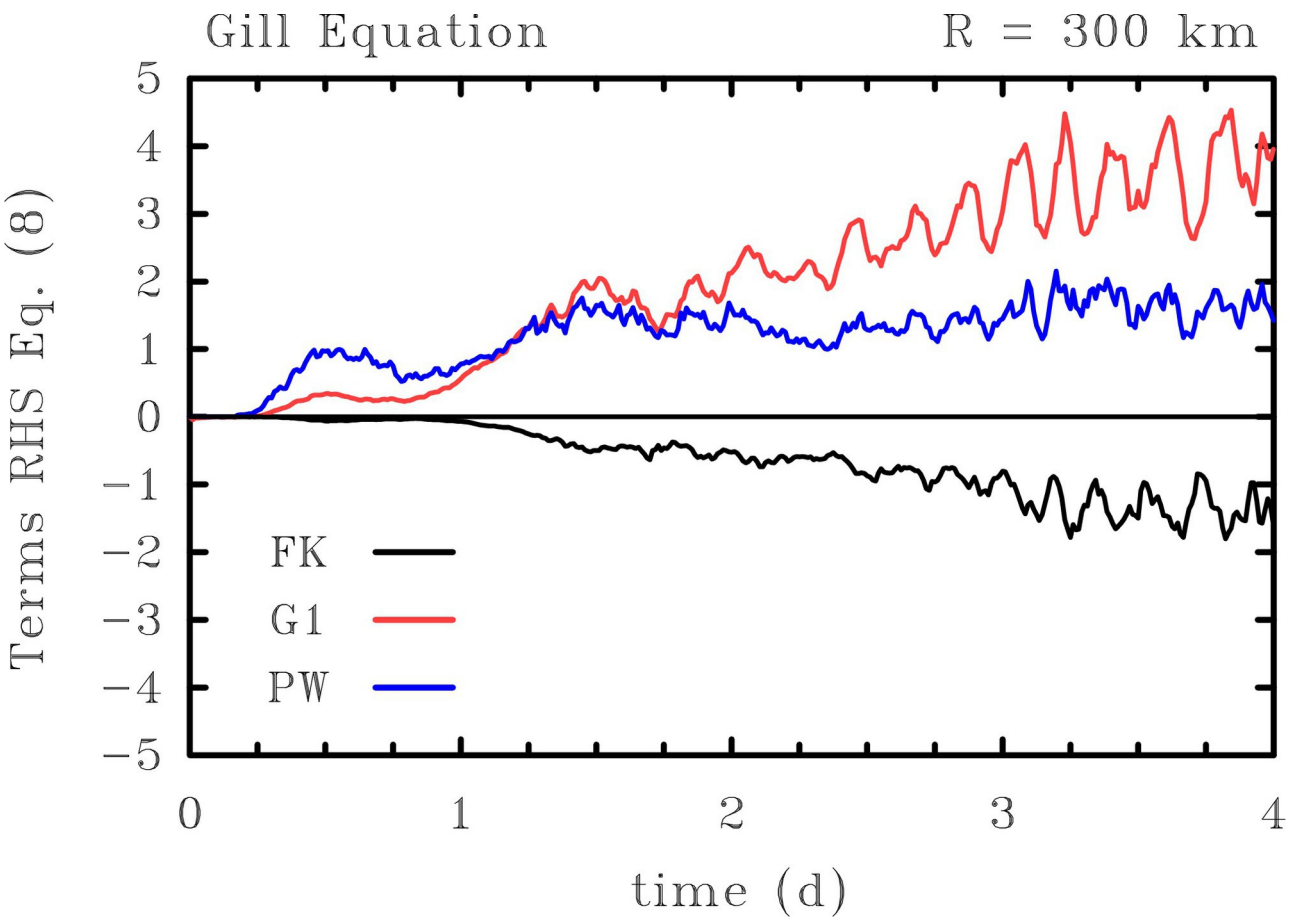

fig6a.eps

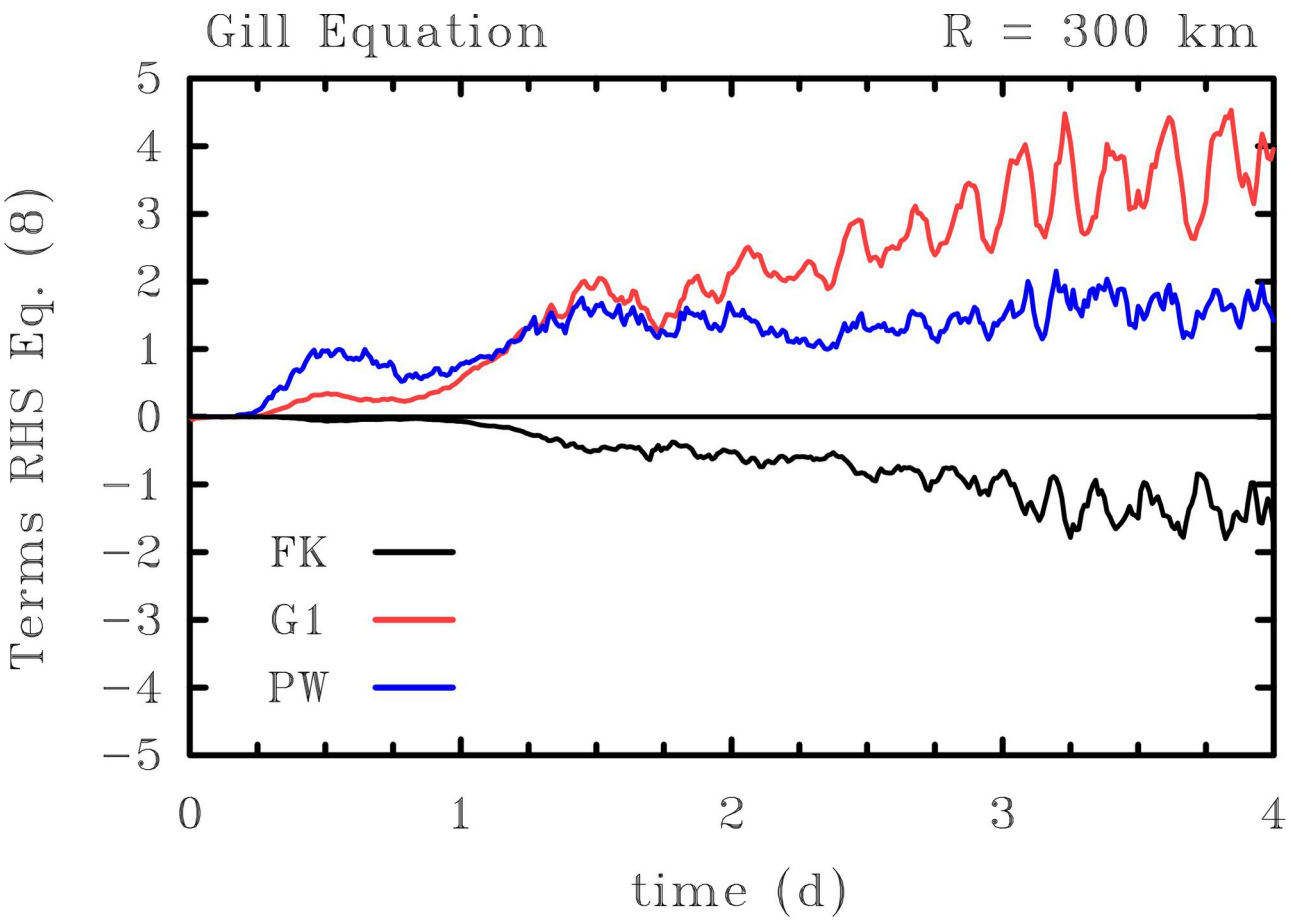

fig6a.eps

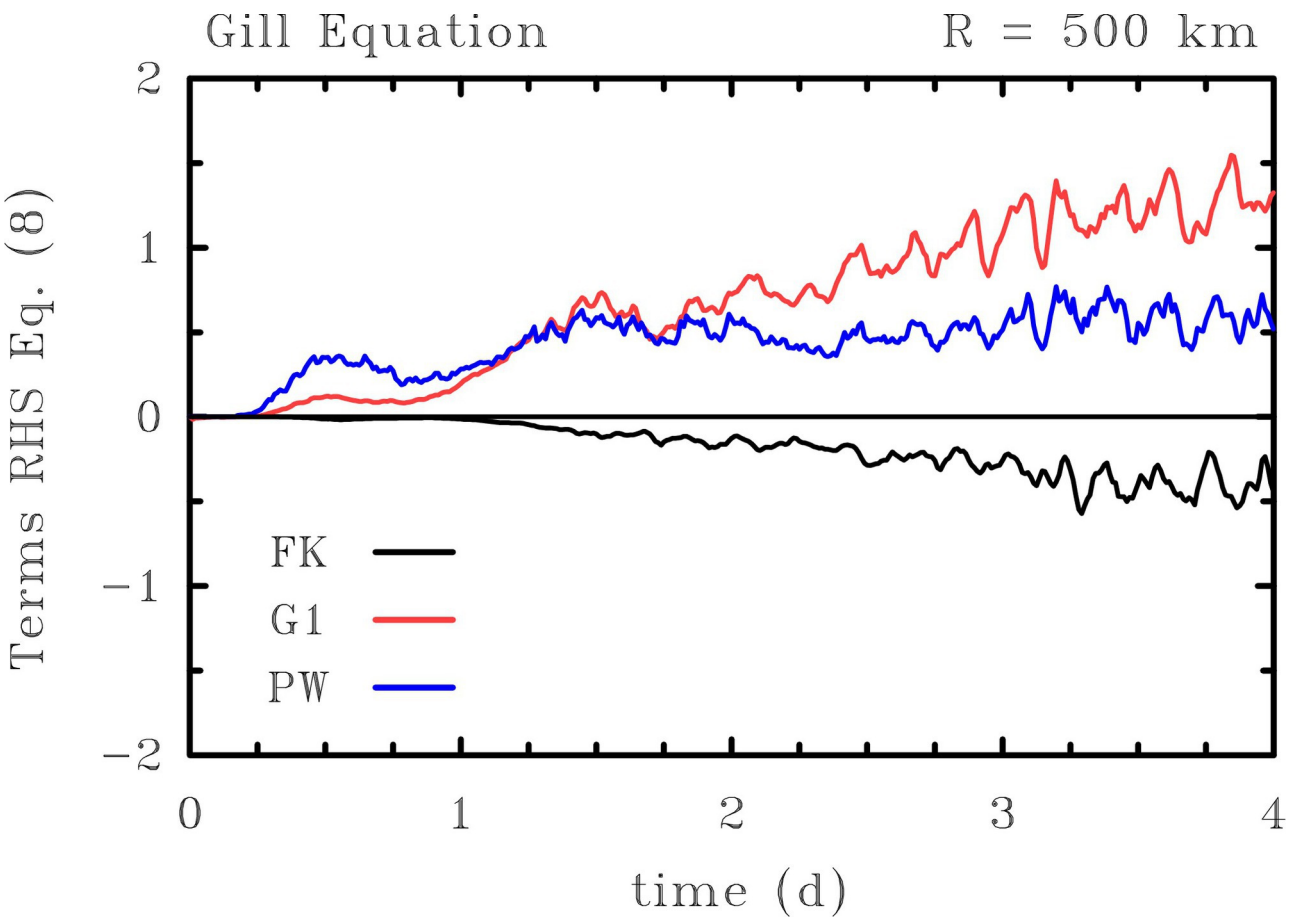

fig6b.eps

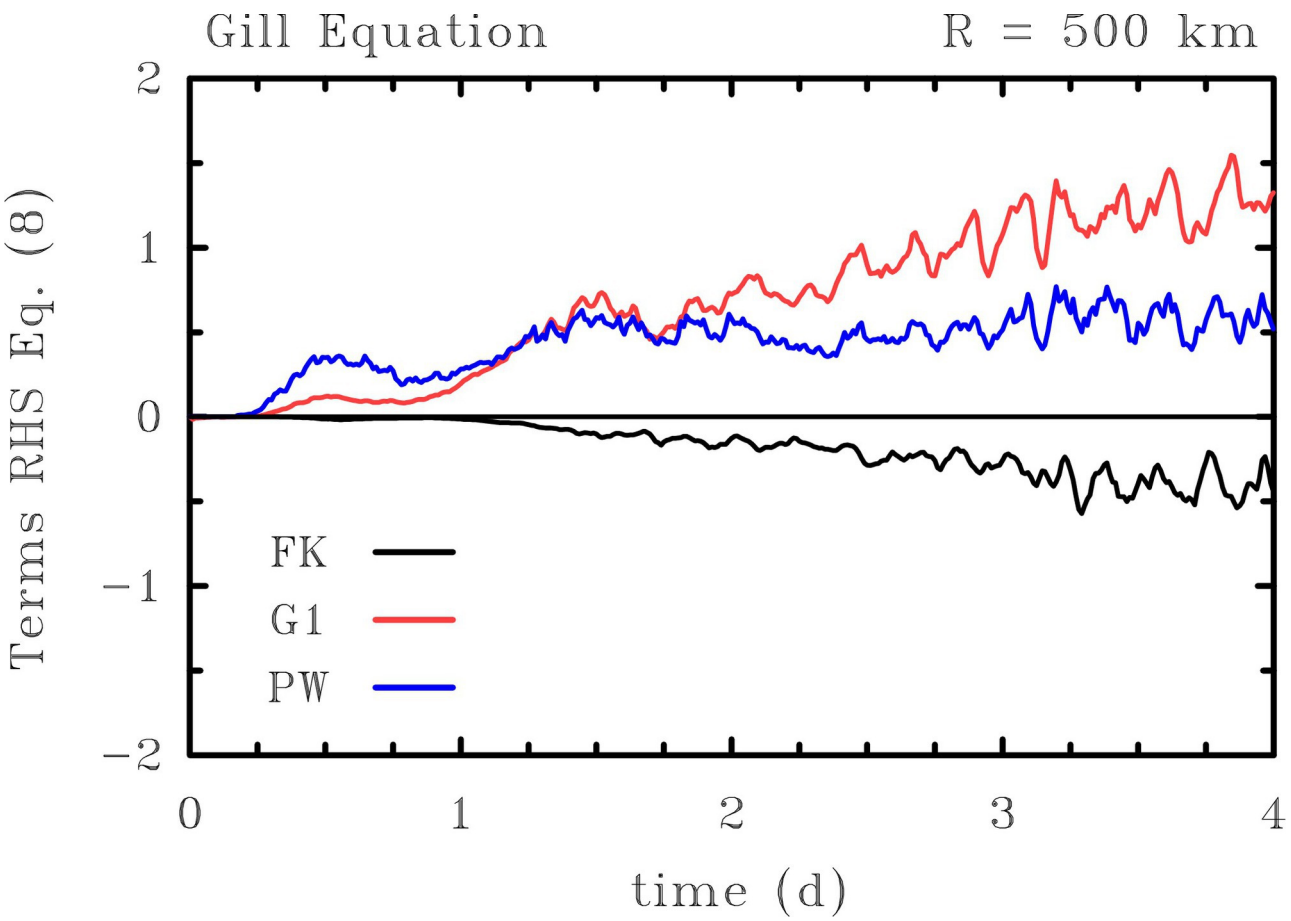

fig6b.eps

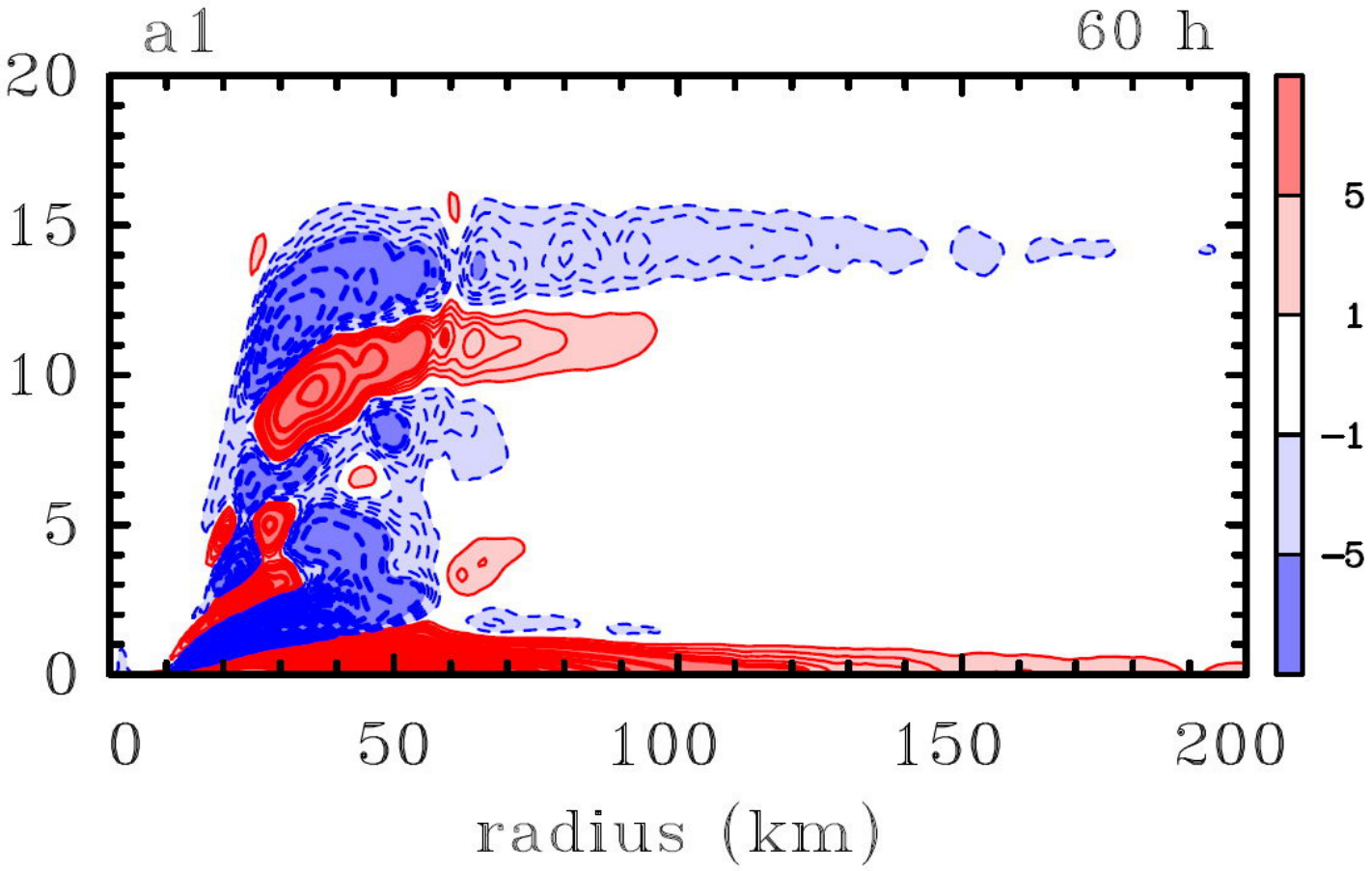

GraphicalFigure.jpg

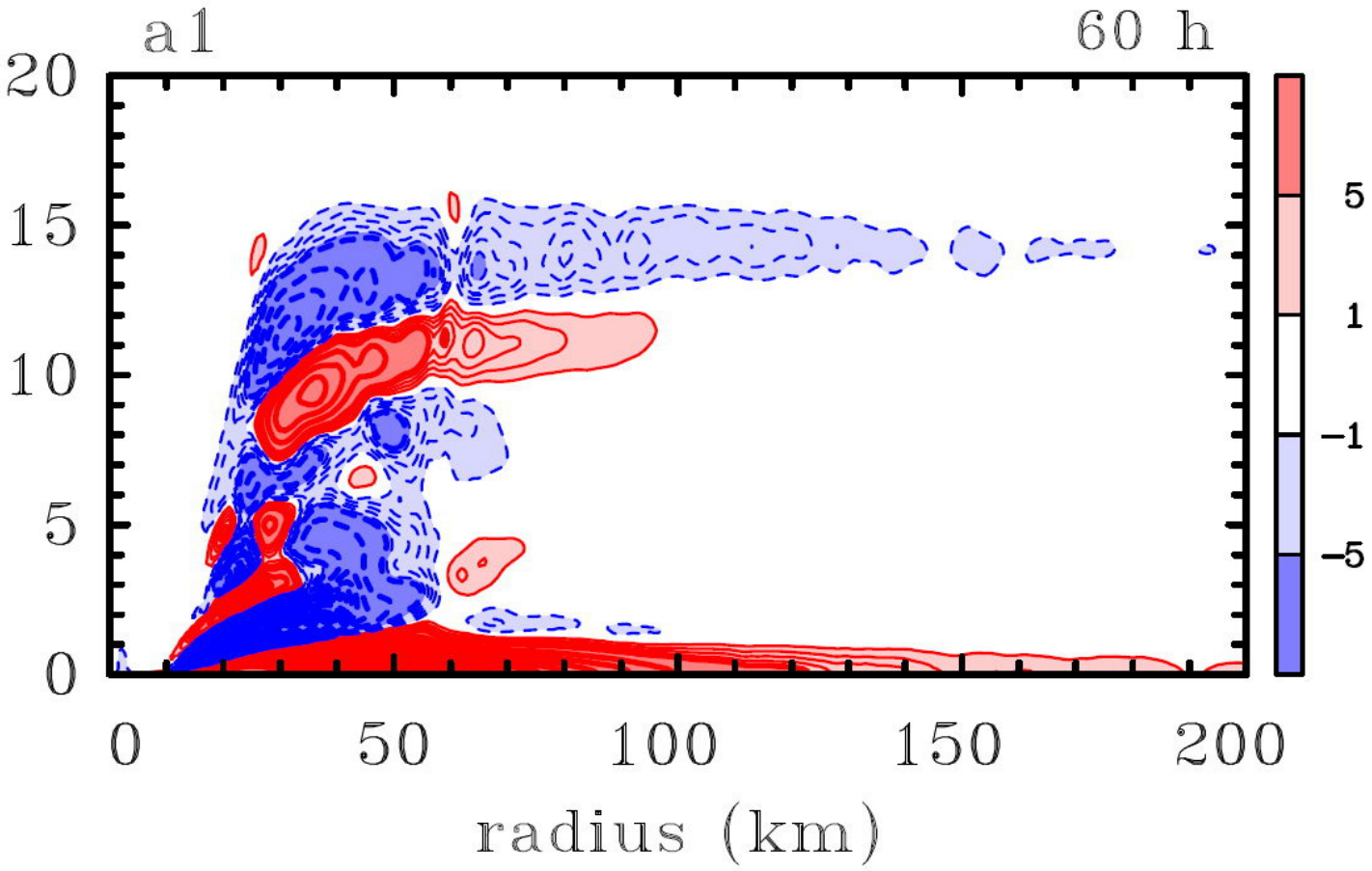

GraphicalFigure.jpg

The generation of kinetic energy in tropical cyclones revisited

Roger K. Smith\affil{a}\corrauth, Michael T. Montgomery\affil{b} and Gerard Kilroy\affil{a}

\address{\affilnum{a} Meteorological Institute, Ludwig Maximilians University of Munich, Munich, Germany \\\affilnum{b} Dept. of Meteorology, Naval Postgraduate School, Monterey, CA }

\corraddr{Prof. Roger K. Smith, Meteorological Institute, Ludwig-Maximilians University of Munich, Theresienstr. 37, 80333 Munich, Germany. E-mail: roger.smith@lmu.de}

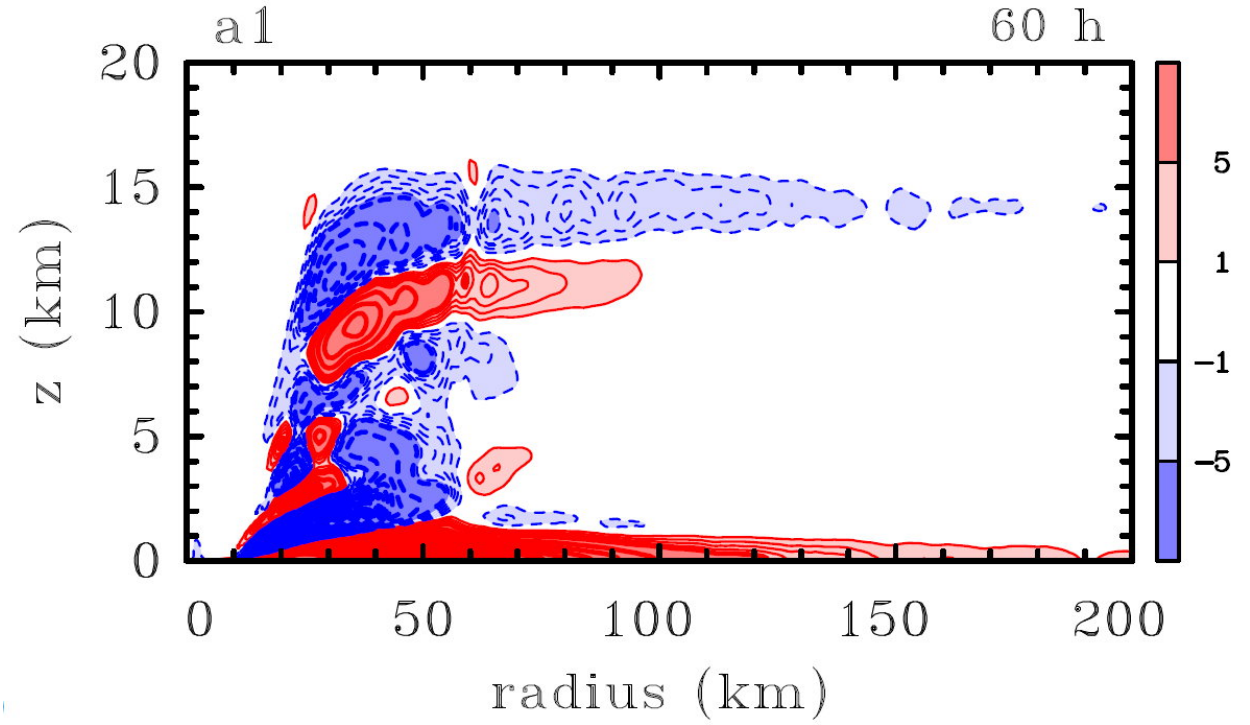

The figure shows the radius-height structure of the azimuthally averaged pressure work term identified by Anthes (1974) as the dominant generation term in the global kinetic energy equation near the end of the period of rapid intensification of an idealized tropical cyclone simulation. It shows several regions of energy generation and consumption, which because the averaged radial pressure gradient is everywhere positive, reflects the structure of the radial velocity. It is seen that the net global generation of kinetic energy is the residual after the cancellation of large positive and negative contributions. There is a large generation of kinetic energy in the frictional boundary layer and only a small contribution from the classical spin up mechanism.

The generation of kinetic energy in tropical cyclones revisited

Roger K. Smith\affil{a}\corrauth, Michael T. Montgomery\affil{b} and Gerard Kilroy\affil{a}

\address{\affilnum{a} Meteorological Institute, Ludwig Maximilians University of Munich, Munich, Germany \\\affilnum{b} Dept. of Meteorology, Naval Postgraduate School, Monterey, CA }

\corraddr{Prof. Roger K. Smith, Meteorological Institute, Ludwig-Maximilians University of Munich, Theresienstr. 37, 80333 Munich, Germany. E-mail: roger.smith@lmu.de}

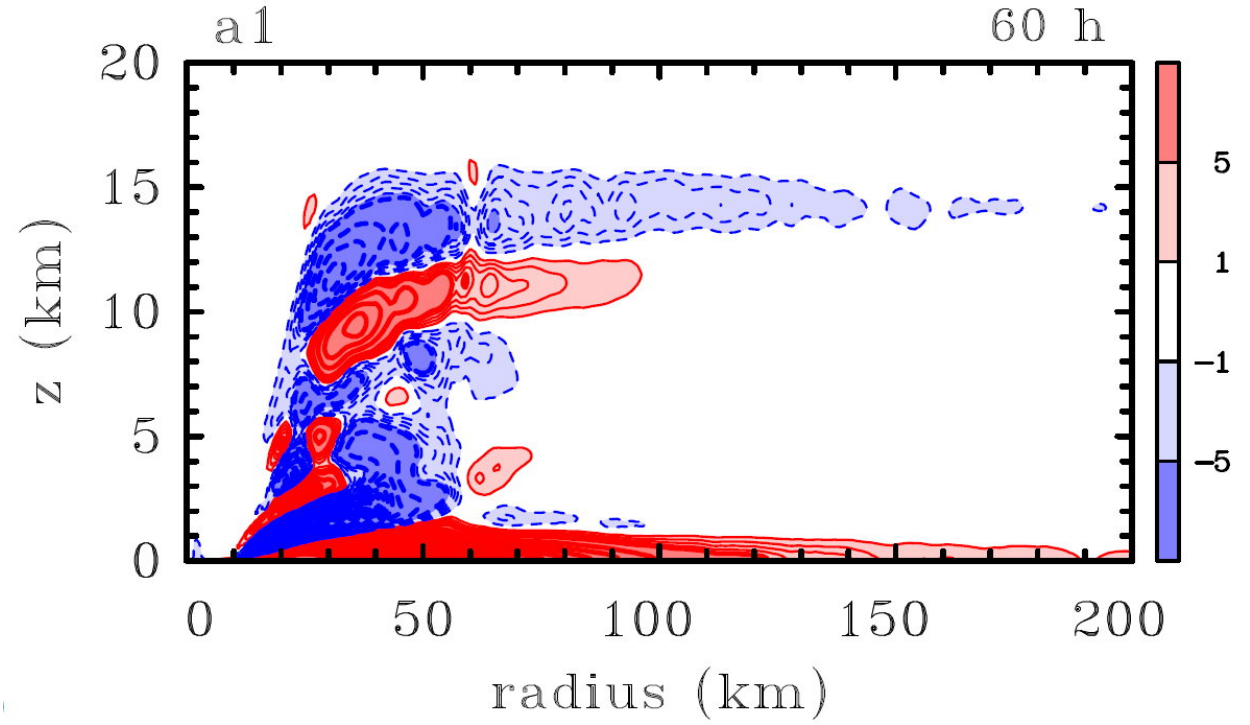

The figure shows the radius-height structure of the azimuthally averaged pressure work term identified by Anthes (1974) as the dominant generation term in the global kinetic energy equation near the end of the period of rapid intensification of an idealized tropical cyclone simulation. It shows several regions of energy generation and consumption, which because the averaged radial pressure gradient is everywhere positive, reflects the structure of the radial velocity. It is seen that the net global generation of kinetic energy is the residual after the cancellation of large positive and negative contributions. There is a large generation of kinetic energy in the frictional boundary layer and only a small contribution from the classical spin up mechanism.

The generation of kinetic energy in tropical cyclones revisited

Roger K. Smith[a]*, Michael T. Montgomery[b] and Gerard Kilroy[a]

[a] *Meteorological Institute, Ludwig Maximilians University of Munich, Munich, Germany*

[b] *Dept. of Meteorology, Naval Postgraduate School, Monterey, CA*

*Correspondence to: Prof. Roger K. Smith, Meteorological Institute, Ludwig-Maximilians University of Munich, Theresienstr. 37, 80333 Munich, Germany. E-mail: roger.smith@lmu.de

Many previous diagnoses of the global kinetic energy for a tropical cyclone have given prominence to a global integral of a pressure-work term in the generation of kinetic energy. However, in his erudite textbook of atmospheric and oceanic dynamics, Gill (1982) derives a form of the kinetic energy equation in which there is no such explicit source term. In this paper we revisit the interpretations of the generation of kinetic energy given previously in the light of Gill's analysis and compare the various interpretations, which are non-unique.

Further, even though global energetics provide a constraint on the flow evolution, in the context of the kinetic energy equation, they conceal important aspects of energy generation and consumption, a finding that highlights the limitations of a global kinetic energy budget in revealing the underlying dynamics of tropical cyclones.

Key Words: Tropical cyclone, hurricane, typhoon, spin-up, energetics

Received April 13, 2018; Revised ; Accepted

1. Introduction

In a classical review paper, Anthes (1974, section DI) summarized the global energetics of tropical cyclones, based in part on the work of Palmén and Jordan (1955) and Palmén and Riehl (1957). In this review he argues that the kinetic energy is dominated by the horizontal velocity components and he derives an expression for the rate-of-generation of kinetic energy, showing that "The important source of kinetic energy production in the hurricane is the radial flow toward lower pressure in the inflow layer, represented by $u\partial p/\partial r$." (Here u is the radial velocity component, r is the radius and p is the pressure). In a similar vein, Palmén and Riehl *op. cit.* note that "the generation depends on the vertical correlation between radial flow component and pressure gradient which, for production of kinetic energy, must be positive, i.e., the strongest inflow must occur at the strongest inward directed pressure gradient. They conclude that "kinetic energy production within the cyclone can take place only if the cyclone is of the warm core type." Anthes goes on to argue that "This inflow is a result of surface friction, which reduces the tangential wind speed and thereby destroys the gradient balance, so that the inward pressure gradient force exceeds the Coriolis and centripetal forces. In the warm core low the maximum pressure gradient ($\partial p/\partial r < 0$)* occurs just above the surface layer, at which the inflow ($u < 0$) is maximum in magnitude. In the outflow layer, where the radial flow is reversed, the pressure gradient is much weaker. The result is a net production of kinetic energy, dominated by the contribution from the inflow region."

The foregoing interpretations seem at odds with the kinetic energy equation in flux form presented by Gill (1982) in which the term $-u\partial p/\partial r$ does not appear. Nevertheless, in the context of tropical cyclones, subsequent work has built on the formulation by Palmén and Riehl as reviewed by Anthes (e.g. Kurihara 1975, Tuleya and Kurihara 1975, Frank 1977, DiMego and Bosart 1982, Hogsett and Zhang 2009, Wang *et al.* 2016). The generation of kinetic energy in the context of the global climate is discussed by Peixoto and Oort (1992, section 13.2).

The purpose of this paper is to reconcile the different interpretations of kinetic energy generation and to calculate the various terms in the kinetic energy budget from an idealized high-resolution numerical simulation of a tropical cyclone.

2. Kinetic energy equations

In its most basic form, the momentum equation may be written as

$$\frac{\partial \mathbf{u}}{\partial t} + \mathbf{u}\cdot\nabla\mathbf{u} + \mathbf{f}\wedge\mathbf{u} = -\frac{1}{\rho}\nabla p - g\mathbf{k} - \mathbf{F} \qquad (1)$$

*Presumably Anthes meant $\partial p/\partial r > 0$.

where $\mathbf{u}$ is the three dimensional velocity vector, p is the pressure, ρ is the density, $\mathbf{F}$ is the frictional force opposing the motion, $\mathbf{f} = f\mathbf{k}$, f is the Coriolis parameter ($2\Omega \sin\phi$, where ϕ is latitude and Ω is the earth's rotation rate), g is the acceleration due to gravity, and $\mathbf{k}$ is the unit vector in the vertical direction (here and below, all vector quantities are in bold type). For simplicity, an f-plane is assumed (f = constant) and the Coriolis terms proportional to the cosine of the latitude have been neglected as is customary for geophysical flow analyses off of the equator (e.g., McWilliams 2011).

The kinetic energy equation is obtained by taking the scalar product Equation (1) with $\mathbf{u}$ using the identity $\mathbf{u}\cdot\nabla\mathbf{u} = \nabla(\frac{1}{2}\mathbf{u^2}) + \omega \wedge \mathbf{u}$, where $\omega = \nabla \wedge \mathbf{u}$ is the vorticity vector. This procedure gives:

$$\frac{\partial}{\partial t}(\tfrac{1}{2}\mathbf{u^2}) + \mathbf{u}\cdot\nabla(\tfrac{1}{2}\mathbf{u^2}) = -\frac{1}{\rho}\mathbf{u}\cdot\nabla p - gw - \mathbf{u}\cdot\mathbf{F}, \tag{2}$$

where $w = \mathbf{k}\cdot\mathbf{u}$ is the vertical component of velocity. Note that the Coriolis force ($-\mathbf{f}\wedge\mathbf{u}$) does not appear in the energy equation because it is orthogonal to $\mathbf{u}$.

An alternative form of the energy equation is obtained by removing some hydrostatically-balanced reference pressure, $p_{ref}(z)$, from (1), where $dp_{ref}/dz = -g\rho_{ref}$ defines a reference density, ρ_{ref}, that is a function of altitude z. Then, with the substitution $p = p_{ref}(z) + p'$ and $\rho = \rho_{ref}(z) + \rho'$, the first two terms on the right-hand-side of Equation (1), $-(1/\rho)\nabla p - g\mathbf{k}$, become $-(1/\rho)\nabla p' + b\mathbf{k}$, where $b = -g(\rho - \rho_{ref})/\rho$ is the buoyancy force of an air parcel per unit mass. Then, Equation (2) becomes

$$\frac{\partial}{\partial t}(\tfrac{1}{2}\mathbf{u^2}) + \mathbf{u}\cdot\nabla(\tfrac{1}{2}\mathbf{u^2}) = -\frac{1}{\rho}\mathbf{u_h}\cdot\nabla_h p' + Pw - \mathbf{u}\cdot\mathbf{F}, \tag{3}$$

where $\mathbf{u_h}$ is the horizontal velocity vector, ∇_h is the horizontal gradient operator and

$$P = -\frac{1}{\rho}\frac{\partial p}{\partial z} - g = -\frac{1}{\rho}\frac{\partial p'}{\partial z} + b \tag{4}$$

is the net vertical perturbation gradient force per unit mass. Despite the explicit appearance of p' in the first term on the right-hand-side, all the terms in Equation (3) are independent of the reference pressure $p_{ref}(z)$, since, in particular, $\mathbf{u_h}\cdot\nabla_h p_{ref}(z) = 0$. For simplicity, we take $p_{ref}(z)$ and $\rho_{ref}(z)$ to be the ambient pressure and density, respectively, assuming that these are in hydrostatic equilibrium. Then p' vanishes at large distances from the vortex axis.

We examine now the different forms of Equation (3) derived by Anthes (1974), Gill (1982), and others beginning with a slight modification of Gill's formulation.

2.1. *Modified Gill's formulation*

In essence, Gill's formulation of the kinetic energy equation is as follows. Using the result that for any scalar field, γ,

$$\rho\frac{D\gamma}{Dt} = \frac{\partial}{\partial t}(\rho\gamma) + \nabla\cdot(\rho\gamma\mathbf{u}), \tag{5}$$

where $D/Dt = \partial/\partial t + \mathbf{u}\cdot\nabla$ is the material derivative (see Gill 1982, Equation 4.3.6)[†], the material form of Equation (3) times ρ may be written in flux form as

$$\frac{\partial}{\partial t}(\tfrac{1}{2}\rho\mathbf{u^2}) + \nabla\cdot\mathbf{F_{KE}} = p'\nabla_h\cdot\mathbf{u_h} + \rho Pw + \frac{\partial(p'w)}{\partial z} - \rho\mathbf{u}\cdot\mathbf{F}, \tag{6}$$

where

$$\mathbf{F_{KE}} = (p' + \tfrac{1}{2}\rho\mathbf{u^2})\mathbf{u}, \tag{7}$$

is the *mechanical energy flux density vector* (Gill, 1982, cf. Equation 4.6.4).

The global kinetic energy budget can be obtained by integrating Equation (6) over a cylindrical volume of space, V, of radius R and height H centred on the storm and using the boundary conditions that $u = 0$ at $r = 0$, and $w = 0$ at $z = 0$ and $z = H$. Here, we use a cylindrical coordinate system (r, λ, z) centred on the vortex, where r is the radius, λ is the azimuth and z is the height. We denote an integral of the quantity χ over the volume V by

$$\overline{[\chi]} = \frac{1}{\pi R^2 H}\int_0^R r dr \int_0^{2\pi} d\lambda \int_0^H \chi dz$$

Then (6) becomes

MODIFIED GILL'S FORM

$$\frac{d}{dt}\overline{[\tfrac{1}{2}\rho\mathbf{u^2}]} = \overline{[p'\nabla_h\cdot\mathbf{u_h}]} + \overline{[\rho Pw]} - F_{KEG} - D, \tag{8}$$

[†]If the density refers to that of a moist air parcel consisting of dry air, water vapour and liquid water, the density is conserved only if the liquid water component is suspended in the parcel. In the presence of precipitation, there will be a small source or sink of density associated with the flux divergence of falling precipitation. In what follows, we will ignore the effects of this source/sink term in the kinetic energy budget.

where

$$F_{KEG} = \frac{1}{\pi R^2 H} \int_0^{2\pi} d\lambda \int_0^H \left[u(p' + \tfrac{1}{2}\rho \mathbf{u^2}) \right]_{r=R} dz, \tag{9}$$

is the *flux of mechanical energy* through the side boundary $r = R$, and for a Newtonian fluid with dynamic viscosity coefficient μ,

$$D = \overline{[\mu \Phi_\nu]}, \tag{10}$$

where, in cylindrical coordinates,

$$\begin{aligned} \Phi_\nu = 2 &\left[\left(\frac{\partial u}{\partial r} \right)^2 + \left(\frac{1}{r}\frac{\partial v}{\partial \lambda} + \frac{u}{r} \right)^2 + \left(\frac{\partial w}{\partial z} \right)^2 \right] \\ &+ \left[r\frac{\partial}{\partial r}\left(\frac{v}{r} \right) + \frac{1}{r}\frac{\partial u}{\partial \lambda} \right]^2 + \left[\frac{1}{r}\frac{\partial w}{\partial \lambda} + \frac{\partial v}{\partial z} \right]^2 \\ &+ \left[\frac{\partial u}{\partial z} + \frac{\partial w}{\partial r} \right]^2 - \frac{2}{3}(\nabla \cdot \mathbf{u})^2 \end{aligned} \tag{11}$$

is the dissipation function[‡]. Here, v is the tangential wind component.

Since $\nabla_h \cdot \mathbf{u_h}$ is the fractional change in the horizontal area of an air parcel per unit time, the first term on the right-hand-side of Equation (8) is the cumulative effect of the kinetic energy generated locally when an air parcel with positive perturbation pressure expands in the horizontal or one with a negative perturbation pressure contracts in the horizontal. The second term on the right-hand-side of this equation represents the rate of kinetic energy production by air rising in the presence of a positive net vertical perturbation pressure gradient force ($P > 0$) and air sinking in the presence of a negative net vertical perturbation pressure gradient force ($P < 0$). In Gill's original formulation, the net vertical perturbation pressure gradient force term in Equation (8) is replaced by a buoyancy force, which, by itself, is a non-unique force, and the second term on the right-hand-side is replaced by $\nabla \cdot \mathbf{u}$, which is the fractional change in volume of an air parcel. Note that, in Gill's formulation, there is no term corresponding with $u\partial p/\partial r$ (or equivalently $u\partial p'/\partial r$) in Anthes' formulation of the problem, which a number of authors have argued is the key term in generating kinetic energy.

2.2. *Generalized Anthes' formulation*

As noted above, Anthes reasonably supposes that the vertical velocity makes only a small contribution to the global kinetic energy and his derivation of the kinetic energy equation is based on the horizontal momentum equations only and the neglect of the contribution from $\frac{1}{2}w^2$ in the kinetic energy. Nevertheless, Anthes retains the vertical velocity component in the advection term $\mathbf{u} \cdot \nabla \mathbf{u}$ in Equation (1) and $\mathbf{u} \cdot \nabla(\frac{1}{2}\mathbf{u^2})$ in Equation (2). A slightly generalized form of Anthes' equation follows directly from ρ times Equation (3), which in flux form analogous to (6) is

$$\begin{aligned} \frac{\partial}{\partial t}(\tfrac{1}{2}\rho \mathbf{u^2}) + \nabla \cdot \mathbf{F_{KEA}} = \\ -\mathbf{u_h} \cdot \nabla_h p' + \rho P w - \rho \mathbf{u} \cdot \mathbf{F}, \end{aligned} \tag{12}$$

where

$$\mathbf{F_{KEA}} = (\tfrac{1}{2}\rho \mathbf{u^2})\mathbf{u}. \tag{13}$$

Again integrating over the cylinder, Equation (12) becomes

GENERALIZED ANTHES' FORM

$$\frac{d}{dt}\overline{[\tfrac{1}{2}\rho \mathbf{u^2}]} = -\overline{[\mathbf{u_h} \cdot \nabla_h p']} + \overline{[\rho P w]} - F_{KEA} - D, \tag{14}$$

where

$$F_{KEA} = \frac{1}{\pi R^2 H} \int_0^{2\pi} d\lambda \int_0^H \left[u(\tfrac{1}{2}\rho \mathbf{u^2}) \right]_{r=R} dz. \tag{15}$$

Equation (14) is a generalization of Anthes' formulation to include the three-dimensional wind vector in the definition of kinetic energy and the rate of working of the net vertical perturbation gradient force per unit volume, $\overline{[\rho P w]}$, which is a non-hydrostatic effect. As in Anthes' original form, the pressure-work term, $-\overline{[\mathbf{u_h} \cdot \nabla_h p']}$, appears explicitly in the global form of the kinetic energy equation. For an axisymmetric flow, this term is simply $\overline{[-u\partial p/\partial r]}$ and, at first sight, one might question its prominence as a source of kinetic energy, since $\partial p/\partial r$ is *not* the only radial force acting on fluid parcels en route to the storm core. Above the frictional boundary layer, the radial pressure gradient is closely balanced by the sum of the centrifugal force and the radial component of the Coriolis force. Moreover, this

[‡]Equation (8) is, in essence, the kinetic energy equation for the Reynolds averaged flow in which the quantity μ is a turbulent eddy counterpart. In this case, we are presuming that a K-theory closure is adequate so that the Reynolds averaged equations look essentially like the Newtonian fluid formulation. Further, in the mechanical energy flux through the side boundary in Equation (9) we have neglected the eddy diffusive radial flux of kinetic energy. Relative to the advective flux of kinetic energy, the diffusive flux scales as the inverse Reynolds number of the flow, which is always small compared to unity outside of the surface layer. This conclusion is based on recently obtained estimates of the turbulent eddy diffusivity observed in major hurricanes on the order of $50 - 100$ m^{2}s^{-1} (Zhang *et al.* 2011).

source term does not appear in Gill's formulation (cf. Eq. (8)), although it is replaced by the term $\overline{[p'\nabla_h \cdot \mathbf{u_h}]}$ and the boundary flux terms are different. Even so, one should bear in mind that even in the axisymmetric case, $\overline{[-u\partial p/\partial r]}$ is generating *not only a radial contribution to the kinetic energy, but also an azimuthal contribution* through the action of the generalized Coriolis force $(f + v/r)u$. The generation of this azimuthal contribution is implicit in the kinetic energy equation as the generalized Coriolis force does no work, but it does convert radial momentum to tangential momentum.

3. Kinetic energy budget for an idealized simulation

We examine now the generation terms in the two forms of the kinetic energy equation for the case of an idealized tropical cyclone simulation. We begin with a brief description of the numerical model and go on to present the results.

3.1. *The numerical model*

The numerical model used for this study is Bryan's three-dimensional, nondydrostatic cloud model (CM1), version 16 (Bryan and Fritsch, 2002). The simulations relate to the prototype problem for tropical cyclone intensification, which considers the evolution of an initially axisymmetric, cloud-free, warm-cored, baroclinic vortex in a quiescent environment on an f-plane. The initial vortex is in thermal wind balance. A latitude of 20^oN and a constant sea surface temperature of 28^oC are assumed. The model configuration is more or less the same as described in section 2 of Črnivec *et al.* (2016). The differences are that, following the work of Mapes and Zuidema (1996), a more realistic time scale for Newtonian relaxation to the temperature field (10 days) is applied here instead of the previous default value in CM1 (12 h). Further, an open boundary condition is taken at lateral boundaries instead of rigid walls and the Dunion moist tropical sounding is used as the environmental sounding (Dunion 2011).

The initial tangential wind speed has a maximum of 15 m s^{-1} at the surface at a radius of 100 km. The tangential wind speed decreases sinusoidally with height, becoming zero at a height of 20 km. Above this height, up to 25 km, the tangential wind is set to zero. The balanced pressure, density and temperature fields consistent with this prescribed tangential wind distribution are obtained using the method described by Smith (2006). The calculations are carried out for a period of 4 days with data output every 15 min.

3.2. *A few details of the simulation*

Figure 1 summarizes the vortex evolution in the simulation. Panel (a) shows time series of the maximum azimuthally-averaged tangential wind speed, V_{max}, and panel (b) shows the radius R_{vmax} at which V_{max} occurs. Typically, V_{max} is located a few hundred meters above the surface, within a shallow inflow layer. The evolution is broadly similar to that described in Kilroy *et al.* (2016), who used a different numerical model and a much coarser horizontal resolution (horizontal grid spacing 5 km compared with 1 km used here). In brief, after a gestation for about a day during which deep convection becomes established inside R_{vmax}, the vortex undergoes a rapid intensification phase lasting about 36 h, before reaching a quasi-steady state. Initially R_{vmax} is located at a radius of 100 km, but contracts to a little more than 20 km after about $2\frac{1}{4}$ days. The most rapid contraction occurs during the rapid intensification phase as absolute angular momentum surfaces are drawn inwards quickly within and above the boundary layer.

Figure 1(c) shows the outermost radius of gale-force winds, R_{gales}, defined here as the radius of 17 m s^{-1} azimuthally-averaged tangential winds at a height of 1 km, which is approximately at the top of the frictional boundary layer. Shown also is R_{galesF}, defined as the (outer) radius at which the total wind speed at any grid point at a height of 10 m is 17 m s^{-1}. Both quantities serve as a measure of the vortex size, R_{galesF} being closest to the quantity used by forecasters[§], but R_{gales} being a preferred measure from a theoretical viewpoint (Kilroy *et al.* 2016). The evolution of storm size based on R_{galesF} is similar to that based on R_{gales}, although R_{gales} always exceeds the value of R_{galesF}. After 4 days, R_{gales} exceeds R_{galesF} by about 80 km.

Figure 2 shows vertical cross sections of the azimuthally-averaged, 3 h time averaged, radial and tangential velocity components, the vertical velocity component, and the M-surfaces during the intensification phase of the vortex. The time averages are centred on 36 h during the period of rapid intensification and at 60 h near the end of this period. The basic features of the flow are qualitatively similar at both times, but all three velocity components strengthen over the period, the M-surfaces moving inwards in the lower troposphere and outwards in the upper troposphere. The flow structure is similar to that which has been described in many previous studies (see e.g. the recent review by Montgomery and Smith 2017a and refs.) with a layer of strong shallow inflow marking the frictional boundary layer, a layer of weaker inflow in the lower troposphere, a region of strong outflow in the upper troposphere and a layer of enhanced inflow below the outflow. The maximum tangential wind speed occurs within, but near the top of the frictional boundary layer[¶]. Much of the ascent occurs in an annular region on the order of 50-60 km in radius. The region inside this annulus shows mostly descent.

3.3. *Kinetic energy evolution*

Figure 3 shows time series of the domain-averaged kinetic energy per unit mass, $\overline{\left[\frac{1}{2}\rho\mathbf{u^2}\right]}$, for domain radii 300 km and 500 km and a domain height of 20 km. As anticipated by Anthes (1974), this quantity is dominated by the horizontal velocity components: in fact, the curves for $\overline{\left[\frac{1}{2}\rho\mathbf{u^2}\right]}$ and $\overline{\left[\frac{1}{2}\rho\mathbf{u_h^2}\right]}$ essentially overlap. It follows that the contribution of the vertical velocity to the global kinetic energy is negligible. Notable features of the curves for both domain sizes are the slight decrease during the first 12 h on account of surface friction, followed by a rapid increase as the vortex intensifies. As time proceeds, the rate of increase progressively declines.

[§] Based on the wind speed in a particular sector and not azimuthally averaged.

[¶] At 60 h, the tangential wind field exhibits a second local maximum in the eyewall. This is a transient feature that is presumably associated with a centrifugal wave near the base of the eyewall (e.g. Montgomery and Smith 2017, p550) excited by an elevated pulse of boundary layer outflow shortly before. This feature is not seen at 48 h or 72 h and its presence doesn't alter the findings concerning the kinetic energy budget.

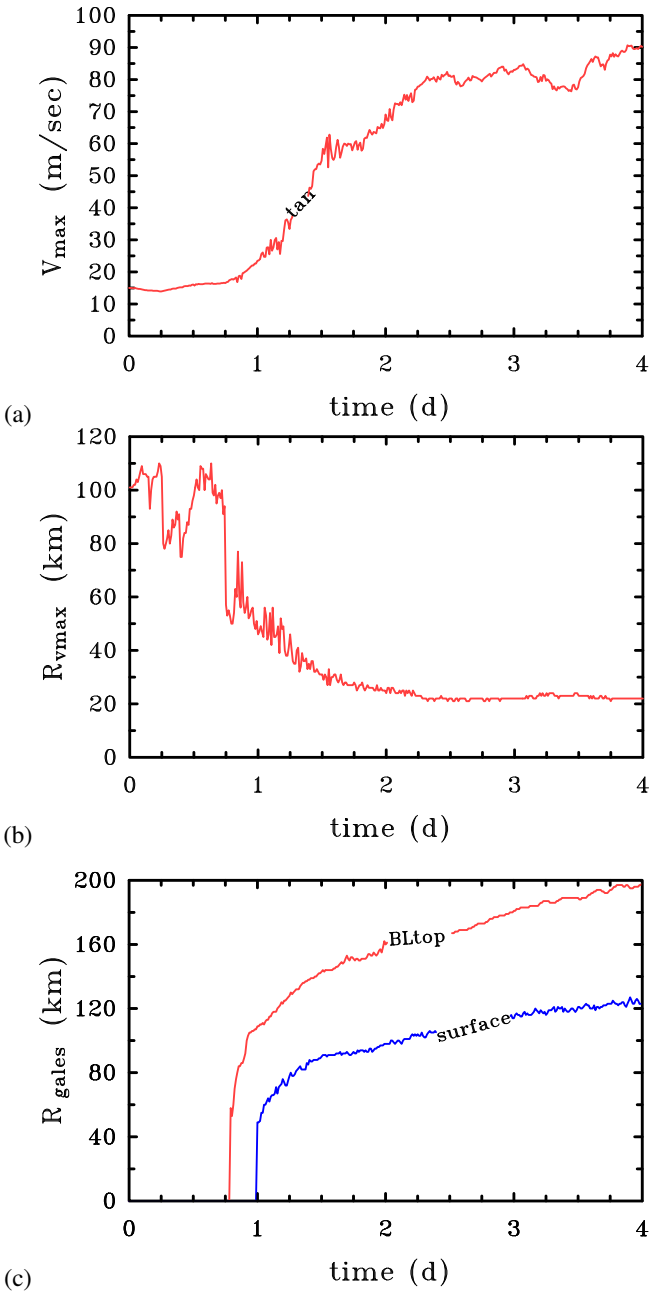

Figure 1. Time series of (a) maximum azimuthally-averaged tangential wind speed (V_{max}). Panel (b) shows the radius R_{vmax} at which the maximum tangential wind speed occurs (V_{max}). Panel (c) shows the radius at which gale force winds occurs (R_{gales}), where R_{gales} calculated at a height of 1 km, and corresponds to the radius of 17 m s^{-1} total winds outside the eyewall.

3.4. Kinetic energy generation: Anthes' formulation

Figure 4 shows time series of the principal terms in the generalized Anthes formulation (the right-hand-side of Equation (14)), excluding only the global dissipation term since the focus of the paper is on kinetic energy generation. For both domain radii, 300 km (Fig. 4(a)) and 500 km (Fig. 4(a)), both the terms $\overline{[-\mathbf{u_h} \cdot \nabla_h p']}$ and $\overline{[\rho P w]}$ are positive, but, perhaps surprisingly, the former term is not appreciably larger than the latter, even beyond 2 days when the differences are largest. The boundary flux term F_{KEA} is virtually zero throughout the calculation. For the larger domain size (R = 500 km), the temporal behaviour of the various terms is similar, but, as expected, the magnitudes of the respective terms are appreciably smaller (Fig. 4(b)), since the largest contributions to the averages are from well inside a 300 km radius (note the different scales on the ordinate in Figs. 4(a) and 4(b)).

The finding that the two terms $\overline{[-\mathbf{u_h} \cdot \nabla_h p']}$ and $\overline{[\rho P w]}$ are not appreciably different in magnitude is at first sight surprising since, as shown in Figure 3, the contribution of the vertical velocity to the total kinetic energy is negligible. Moreover, the $\overline{[\rho P w]}$ term does not appear in Anthes' original formulation because the formulation was based on the horizontal momentum equations only. An explanation of this result is suggested by an examination of the radial-height structure of the azimuthally-averaged generation term before completing the columnar average, i.e. $< -\mathbf{u_h} \cdot \nabla_h p' >$, where the angle brackets denote an azimuthal average. The structure of this average together with those of the other generation term, $< \rho P w >$, at 36 h and 60 h, is shown in Figure 5. At both times, the Anthes generation term $< -\mathbf{u_h} \cdot \nabla_h p' >$ shows coherent regions of large kinetic energy generation and of large kinetic energy destruction. The main region of generation in panels (a) and (b) is at low levels, below about 2 km, where the strongest inflow occurs and where the inward directed radial pressure gradient force is particularly strong (panels (c) and (d) of Figure 5). There is a second region of generation in an annular column, mostly on the outer side of the eyewall updraught below about 9 km at 36 h and below

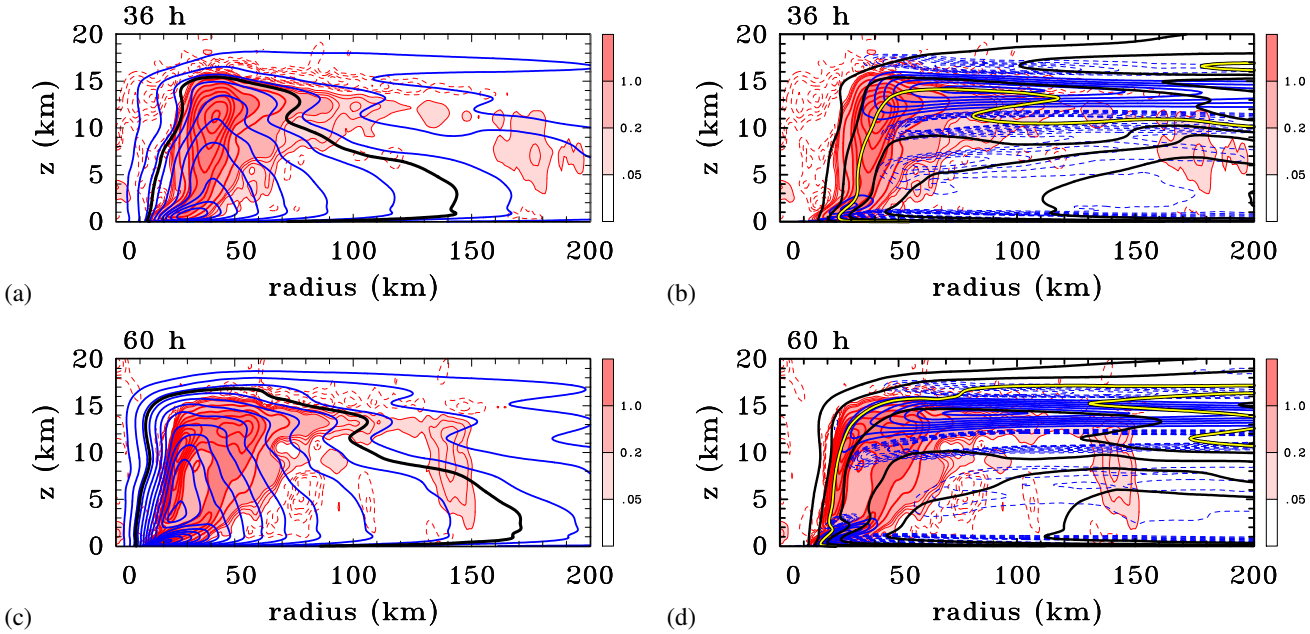

Figure 2. Left panels: Vertical cross sections of the azimuthally-averaged, 3 hour time averaged tangential velocity component (blue contours) centred at 36 h and 60 h. Superimposed are contours and shading of the averaged vertical velocity. Contour intervals are as follows. Tangential velocity: blue contours every 5 m s^{-1}, with a thick black contour highlighting the 17 m s^{-1} contour. Vertical velocity: thin red contours every 0.05 m s^{-1} to 0.2 m s^{-1}, thick red contour interval 0.5 m s^{-1}, thin dashed red contours indicate subsidence at intervals of 0.02 m s^{-1}. Right Panels: Vertical cross sections of the azimuthally-averaged, 3 hour time averaged radial velocity component together with the averaged vertical velocity centred at the same times. Contour intervals are as follows. Radial velocity: thick blue contours 4 m s^{-1}, dashed negative, thin blue dashed contours every 0.5 m s^{-1} down to -3.5 m s^{-1}. Absolute angular momentum: thick black contours every 2×10^5 m^2 s^{-1}, with the 6×10^5 m^2 s^{-1} contour highlighted in yellow.

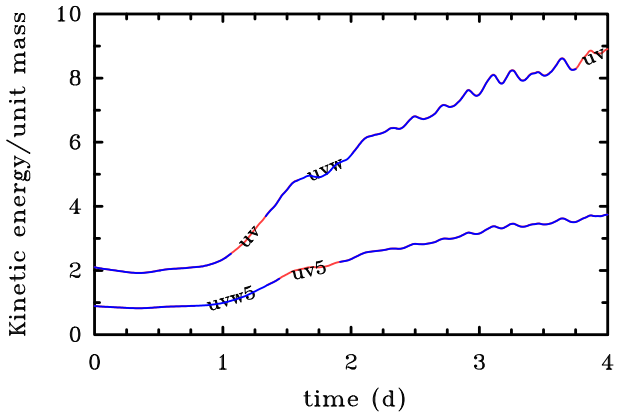

Figure 3. Time series of the left-hand-side of Equation 14, $\overline{\left[\frac{1}{2}\rho \mathbf{u}^2\right]}$ (curves labelled uvw) compared to $\overline{\left[\frac{1}{2}\rho \mathbf{u}_\mathbf{h}^2\right]}$ (curves labelled uv) for cylinders of 300 km and 500 km. The curves for each cylinder size lie essentially on top of each other so that only a single curve is evident. The curves for the 500 km domain are labelled with a '5'.

about 12 km at 60 h. The generation terms in panels (a) and (b) are similar in structure and magnitude to that shown by Kurihara (1975, Figure 42, upper right) for a lower resolution axisymmetric simuulation.

Since the radial pressure gradient is positive at all heights [panels (c) and (d) of Figure 5], these generation regions must be ones in which there is generally inflow[‖]. For the same reason, where there is outflow, there is kinetic energy removal as seen in the two principal coherent regions in panels (a) and (b) where $< -\mathbf{u_h} \cdot \nabla_h p' >< 0$. It follows that the computed value of $\overline{[-\mathbf{u_h} \cdot \nabla_h p']}$ is the remainder resulting from the cancellation of two comparatively large contributions from $< \mathbf{u_h} \cdot \nabla_h p' >$ of opposite sign, namely $< -\mathbf{u_h} \cdot \nabla_h p' >_+$ and $< -\mathbf{u_h} \cdot \nabla_h p' >_-$, the former being the sum of all positive values of $-\mathbf{u_h} \cdot \nabla_h p'$ and the latter $< -\mathbf{u_h} \cdot \nabla_h p' >_-$ to be the sum of all negative values. This large cancellation is evident in the time series shown in Figure 4.

In summary, a substantial fraction of the kinetic energy that is generated is removed in regions where there is outflow and the residual is relatively small, comparable, indeed, with the kinetic energy generated by the rate-of-working of the net vertical perturbation pressure gradient force (buoyancy plus perturbation pressure gradient), principally in the region of diabatically-forced ascent. The structure of the net vertical perturbation pressure gradient force at 36 h and 60 h is shown in panels (e) and (f) of Figure 5. As expected, this force is concentrated in an annular region overlapping the region of diabatic heating.

3.5. *Kinetic energy generation (Gill's formulation)*

Figure 6 shows time series of the principal terms in the modified Gill formulation (the right-hand-side of Equation (8)), excluding again the global dissipation term. In this formulation, the term $\overline{[p' \nabla_h \cdot \mathbf{u_h}]}$ is positive with mean amplitude and fluctuations about this mean

[‖] Note that eddy effects are included in all generation terms.

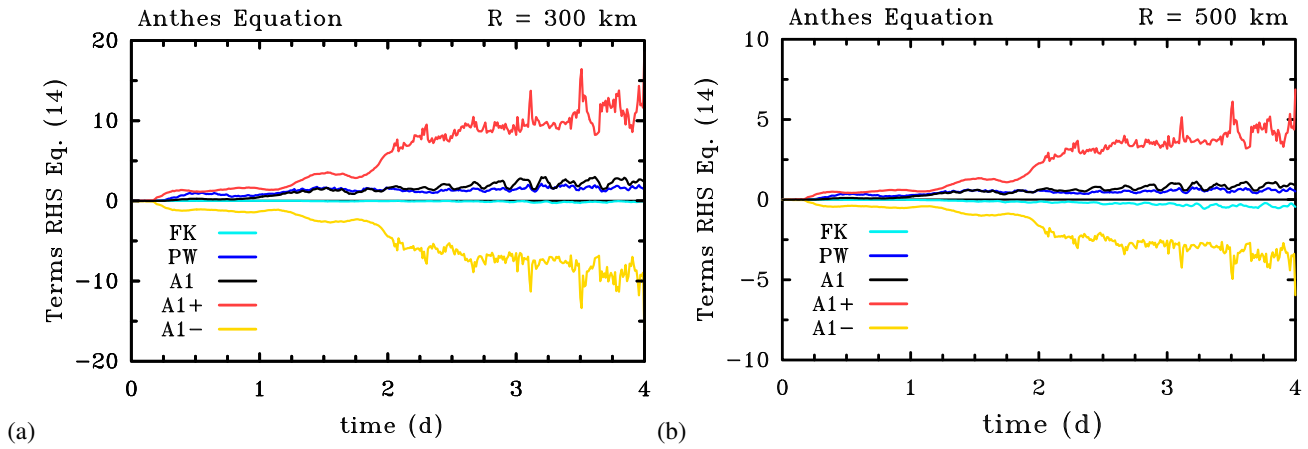

Figure 4. Time series of the kinetic energy tendency terms on the right-hand-side of Equation (14), the Anthes' formulation, averaged over a cylinder of size (a) 300 km and (b) 500 km. Units on the ordinate are 10^{-3} W m^{-3}. The dissipation term is not shown. A1 stands for $\overline{[-\mathbf{u_h} \cdot \nabla_h p']}$, FK for F_{KEA} and PW for $\overline{[\rho P w]}$. A1+ and A1- stand for the contributions to A1 from regions where the argument $-\mathbf{u_h} \cdot \nabla_h p'$ is positive and negative, respectively.

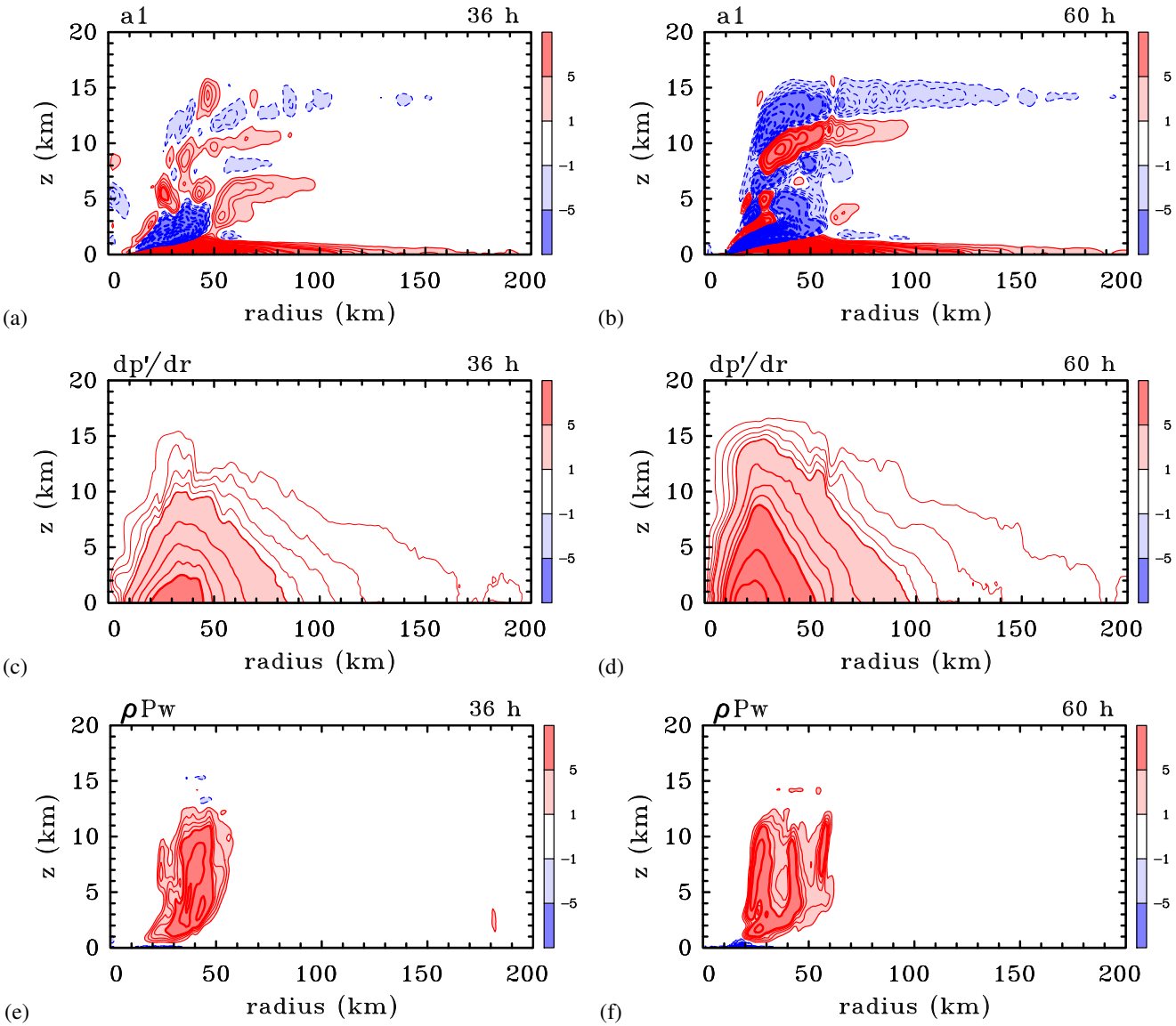

Figure 5. Radius-height cross sections of azimuthally-averaged quantities in Equation (14), before performing the columnar average: $< -\mathbf{u_h} \cdot \nabla_h p' >$ (panels (a), (b)); and $< \rho P w >$ (panels (e), (f)), at 36 h (left panels) and 60 h (right panels). Panels (c) and (d) show similar cross sections of $< \partial p'/\partial r >$ at these times. Contour intervals are as follows. Panels (a), (b), (e) and (f): thick contours 5×10^{-2} W m^{-3}: thin contours 1×10^{-2} W m^{-3}. Solid red contours positive, dashed blue contours negative. Panels (c) and (d): thin contours 0.2×10^{-2} Pa m^{-1} to 0.8×10^{-2} Pa m^{-1}; medium thick contours 1.0×10^{-2} Pa m^{-1} to 5.0×10^{-2} Pa m^{-1}; thick contours every 5.0×10^{-2} Pa m^{-1}. Numbers indicated on the side bar should be multiplied by 10^{-2}.

increasing with time during the 4 day calculation [Fig. 6(b)]. For the first day, the term is a little less than the $\overline{[\rho P w]}$ term, but thereafter becomes progressively larger. The increasing energy source represented by the sum of the two foregoing terms is opposed, in part, by the net outward flux of mechanical energy through the radial boundary, F_{KEG}.

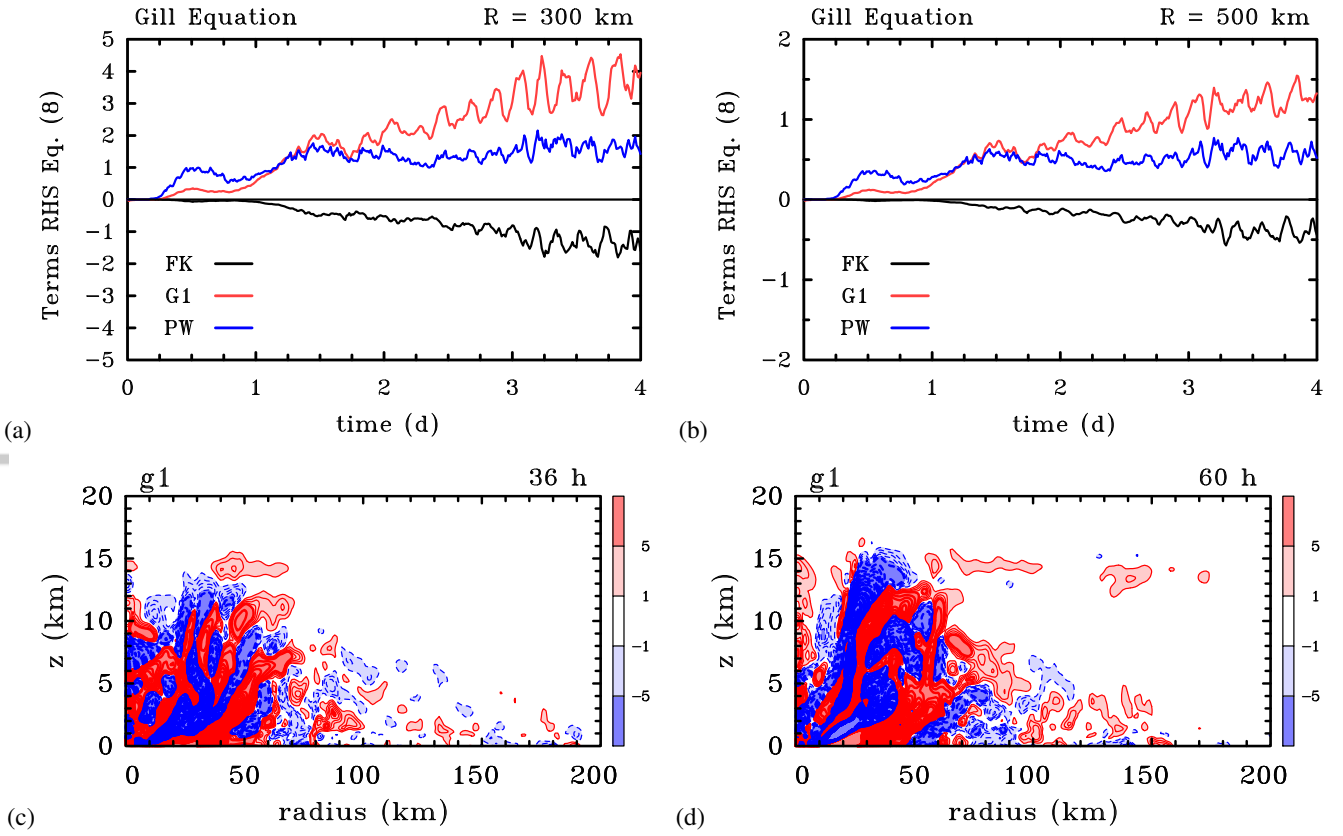

Figure 6. Time series of the kinetic energy tendency terms: $\overline{[p'\nabla_h \cdot \mathbf{u_h}]}$ (denoted by G1); $\overline{[\rho Pw]}$ (denoted PW) and F_{KEG} (denoted FK) in the modified Gill formulation [Equation (8) averaged over a cylinder of size (a) 300 km and (b) 500 km. Units on the ordinate are 10^{-3} W m^{-3}. Panels (c) and (d) show the azimuthally averaged terms $< p'\nabla_h \cdot \mathbf{u_h} >$ in Equation (8) at 36 h and 60 h, respectively. Contour intervals are: thick contours 5×10^{-2} W m^{-3}: thin contours 1×10^{-2} W m^{-3}. Solid red contours positive, dashed blue contours negative. Numbers indicated on the side bar should be multiplied by 10^{-2}.

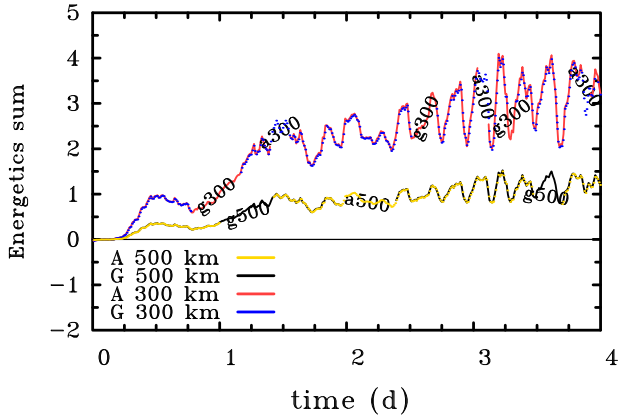

Figure 7. Sum of the terms for Gill's and Anthes' formulation excluding the dissipation term for cylinders of radius $R = 300$ km and 500 km. Values on the ordinate have been multiplied by 10^3 for plotting purposes. The two curves for each value of R lie essentially on top of each other.

Panels (c) and (d) of Figure 6 show the structure of the term $< p'\nabla_h \cdot \mathbf{u_h} >$, again 36 h and 60 h. The radial and vertical integral of this term form the cylindrical average $\overline{[p'\nabla_h \cdot \mathbf{u_h}]}$ in the modified Gill's formulation of the energy equation. The qualitative radius-height structure of $< p'\nabla_h \cdot \mathbf{u_h} >$ at the two times shown is less easy to infer from the solutions in Figure 2. Moreover, as shown in Figure 6, there is significant cancellation between the term $\overline{[p'\nabla_h \cdot \mathbf{u_h}]}$ and the boundary flux term in Gill's formulation [Equation (8)]. For this reason, the Anthes' formulation of the energy equation would seem to be preferable to Gill's formulation, even though both formulations are correct and give the same tendency of kinetic energy over the control volume of integration (see next subsection).

3.6. Total kinetic energy generation

A check on the foregoing calculations is provided by calculating the total tendency of kinetic energy generation, which is the sum of all the terms on the right-hand-side of Equations (8) or (14). This sum should be the same for each formulation. That this is the case is verified in Figure 7, which shows the sum for each domain size. As expected, the curves for the two formulations are coincident.

4. Discussion

Anthes' statement noted in the Introduction that "the important source of kinetic energy production in the hurricane is the radial flow toward lower pressure in the inflow layer, represented by $-u\partial p/\partial r$" may seem at first sight problematic because, above the boundary

layer, the radial pressure gradient is very closely in balance with sum of centrifugal and Coriolis forces. Thus the energy source associated with $-u\partial p/\partial r$ might appear, at least at first sight, to be a gross overestimate. However, the kinetic energy equation doesn't recognize the balance constraint and, in this equation, the radial pressure gradient acts to generate not only kinetic energy of radial motion, but also that of tangential motion through the action of the generalized Coriolis force $(f + v/r)u$, a term that appears in the tangential momentum equation in cylindrical coordinates. This is despite the fact that the generalized Coriolis force does not appear explicitly in the kinetic energy equation.

As noted also in the Introduction, Anthes recognized that much of the inflow into the storm is " ... a result of surface friction, which reduces the tangential wind speed and thereby destroys the gradient balance, so that the inward pressure gradient force exceeds the Coriolis and centripetal** forces" and he pointed out that "In the warm core low the maximum pressure gradient ($-\partial p/\partial r < 0$ [sign corrected: our insertion]) occurs at the lowest level, at which the inflow ($u < 0$) is maximum. In the outflow layer, where the radial flow is reversed, the pressure gradient is much weaker. The result is a net production of kinetic energy, dominated by the contribution from the inflow region". While this view is broadly supported by the calculations presented herein, the calculations provide a sharper view of the *net* production of kinetic energy indicating a region of significant kinetic energy generation accompanying inflow *throughout* the lower troposphere above the boundary layer as well as significant regions where kinetic energy is consumed as air flows outwards, against the radial pressure gradient, above the boundary layer. Indeed, the generation above the boundary layer is a manifestation of spin up by the classical mechanism articulated by Ooyama (1969), while the generation within the boundary layer, highlighted by Anthes, is a manifestation of the nonlinear boundary layer spin up mechanism articulated by Smith and Vogl (2008), Smith *et al.* (2009), Smith and Montgomery (2016) and Montgomery and Smith (2017b).

Anthes argues that the boundary layer " ... must be responsible for a net gain of kinetic energy" even though "a substantial dissipation of kinetic energy in the hurricane occurs in the boundary layer through turbulent diffusion and ultimate loss of energy to the sea surface". As a result, he is led to the paradox that "surface friction is responsible for a net increase in kinetic energy and without friction the hurricane could not exist." The resolution of this paradox would appear to be Anthes' de-emphasis of the role of the classical mechanism for spin up in the kinetic energy budget.

The results of our study, especially the noted cancellation of relatively large generation and consumption contributions to the term $\overline{[-\mathbf{u_h} \cdot \nabla_h p']}$ points to limitations in the utility of a global kinetic energy budget in revealing the underlying dynamics of tropical cyclone intensification. An alternative approach would be to examine the energetics of individual air parcels as they move around some hypothetical circuit (see Emanuel (2004) and references), but this approach relies on assumptions about the circuits traversed, circuits that may or may not be realizable in reality.

5. Conclusions

We have re-examined the traditional theory for kinetic energy generation in a tropical cyclone used by Palmén and Jordan (1955), Palmén and Riehl (1957), Frank (1977), Hogsett and Zhang (2009) and succinctly summarized in the review article by Anthes (1974). We have compared this with an alternative interpretation of global kinetic energy generation in geophysical flows inspired by Gill (1982), noting that such interpretations are non-unique.

We have shown that the *net* rate of production of kinetic energy is a comparatively small difference between the generation in regions of inflow and the magnitude of the consumption in regions of outflow, so much so, that this difference is comparable in magnitude with the rate of generation by the net vertical perturbation pressure gradient force. The latter effect was not contained in Anthes' original formulation, which was based only on the horizontal momentum equations.

We pointed out that the kinetic energy generation term in Anthes' formulation involving the radial pressure gradient does not appear in Gill's formulation of the kinetic energy equation or our modification thereof. It is replaced by a term comprising the global integral of the rate of working by perturbation pressure ($\overline{[p'\nabla_h \cdot \mathbf{u_h}]}$) as the flow expands in the horizontal. However, this generation term is largely compensated in the modified Gill formulation by the boundary flux of mechanical energy (F_{KEG}). The fact that the boundary flux of kinetic energy in the Anthes formulation (F_{KEA}) is typically negligible, as well as the difficulty in anticipating the structure of the term $\overline{[p'\nabla_h \cdot \mathbf{u_h}]}$ in a tropical cyclone are factors weighing in favour of using Anthes' formulation when applied to the generation of kinetic energy in a tropical cyclone. However, in the light of the large cancellation of positive and negative values in the radial pressure-work term, the contribution from the rate of working of the net vertical force is non-negligible in comparison and should be included in any global kinetic energy budget.

While global energetics provide a constraint on flow evolution, we have shown in the context of the kinetic energy equation that they conceal important aspects of energy generation and consumption. This finding highlights the limitations of a global kinetic energy budget in revealing the underlying dynamics of tropical cyclones.

6. Acknowledgements

We thank Drs. Chris Landsea, Anastassia Makarieva and an anonymous reviewer for their perceptive comments on the original manuscript. GK and RKS acknowledge financial support for tropical cyclone research from the Office of Naval Research Global under Grant No. N62909-15-1-N021. MTM acknowledges the support of NSF grant AGS-1313948, NOAA HFIP grant N0017315WR00048, NASA grant NNG11PK021, ONR grant N0001417WX00336, and the U. S. Naval Postgraduate School.

7. Appendix: Calculation of the net vertical force, P

The net vertical force per unit mass, P, defined in Equation (4) and used to construct Figures 5(e) and 5(f) was first calculated on the stretched model grid at the levels where thermodynamic quantities are defined. The vertical perturbation pressure gradient was determined by fitting a quadratic function to three successive levels z_{i-1}, z_i and z_{i+1} at which the perturbation pressure has values

**Presumably, Anthes means the centrifugal force.

p'_{i-1}, p'_i and p'_{i+1}, respectively. Then

$$\left(\frac{\partial p'}{\partial z}\right)_i = \frac{(p'_{i+1} - p'_i)dz_i^2 - (p'_{i-1} - p'_i)dz_{i+1}^2}{dz_{i+1}dz_i(z_{i+1} - z_{i-1})} \tag{16}$$

where $dz_i = z_i - z_{i-1}$.

8. References

Anthes RA. 1974. The dynamics and energetics of mature tropical cyclones. *Rev. Geophys. Space Phys*,**12**: 495-522

Bryan GH, Fritsch JM. 2002. A benchmark simulation for moist nonhydrostatic numerical models. *Mon. Weather Rev.*, bf 130: 29172928.

Črnivec N, Smith RK, Kilroy G. 2016. Dependence of tropical cyclone intensification rate on sea surface temperature. *Q. J. R. Meteorol. Soc.*, **142**: 1618-1627.

DiMego GJ, Bosart LF. 1982. The transformation of tropical storm Agnes into an extratropical cyclone. Part II: Moisture, vorticity and kinetic energy budget

Dunion JP. 2011. Rewriting the climatology of the tropical North Atlantic and Carribean sea atmosphere. *J. Clim*, **24**: 893908.

Emanuel K. 2004. Tropical cyclone energetics and structure. In *Atmospheric turbulence and mesoscale meteorology*, E. Fedorovich, R. Rotunno and B. Stevens, editors, Cambridge University Press, pp280.

Frank WM. 1977. The structure and energetics of the tropical cyclone ll. Dynamics and energetics. *Mon. Weather Rev.*, **105**: 1136-1160.

Gill AE. 1982. *Atmosphere-Ocean Dynamics*. New York: Academic. 4th ed., 662pp

Hogsett W, Zhang D-L. 2009. Numerical simulation of Hurricane Bonnie (1998). Part III: Energetics. *J. Atmos. Sci.*, **66**: 2678-2696.

Kilroy G, Smith RK, Montgomery MT. 2016. Why do model tropical cyclones grow progressively in size and decay in intensity after reaching maturity? *J. Atmos. Sci.*, **73**: 487-503.

Kurihara Y. 1975. 1975: Budget analysis of a tropical cyclone simulated in an axisymmetric numerical model. *J. Atmos. Sci.*, , **32**: 25-59.

McWilliams JC. 2011. *Fundamentals of geophysical fluid dynamics*. Cambridge University Press, 283pp.

Mapes BE, Zuidema P. 1996: Radiative-dynamical consequences of dry tongues in the tropical troposphere. *J. Atmos. Sci.*, **53**: 620-638.

Montgomery MT, Smith RK. 2017a: Recent developments in the fluid dynamics of tropical cyclones. *Annu. Rev. Fluid Mech.*, **49**: 1-33, doi:10.1146/annurev-fluid-010816-060022.

Montgomery MT, Smith RK. 2017b: On the applicability of linear, axisymmetric dynamics in intensifying and mature tropical cyclones. *Fluids*, **2**: 69. doi:10.3390/fluids2040069.

Ooyama K. 1969: Numerical simulation of the life-cycle of tropical cyclones. *J. Atmos. Sci.*, **26**: 3-40.

Palmén E, Jordan CL. 1955. Note on the release of kinetic energy in tropical cyclones. *Tellus*, **7**: 186-189.

Palmén E, Riehl H. 1957. Budget of angular momentum and energy in tropical storms. *J. Meteor.*, **14**: 150-159.

Peixoto JP, Oort AH. 1992 *Physics of climate*. American Institute of Physics, New York, p 520.

Smith RK. 2006. Accurate determination of a balanced axisymmetric vortex. *Tellus*, **58A**: 98-103.

Smith RK, Vogl S, 2008: A simple model of the hurricane boundary layer revisited. *Q. J. R. Meteorol. Soc.*, **134**: 337-351.

Smith RK, Montgomery MT, 2016: The efficiency of diabatic heating and tropical cyclone intensification. *Q. J. R. Meteorol. Soc.*, **142**: 2081-2086.

Smith RK Montgomery MT Nguyen SV. 2009: Tropical cyclone spin up revisited. *Q. J. R. Meteorol. Soc.*, **135**: 1321-1335.

Tuleya RE, Kurihra Y. 1975. The energy and angular momentum budgets of a three-dimensional tropical cyclone model. *J. Atmos. Sci.*, **32**: 287-301.

Wang Y, Cui X, Li, X, Zhang W, Huang Y. 2016. Kinetic energy budget during the genesis period of Tropical Cyclone Durian (2001) in the South China Sea. *Mon. Weather Rev.*, **144**: 2831-854.

Zhang JA Rogers RF Nolan DS and Marks FD 2011: On the characteristic height scales of the hurricane boundary layer. *Mon. Weather Rev.*, **139**: 2523-2535.

Quarterly Journal of the Royal Meteorological Society *Q. J. R. Meteorol. Soc.* **144: 1–9 (2018)**

The generation of kinetic energy in tropical cyclones revisited

Roger K. Smith[a]*, Michael T. Montgomery[b] and Gerard Kilroy[a]
[a] *Meteorological Institute, Ludwig Maximilians University of Munich, Munich, Germany*
[b] *Dept. of Meteorology, Naval Postgraduate School, Monterey, CA*
*Correspondence to: Prof. Roger K. Smith, Meteorological Institute, Ludwig-Maximilians University of Munich, Theresienstr. 37, 80333 Munich, Germany. E-mail: roger.smith@lmu.de

Many previous diagnoses of the global kinetic energy for a tropical cyclone have given prominence to a global integral of a pressure-work term in the generation of kinetic energy. However, in his erudite textbook of atmospheric and oceanic dynamics, Gill (1982) derives a form of the kinetic energy equation in which there is no such explicit source term. In this paper we revisit the interpretations of the generation of kinetic energy given previously in the light of Gill's analysis and compare the various interpretations, which are non-unique.
Further, even though global energetics provide a constraint on the flow evolution, in the context of the kinetic energy equation, they conceal important aspects of energy generation and consumption, a finding that highlights the limitations of a global kinetic energy budget in revealing the underlying dynamics of tropical cyclones.

Key Words: Tropical cyclone, hurricane, typhoon, spin-up, energetics

Received May 17, 2018; Revised ; Accepted

Citation: . . .

1. Introduction

In a classical review paper, Anthes (1974, section DI) summarized the global energetics of tropical cyclones, based in part on the work of Palmén and Jordan (1955) and Palmén and Riehl (1957). In this review he argues that the kinetic energy is dominated by the horizontal velocity components and he derives an expression for the rate-of-generation of kinetic energy, showing that "The important source of kinetic energy production in the hurricane is the radial flow toward lower pressure in the inflow layer, represented by $u\partial p/\partial r$." (Here u is the radial velocity component, r is the radius and p is the pressure). In a similar vein, Palmén and Riehl *op. cit.* note that "the generation depends on the vertical correlation between radial flow component and pressure gradient which, for production of kinetic energy, must be positive, i.e., the strongest inflow must occur at the strongest inward directed pressure gradient. They conclude that "kinetic energy production within the cyclone can take place only if the cyclone is of the warm core type." Anthes goes on to argue that "This inflow is a result of surface friction, which reduces the tangential wind speed and thereby destroys the gradient balance, so that the inward pressure gradient force exceeds the Coriolis and centripetal forces. In the warm core low the maximum pressure gradient ($\partial p/\partial r < 0$)[1] occurs just above the surface layer, at which the inflow ($u < 0$) is maximum in magnitude. In the outflow layer, where the radial flow is reversed, the pressure gradient is much weaker. The result is a net production of kinetic energy, dominated by the contribution from the inflow region."

The foregoing interpretations seem at odds with the kinetic energy equation in flux form presented by Gill (1982) in which the term $-u\partial p/\partial r$ does not appear. Nevertheless, in the context of tropical cyclones, subsequent work has built on the formulation by Palmén and Riehl as reviewed by Anthes (e.g. Kurihara 1975, Tuleya and Kurihara 1975, Frank 1977, DiMego and Bosart 1982, Hogsett and Zhang 2009, Wang *et al.* 2016). The generation of kinetic energy in the context of the global climate is discussed by Peixoto and Oort (1992, section 13.2).

The purpose of this paper is to reconcile the different interpretations of kinetic energy generation and to calculate the various terms in the kinetic energy budget from an

[1] Presumably Anthes meant $\partial p/\partial r > 0$.

idealized high-resolution numerical simulation of a tropical cyclone.

2. Kinetic energy equations

In its most basic form, the momentum equation may be written as

$$\frac{\partial \mathbf{u}}{\partial t} + \mathbf{u}\cdot\nabla\mathbf{u} + \mathbf{f}\wedge\mathbf{u} = -\frac{1}{\rho}\nabla p - g\mathbf{k} - \mathbf{F} \qquad (1)$$

where $\mathbf{u}$ is the three dimensional velocity vector, p is the pressure, ρ is the density, $\mathbf{F}$ is the frictional force opposing the motion, $\mathbf{f} = f\mathbf{k}$, f is the Coriolis parameter ($2\Omega\sin\phi$, where ϕ is latitude and Ω is the earth's rotation rate), g is the acceleration due to gravity, and $\mathbf{k}$ is the unit vector in the vertical direction (here and below, all vector quantities are in bold type). For simplicity, an f-plane is assumed (f = constant) and the Coriolis terms proportional to the cosine of the latitude have been neglected as is customary for geophysical flow analyses off of the equator (e.g., McWilliams 2011).

The kinetic energy equation is obtained by taking the scalar product Equation (1) with $\mathbf{u}$ using the identity $\mathbf{u}\cdot\nabla\mathbf{u} = \nabla(\frac{1}{2}\mathbf{u^2}) + \omega\wedge\mathbf{u}$, where $\omega = \nabla\wedge\mathbf{u}$ is the vorticity vector. This procedure gives:

$$\frac{\partial}{\partial t}(\tfrac{1}{2}\mathbf{u^2}) + \mathbf{u}\cdot\nabla(\tfrac{1}{2}\mathbf{u^2}) = -\frac{1}{\rho}\mathbf{u}\cdot\nabla p - gw - \mathbf{u}\cdot\mathbf{F}, \quad (2)$$

where $w = \mathbf{k}\cdot\mathbf{u}$ is the vertical component of velocity. Note that the Coriolis force ($-\mathbf{f}\wedge\mathbf{u}$) does not appear in the energy equation because it is orthogonal to $\mathbf{u}$.

An alternative form of the energy equation is obtained by removing some hydrostatically-balanced reference pressure, $p_{ref}(z)$, from (1), where $dp_{ref}/dz = -g\rho_{ref}$ defines a reference density, ρ_{ref}, that is a function of altitude z. Then, with the substitution $p = p_{ref}(z) + p'$ and $\rho = \rho_{ref}(z) + \rho'$, the first two terms on the right-hand-side of Equation (1), $-(1/\rho)\nabla p - g\mathbf{k}$, become $-(1/\rho)\nabla p' + b\mathbf{k}$, where $b = -g(\rho - \rho_{ref})/\rho$ is the buoyancy force of an air parcel per unit mass. Then, Equation (2) becomes

$$\frac{\partial}{\partial t}(\tfrac{1}{2}\mathbf{u^2}) + \mathbf{u}\cdot\nabla(\tfrac{1}{2}\mathbf{u^2}) = -\frac{1}{\rho}\mathbf{u_h}\cdot\nabla_h p' + Pw - \mathbf{u}\cdot\mathbf{F}, \quad (3)$$

where $\mathbf{u_h}$ is the horizontal velocity vector, ∇_h is the horizontal gradient operator and

$$P = -\frac{1}{\rho}\frac{\partial p}{\partial z} - g = -\frac{1}{\rho}\frac{\partial p'}{\partial z} + b \qquad (4)$$

is the net vertical perturbation gradient force per unit mass. Despite the explicit appearance of p' in the first term on the right-hand-side, all the terms in Equation (3) are independent of the reference pressure $p_{ref}(z)$, since, in particular, $\mathbf{u_h}\cdot\nabla_h p_{ref}(z) = 0$. For simplicity, we take $p_{ref}(z)$ and $\rho_{ref}(z)$ to be the ambient pressure and density, respectively, assuming that these are in hydrostatic equilibrium. Then p' vanishes at large distances from the vortex axis.

We examine now the different forms of Equation (3) derived by Anthes (1974), Gill (1982), and others beginning with a slight modification of Gill's formulation.

2.1. *Modified Gill's formulation*

In essence, Gill's formulation of the kinetic energy equation is as follows. Using the result that for any scalar field, γ,

$$\rho\frac{D\gamma}{Dt} = \frac{\partial}{\partial t}(\rho\gamma) + \nabla\cdot(\rho\gamma\mathbf{u}), \qquad (5)$$

where $D/Dt = \partial/\partial t + \mathbf{u}\cdot\nabla$ is the material derivative (see Gill 1982, Equation 4.3.6)[2], the material form of Equation (3) times ρ may be written in flux form as

$$\frac{\partial}{\partial t}(\tfrac{1}{2}\rho\mathbf{u^2}) + \nabla\cdot\mathbf{F_{KE}} = p'\nabla_h\cdot\mathbf{u_h} + \rho Pw + \frac{\partial(p'w)}{\partial z} - \rho\mathbf{u}\cdot\mathbf{F}, \qquad (6)$$

where

$$\mathbf{F_{KE}} = (p' + \tfrac{1}{2}\rho\mathbf{u^2})\mathbf{u}, \qquad (7)$$

is the *mechanical energy flux density vector* (Gill, 1982, cf. Equation 4.6.4).

The global kinetic energy budget can be obtained by integrating Equation (6) over a cylindrical volume of space, V, of radius R and height H centred on the storm and using the boundary conditions that $u = 0$ at $r = 0$, and $w = 0$ at $z = 0$ and $z = H$. Here, we use a cylindrical coordinate system (r, λ, z) centred on the vortex, where r is the radius, λ is the azimuth and z is the height. We denote an integral of the quantity χ over the volume V by

$$\overline{[\chi]} = \frac{1}{\pi R^2 H}\int_0^R r dr \int_0^{2\pi} d\lambda \int_0^H \chi dz$$

Then (6) becomes

MODIFIED GILL'S FORM

$$\frac{d}{dt}\overline{[\tfrac{1}{2}\rho\mathbf{u^2}]} = \overline{[p'\nabla_h\cdot\mathbf{u_h}]} + \overline{[\rho Pw]} - F_{KEG} - D, \qquad (8)$$

where

$$F_{KEG} = \frac{1}{\pi R^2 H}\int_0^{2\pi} d\lambda \int_0^H \left[u(p' + \tfrac{1}{2}\rho\mathbf{u^2})\right]_{r=R} dz, \qquad (9)$$

is the *flux of mechanical energy* through the side boundary $r = R$, and for a Newtonian fluid with dynamic viscosity coefficient μ,

$$D = \overline{[\mu\Phi_\nu]}, \qquad (10)$$

where, in cylindrical coordinates,

$$\Phi_\nu = 2\left[\left(\frac{\partial u}{\partial r}\right)^2 + \left(\frac{1}{r}\frac{\partial v}{\partial\lambda} + \frac{u}{r}\right)^2 + \left(\frac{\partial w}{\partial z}\right)^2\right] + \left[r\frac{\partial}{\partial r}\left(\frac{v}{r}\right) + \frac{1}{r}\frac{\partial u}{\partial\lambda}\right]^2 + \left[\frac{1}{r}\frac{\partial w}{\partial\lambda} + \frac{\partial v}{\partial z}\right]^2 + \left[\frac{\partial u}{\partial z} + \frac{\partial w}{\partial r}\right]^2 - \frac{2}{3}(\nabla\cdot\mathbf{u})^2 \qquad (11)$$

[2] If the density refers to that of a moist air parcel consisting of dry air, water vapour and liquid water, the density is conserved only if the liquid water component is suspended in the parcel. In the presence of precipitation, there will be a small source or sink of density associated with the flux divergence of falling precipitation. In what follows, we will ignore the effects of this source/sink term in the kinetic energy budget.

is the dissipation function[3]. Here, v is the tangential wind component.

Since $\nabla_h \cdot \mathbf{u_h}$ is the fractional change in the horizontal area of an air parcel per unit time, the first term on the right-hand-side of Equation (8) is the cumulative effect of the kinetic energy generated locally when an air parcel with positive perturbation pressure expands in the horizontal or one with a negative perturbation pressure contracts in the horizontal. The second term on the right-hand-side of this equation represents the rate of kinetic energy production by air rising in the presence of a positive net vertical perturbation pressure gradient force ($P > 0$) and air sinking in the presence of a negative net vertical perturbation pressure gradient force ($P < 0$). In Gill's original formulation, the net vertical perturbation pressure gradient force term in Equation (8) is replaced by a buoyancy force, which, by itself, is a non-unique force, and the second term on the right-hand-side is replaced by $\nabla \cdot \mathbf{u}$, which is the fractional change in volume of an air parcel. Note that, in Gill's formulation, there is no term corresponding with $u\partial p/\partial r$ (or equivalently $u\partial p'/\partial r$) in Anthes' formulation of the problem, which a number of authors have argued is the key term in generating kinetic energy.

2.2. *Generalized Anthes' formulation*

As noted above, Anthes reasonably supposes that the vertical velocity makes only a small contribution to the global kinetic energy and his derivation of the kinetic energy equation is based on the horizontal momentum equations only and the neglect of the contribution from $\frac{1}{2}w^2$ in the kinetic energy. Nevertheless, Anthes retains the vertical velocity component in the advection term $\mathbf{u} \cdot \nabla \mathbf{u}$ in Equation (1) and $\mathbf{u} \cdot \nabla(\frac{1}{2}\mathbf{u^2})$ in Equation (2). A slightly generalized form of Anthes' equation follows directly from ρ times Equation (3), which in flux form analogous to (6) is

$$\frac{\partial}{\partial t}(\tfrac{1}{2}\rho\mathbf{u^2}) + \nabla \cdot \mathbf{F_{KEA}} = -\mathbf{u_h} \cdot \nabla_h p' + \rho P w - \rho \mathbf{u} \cdot \mathbf{F}, \qquad (12)$$

where

$$\mathbf{F_{KEA}} = (\tfrac{1}{2}\rho\mathbf{u^2})\mathbf{u}. \qquad (13)$$

Again integrating over the cylinder, Equation (12) becomes

GENERALIZED ANTHES' FORM

$$\frac{d}{dt}\overline{[\tfrac{1}{2}\rho\mathbf{u^2}]} = -\overline{[\mathbf{u_h} \cdot \nabla_h p']} + \overline{[\rho P w]} - F_{KEA} - D, \qquad (14)$$

[3]Equation (8) is, in essence, the kinetic energy equation for the Reynolds averaged flow in which the quantity μ is a turbulent eddy counterpart. In this case, we are presuming that a K-theory closure is adequate so that the Reynolds averaged equations look essentially like the Newtonian fluid formulation. Further, in the mechanical energy flux through the side boundary in Equation (9) we have neglected the eddy diffusive radial flux of kinetic energy. Relative to the advective flux of kinetic energy, the diffusive flux scales as the inverse Reynolds number of the flow, which is always small compared to unity outside of the surface layer. This conclusion is based on recently obtained estimates of the turbulent eddy diffusivity observed in major hurricanes on the order of $50 - 100$ m^{2}s^{-1} (Zhang *et al.* 2011).

where

$$F_{KEA} = \frac{1}{\pi R^2 H}\int_0^{2\pi} d\lambda \int_0^H \left[u(\tfrac{1}{2}\rho\mathbf{u^2})\right]_{r=R} dz. \qquad (15)$$

Equation (14) is a generalization of Anthes' formulation to include the three-dimensional wind vector in the definition of kinetic energy and the rate of working of the net vertical perturbation gradient force per unit volume, $\overline{[\rho P w]}$, which is a non-hydrostatic effect. As in Anthes' original form, the pressure-work term, $-\overline{[\mathbf{u_h} \cdot \nabla_h p']}$, appears explicitly in the global form of the kinetic energy equation. For an axisymmetric flow, this term is simply $\overline{[-u\partial p/\partial r]}$ and, at first sight, one might question its prominence as a source of kinetic energy, since $\partial p/\partial r$ is *not* the only radial force acting on fluid parcels en route to the storm core. Above the frictional boundary layer, the radial pressure gradient is closely balanced by the sum of the centrifugal force and the radial component of the Coriolis force. Moreover, this source term does not appear in Gill's formulation (cf. Eq. (8)), although it is replaced by the term $\overline{[p'\nabla_h \cdot \mathbf{u_h}]}$ and the boundary flux terms are different. Even so, one should bear in mind that even in the axisymmetric case, $\overline{[-u\partial p/\partial r]}$ is generating *not only a radial contribution to the kinetic energy, but also an azimuthal contribution* through the action of the generalized Coriolis force $(f + v/r)u$. The generation of this azimuthal contribution is implicit in the kinetic energy equation as the generalized Coriolis force does no work, but it does convert radial momentum to tangential momentum.

3. Kinetic energy budget for an idealized simulation

We examine now the generation terms in the two forms of the kinetic energy equation for the case of an idealized tropical cyclone simulation. We begin with a brief description of the numerical model and go on to present the results.

3.1. *The numerical model*

The numerical model used for this study is Bryan's three-dimensional, nondydrostatic cloud model (CM1), version 16 (Bryan and Fritsch, 2002). The simulations relate to the prototype problem for tropical cyclone intensification, which considers the evolution of an initially axisymmetric, cloud-free, warm-cored, baroclinic vortex in a quiescent environment on an f-plane. The initial vortex is in thermal wind balance. A latitude of 20^{o}N and a constant sea surface temperature of 28^{o}C are assumed. The model configuration is more or less the same as described in section 2 of Črnivec *et al.* (2016). The differences are that, following the work of Mapes and Zuidema (1996), a more realistic time scale for Newtonian relaxation to the temperature field (10 days) is applied here instead of the previous default value in CM1 (12 h). Further, an open boundary condition is taken at lateral boundaries instead of rigid walls and the Dunion moist tropical sounding is used as the environmental sounding (Dunion 2011).

The initial tangential wind speed has a maximum of 15 m s^{-1} at the surface at a radius of 100 km. The tangential wind speed decreases sinusoidally with height, becoming zero at a height of 20 km. Above this height, up

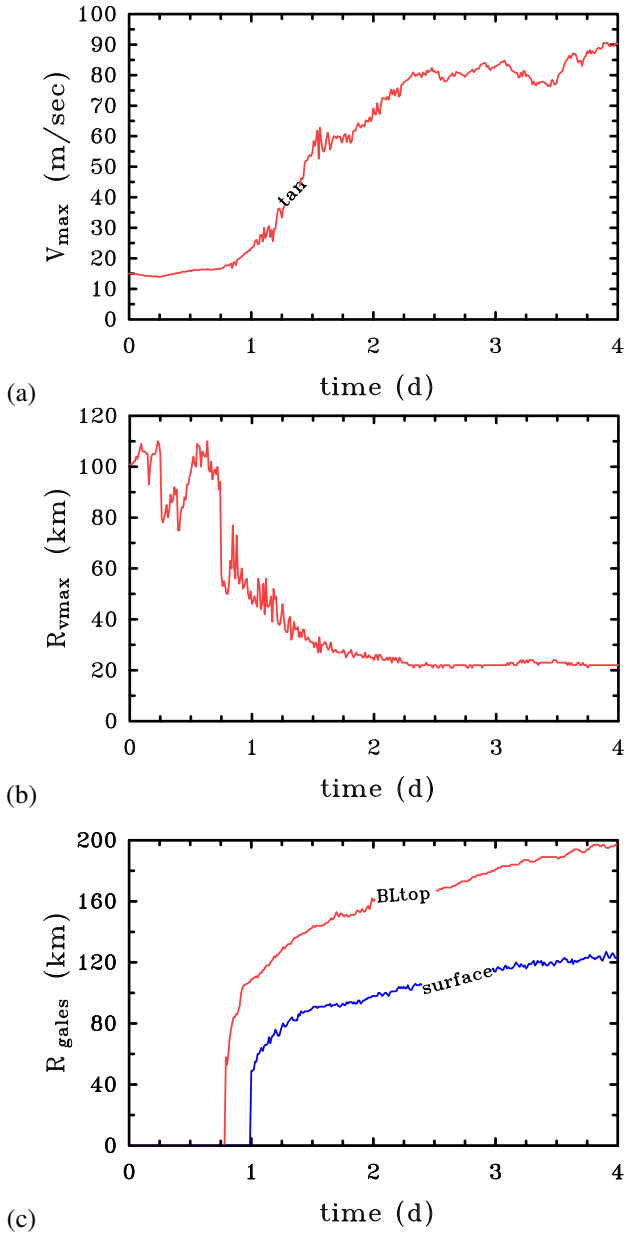

Figure 1. Time series of (a) maximum azimuthally-averaged tangential wind speed (V_{max}). Panel (b) shows the radius R_{vmax} at which the maximum tangential wind speed occurs (V_{max}). Panel (c) shows the radius at which gale force winds occurs (R_{gales}), where R_{gales} calculated at a height of 1 km, and corresponds to the radius of 17 m s^{-1} total winds outside the eyewall.

to 25 km, the tangential wind is set to zero. The balanced pressure, density and temperature fields consistent with this prescribed tangential wind distribution are obtained using the method described by Smith (2006). The calculations are carried out for a period of 4 days with data output every 15 min.

3.2. *A few details of the simulation*

Figure 1 summarizes the vortex evolution in the simulation. Panel (a) shows time series of the maximum azimuthally-averaged tangential wind speed, V_{max}, and panel (b) shows the radius R_{vmax} at which V_{max} occurs. Typically, V_{max} is located a few hundred meters above the surface, within a shallow inflow layer. The evolution is broadly similar to that described in Kilroy *et al.* (2016), who used a different numerical model and a much coarser horizontal resolution (horizontal grid spacing 5 km compared with 1 km used here). In brief, after a gestation for about a day during which deep convection becomes established inside R_{vmax}, the vortex undergoes a rapid intensification phase lasting about 36 h, before reaching a quasi-steady state. Initially R_{vmax} is located at a radius of 100 km, but contracts to a little more than 20 km after about $2\frac{1}{4}$ days. The most rapid contraction occurs during the rapid intensification phase as absolute angular momentum surfaces are drawn inwards quickly within and above the boundary layer.

Figure 1(c) shows the outermost radius of gale-force winds, R_{gales}, defined here as the radius of 17 m s^{-1} azimuthally-averaged tangential winds at a height of 1 km, which is approximately at the top of the frictional boundary layer. Shown also is R_{galesF}, defined as the (outer) radius at which the total wind speed at any grid point at a height of 10 m is 17 m s^{-1}. Both quantities serve as a measure of the vortex size, R_{galesF} being closest to the quantity used by forecasters[4], but R_{gales} being a preferred measure from a theoretical viewpoint (Kilroy *et al.* 2016). The evolution of storm size based on R_{galesF} is similar to that based on R_{gales}, although R_{gales} always exceeds the value of R_{galesF}. After 4 days, R_{gales} exceeds R_{galesF} by about 80 km.

Figure 2 shows vertical cross sections of the azimuthally-averaged, 3 h time averaged, radial and tangential velocity components, the vertical velocity component, and the M-surfaces during the intensification phase of the vortex. The time averages are centred on 36 h during the period of rapid intensification and at 60 h near the end of this period. The basic features of the flow are qualitatively similar at both times, but all three velocity components strengthen over the period, the M-surfaces moving inwards in the lower troposphere and outwards in the upper troposphere. The flow structure is similar to that which has been described in many previous studies (see e.g. the recent review by Montgomery and Smith 2017a and refs.) with a layer of strong shallow inflow marking the frictional boundary layer, a layer of weaker inflow in the lower troposphere, a region of strong outflow in the upper troposphere and a layer of enhanced inflow below the outflow. The maximum tangential wind speed occurs within, but near the top of the frictional boundary layer[5]. Much of the ascent occurs in an annular region on the order of 50-60 km in radius. The region inside this annulus shows mostly descent.

3.3. *Kinetic energy evolution*

Figure 3 shows time series of the domain-averaged kinetic energy per unit mass, $\overline{\left[\frac{1}{2}\rho\mathbf{u^2}\right]}$, for domain radii 300 km and 500 km and a domain height of 20 km. As anticipated by Anthes (1974), this quantity is dominated by the horizontal velocity components: in fact, the curves for $\overline{\left[\frac{1}{2}\rho\mathbf{u^2}\right]}$ and $\overline{\left[\frac{1}{2}\rho\mathbf{u_h^2}\right]}$ essentially overlap. It follows that the contribution of the vertical velocity to the global kinetic energy is

[4]Based on the wind speed in a particular sector and not azimuthally averaged.

[5]At 60 h, the tangential wind field exhibits a second local maximum in the eyewall. This is a transient feature that is presumably associated with a centrifugal wave near the base of the eyewall (e.g. Montgomery and Smith 2017, p550) excited by an elevated pulse of boundary layer outflow shortly before. This feature is not seen at 48 h or 72 h and its presence doesn't alter the findings concerning the kinetic energy budget.

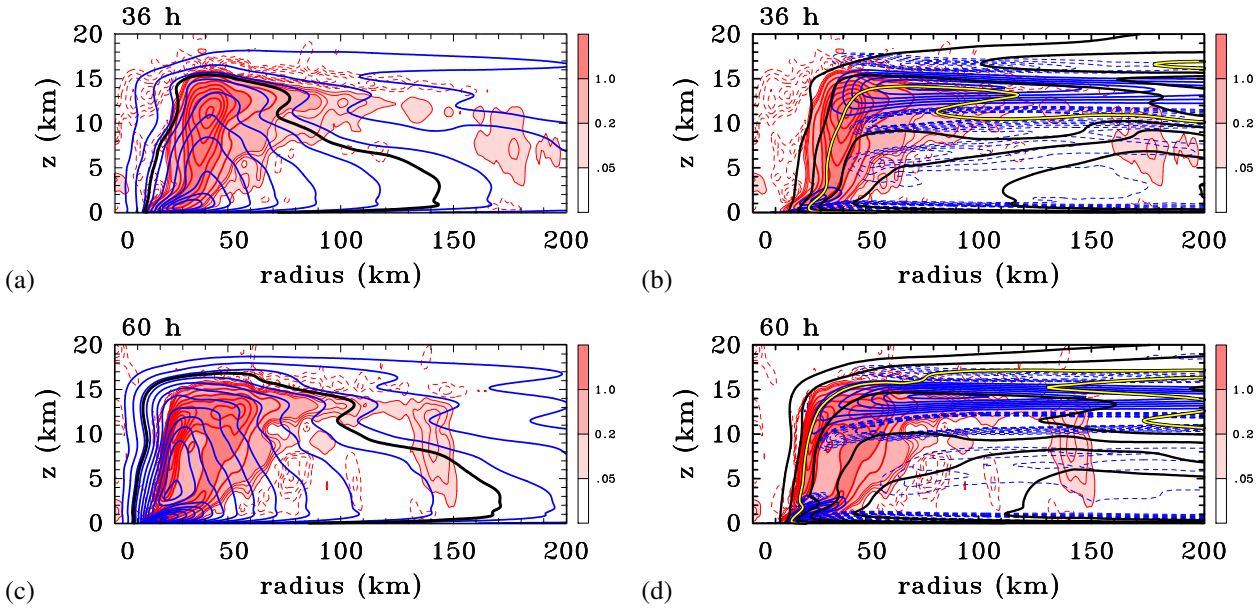

Figure 2. Left panels: Vertical cross sections of the azimuthally-averaged, 3 hour time averaged tangential velocity component (blue contours) centred at 36 h and 60 h. Superimposed are contours and shading of the averaged vertical velocity. Contour intervals are as follows. Tangential velocity: blue contours every 5 m s^{-1}, with a thick black contour highlighting the 17 m s^{-1} contour. Vertical velocity: thin red contours every 0.05 m s^{-1} to 0.2 m s^{-1}, thick red contour interval 0.5 m s^{-1}, thin dashed red contours indicate subsidence at intervals of 0.02 m s^{-1}. Right Panels: Vertical cross sections of the azimuthally-averaged, 3 hour time averaged radial velocity component together with the averaged vertical velocity centred at the same times. Contour intervals are as follows. Radial velocity: thick blue contours 4 m s^{-1}, dashed negative, thin blue dashed contours every 0.5 m s^{-1} down to -3.5 m s^{-1}. Absolute angular momentum: thick black contours every 2×10^5 m^2 s^{-1}, with the 6×10^5 m^2 s^{-1} contour highlighted in yellow.

negligible. Notable features of the curves for both domain sizes are the slight decrease during the first 12 h on account of surface friction, followed by a rapid increase as the vortex intensifies. As time proceeds, the rate of increase progressively declines.

3.4. *Kinetic energy generation: Anthes' formulation*

Figure 4 shows time series of the principal terms in the generalized Anthes formulation (the right-hand-side of Equation (14)), excluding only the global dissipation term since the focus of the paper is on kinetic energy generation. For both domain radii, 300 km (Fig. 4(a)) and 500 km (Fig. 4(a)), both the terms $\overline{[-\mathbf{u_h} \cdot \nabla_h p']}$ and $\overline{[\rho P w]}$ are positive[6], but, perhaps surprisingly, the former term is not appreciably larger than the latter, even beyond 2 days when the differences are largest. The boundary flux term F_{KEA} is virtually zero throughout the calculation. For the larger domain size (R = 500 km), the temporal behaviour of the various terms is similar, but, as expected, the magnitudes of the respective terms are appreciably smaller (Fig. 4(b)), since the largest contributions to the averages are from well inside a 300 km radius (note the different scales on the ordinate in Figs. 4(a) and 4(b)).

The finding that the two terms $\overline{[-\mathbf{u_h} \cdot \nabla_h p']}$ and $\overline{[\rho P w]}$ are not appreciably different in magnitude is at first sight surprising since, as shown in Figure 3, the contribution of the vertical velocity to the total kinetic energy is negligible. Moreover, the $\overline{[\rho P w]}$ term does not appear in Anthes' original formulation because the formulation was based on the horizontal momentum equations only. An explanation of this result is suggested by an examination of the radial-height structure of the azimuthally-averaged generation term before completing the columnar average, i.e. $< -\mathbf{u_h} \cdot \nabla_h p' >$, where the angle brackets denote an azimuthal average. The structure of this average together with those of the other generation term, $< \rho P w >$, at 36 h and 60 h, is shown in Figure 5. At both times, the Anthes generation term $< -\mathbf{u_h} \cdot \nabla_h p' >$ shows coherent regions of large kinetic energy generation and of large kinetic energy destruction. The main region of generation in panels (a) and (b) is at low levels, below about 2 km, where the strongest inflow occurs and where the inward directed radial pressure gradient force is particularly strong (panels (c) and (d) of Figure 5). There is a second region of generation in an annular column, mostly on the outer side of the eyewall updraught below about 9 km at 36 h and below about 12 km at 60 h. The generation terms in panels (a) and (b) are similar in structure and magnitude to that shown by Kurihara (1975, Figure 42, upper right) for a lower resolution axisymmetric simuulation.

Since the radial pressure gradient is positive at all heights [panels (c) and (d) of Figure 5], these generation regions must be ones in which there is generally inflow[7]. For the same reason, where there is outflow, there is kinetic energy removal as seen in the two principal coherent regions in panels (a) and (b) where $< -\mathbf{u_h} \cdot \nabla_h p' ><< 0$. It follows that the computed value of $\overline{[-\mathbf{u_h} \cdot \nabla_h p']}$ is the remainder resulting from the cancellation of two comparatively large contributions from $< \mathbf{u_h} \cdot \nabla_h p' >$ of opposite sign, namely $< -\mathbf{u_h} \cdot \nabla_h p' >_+$ and $< -\mathbf{u_h} \cdot \nabla_h p' >_-$, the former being the sum of all positive values of $-\mathbf{u_h} \cdot \nabla_h p'$ and the latter $< -\mathbf{u_h} \cdot \nabla_h p' >_-$ to be the sum

[6]The finite difference form of the vertical perturbation pressure gradient in calculating the term $\overline{[\rho P w]}$ is detailed in the appendix.

[7]Note that eddy effects are included in all generation terms.

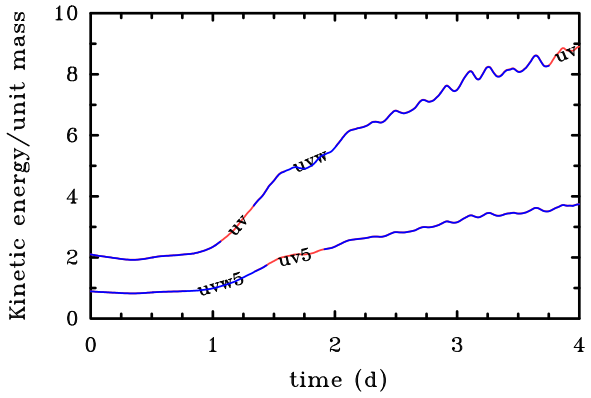

Figure 3. Time series of the left-hand-side of Equation 14, $\overline{[\frac{1}{2}\rho \mathbf{u^2}]}$ (curves labelled uvw) compared to $\overline{[\frac{1}{2}\rho \mathbf{u_h^2}]}$ (curves labelled uv) for cylinders of 300 km and 500 km. The curves for each cylinder size lie essentially on top of each other so that only a single curve is evident. The curves for the 500 km domain are labelled with a '5'.

of all negative values. This large cancellation is evident in the time series shown in Figure 4.

In summary, a substantial fraction of the kinetic energy that is generated is removed in regions where there is outflow and the residual is relatively small, comparable, indeed, with the kinetic energy generated by the rate-of-working of the net vertical perturbation pressure gradient force (buoyancy plus perturbation pressure gradient), principally in the region of diabatically-forced ascent. The structure of the net vertical perturbation pressure gradient force at 36 h and 60 h is shown in panels (e) and (f) of Figure 5. As expected, this force is concentrated in an annular region overlapping the region of diabatic heating.

3.5. *Kinetic energy generation (Gill's formulation)*

Figure 6 shows time series of the principal terms in the modified Gill formulation (the right-hand-side of Equation (8)), excluding again the global dissipation term. In this formulation, the term $\overline{[p'\nabla_h \cdot \mathbf{u_h}]}$ is positive with mean amplitude and fluctuations about this mean increasing with time during the 4 day calculation [Fig. 6(b)]. For the first day, the term is a little less than the $\overline{[\rho P w]}$ term, but thereafter becomes progressively larger. The increasing energy source represented by the sum of the two foregoing terms is opposed, in part, by the net outward flux of mechanical energy through the radial boundary, F_{KEG}.

Panels (c) and (d) of Figure 6 show the structure of the term $< p'\nabla_h \cdot \mathbf{u_h} >$, again 36 h and 60 h. The radial and vertical integral of this term form the cylindrical average $\overline{[p'\nabla_h \cdot \mathbf{u_h}]}$ in the modified Gill's formulation of the energy equation. The qualitative radius-height structure of $< p'\nabla_h \cdot \mathbf{u_h} >$ at the two times shown is less easy to infer from the solutions in Figure 2. Moreover, as shown in Figure 6, there is significant cancellation between the term $\overline{[p'\nabla_h \cdot \mathbf{u_h}]}$ and the boundary flux term in Gill's formulation [Equation (8)]. For this reason, the Anthes' formulation of the energy equation would seem to be preferable to Gill's formulation, even though both formulations are correct and give the same tendency of kinetic energy over the control volume of integration (see next subsection).

3.6. *Total kinetic energy generation*

A check on the foregoing calculations is provided by calculating the total tendency of kinetic energy generation, which is the sum of all the terms on the right-hand-side of Equations (8) or (14). This sum should be the same for each formulation. That this is the case is verified in Figure 7, which shows the sum for each domain size. As expected, the curves for the two formulations are coincident.

4. Discussion

Anthes' statement noted in the Introduction that "the important source of kinetic energy production in the hurricane is the radial flow toward lower pressure in the inflow layer, represented by $-u\partial p/\partial r$" may seem at first sight problematic because, above the boundary layer, the radial pressure gradient is very closely in balance with sum of centrifugal and Coriolis forces. Thus the energy source associated with $-u\partial p/\partial r$ might appear, at least at first sight, to be a gross overestimate. However, the kinetic energy equation doesn't recognize the balance constraint and, in this equation, the radial pressure gradient acts to generate not only kinetic energy of radial motion, but also that of tangential motion through the action of the generalized Coriolis force $(f + v/r)u$, a term that appears in the tangential momentum equation in cylindrical coordinates. This is despite the fact that the generalized Coriolis force does not appear explicitly in the kinetic energy equation.

As noted also in the Introduction, Anthes recognized that much of the inflow into the storm is " ... a result of surface friction, which reduces the tangential wind speed and thereby destroys the gradient balance, so that the inward pressure gradient force exceeds the Coriolis and centripetal[8] forces" and he pointed out that "In the warm core low the maximum pressure gradient ($-\partial p/\partial r < 0$ [sign corrected: our insertion]) occurs at the lowest level, at which the inflow ($u < 0$) is maximum. In the outflow layer, where the radial flow is reversed, the pressure gradient is much weaker. The result is a net production of kinetic energy, dominated by the contribution from the inflow region". While this view is broadly supported by the calculations presented herein, the calculations provide a sharper view of the *net* production of kinetic energy indicating a region of significant kinetic energy generation accompanying inflow *throughout* the lower troposphere above the boundary layer as well as significant regions where kinetic energy is consumed as air flows outwards, against the radial pressure gradient, above the boundary layer. Indeed, the generation above the boundary layer is a manifestation of spin up by the classical mechanism articulated by Ooyama (1969), while the generation within the boundary layer, highlighted by Anthes, is a manifestation of the nonlinear boundary layer spin up mechanism articulated by Smith and Vogl (2008), Smith *et al.* (2009), Smith and Montgomery (2016) and Montgomery and Smith (2017b).

Anthes argues that the boundary layer " ... must be responsible for a net gain of kinetic energy" even though "a substantial dissipation of kinetic energy in the hurricane occurs in the boundary layer through turbulent diffusion and ultimate loss of energy to the sea surface". As a result, he

[8]Presumably, Anthes means the centrifugal force.

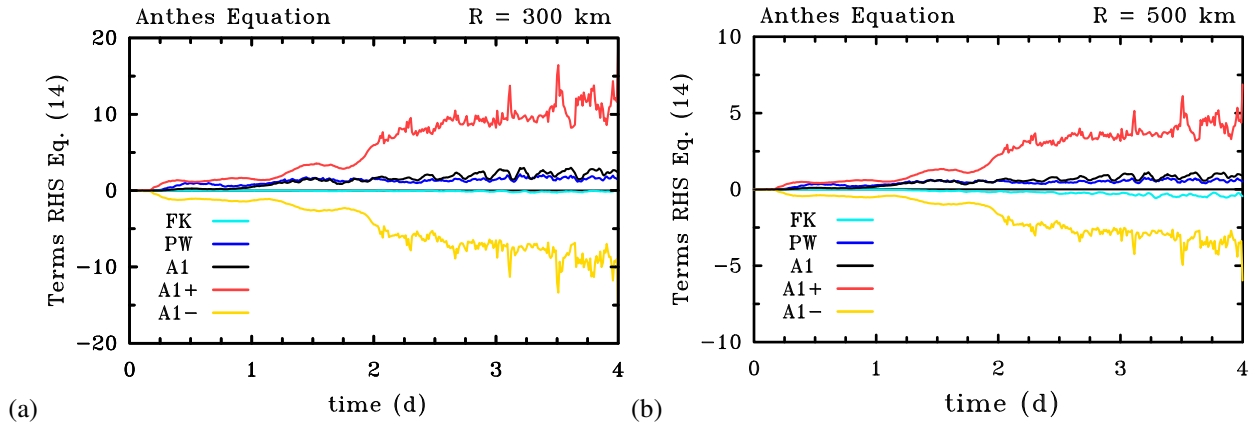

Figure 4. Time series of the kinetic energy tendency terms on the right-hand-side of Equation (14), the Anthes' formulation, averaged over a cylinder of size (a) 300 km and (b) 500 km. Units on the ordinate are 10^{-3} W m^{-3}. The dissipation term is not shown. A1 stands for $\overline{[-\mathbf{u_h} \cdot \nabla_h p']}$, FK for F_{KEA} and PW for $\overline{[\rho P w]}$. A1+ and A1- stand for the contributions to A1 from regions where the argument $-\mathbf{u_h} \cdot \nabla_h p'$ is positive and negative, respectively.

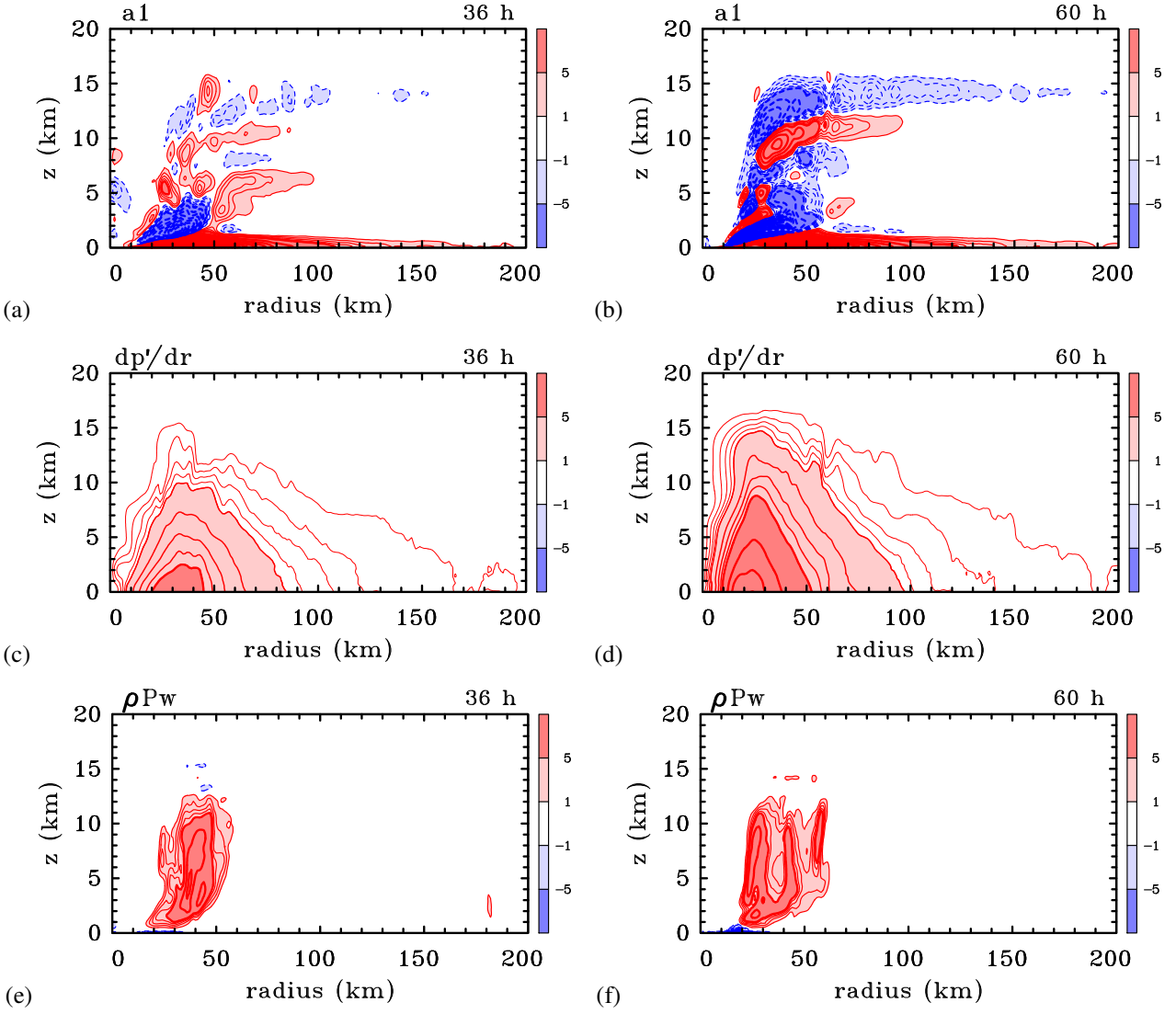

Figure 5. Radius-height cross sections of azimuthally-averaged quantities in Equation (14), before performing the columnar average: $< -\mathbf{u_h} \cdot \nabla_h p' >$ (panels (a), (b)); and $< \rho P w >$ (panels (e), (f)), at 36 h (left panels) and 60 h (right panels). Panels (c) and (d) show similar cross sections of $< \partial p'/\partial r >$ at these times. Contour intervals are as follows. Panels (a), (b), (e) and (f): thick contours 5×10^{-2} W m^{-3}: thin contours 1×10^{-2} W m^{-3}. Solid red contours positive, dashed blue contours negative. Panels (c) and (d): thin contours 0.2×10^{-2} Pa m^{-1} to 0.8×10^{-2} Pa m^{-1}; medium thick contours 1.0×10^{-2} Pa m^{-1} to 5.0×10^{-2} Pa m^{-1}; thick contours every 5.0×10^{-2} Pa m^{-1}. Numbers indicated on the side bar should be multiplied by 10^{-2}.

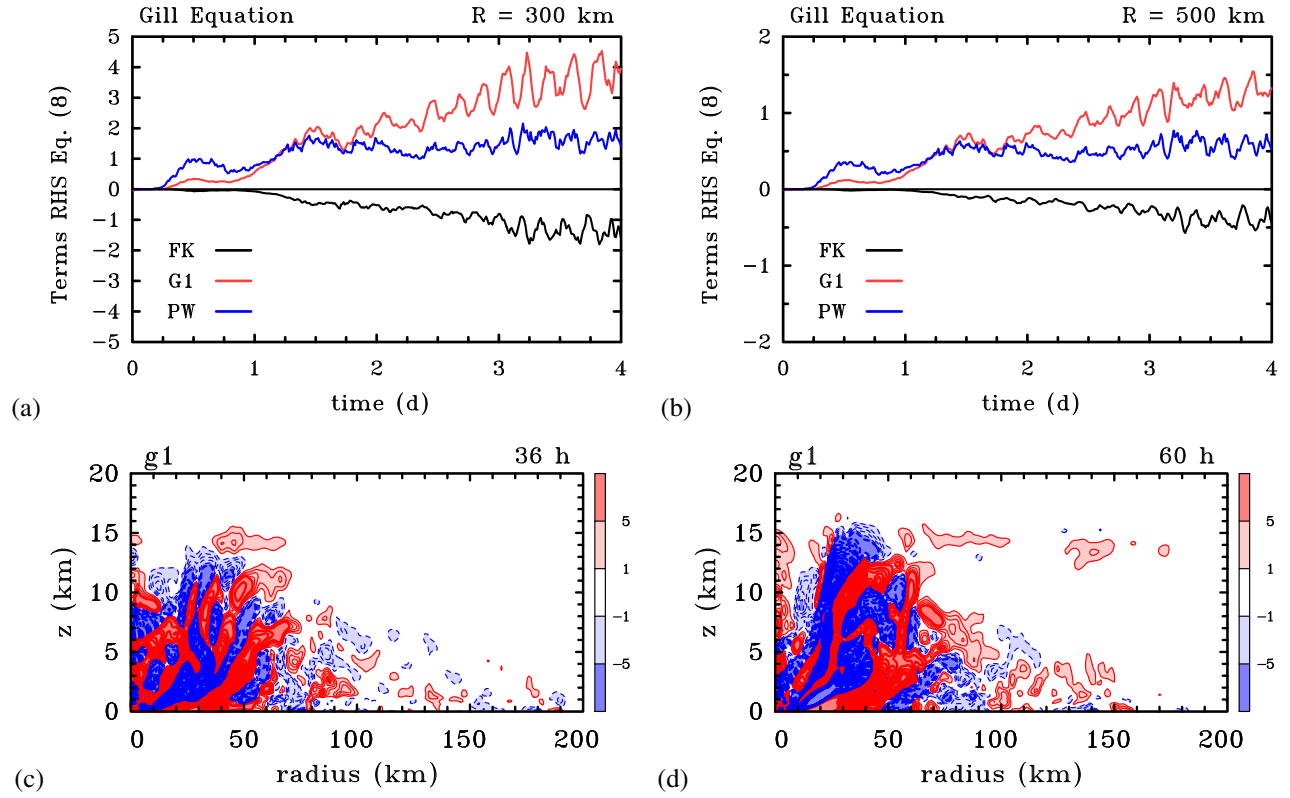

Figure 6. Time series of the kinetic energy tendency terms: $\overline{[p'\nabla_h \cdot \mathbf{u_h}]}$ (denoted by G1); $\overline{[\rho Pw]}$ (denoted PW) and F_{KEG} (denoted FK) in the modified Gill formulation [Equation (8) averaged over a cylinder of size (a) 300 km and (b) 500 km. Units on the ordinate are 10^{-3} W m^{-3}. Panels (c) and (d) show the azimuthally averaged terms $< p'\nabla_h \cdot \mathbf{u_h} >$ in Equation (8) at 36 h and 60 h, respectively. Contour intervals are: thick contours 5×10^{-2} W m^{-3}: thin contours 1×10^{-2} W m^{-3}. Solid red contours positive, dashed blue contours negative. Numbers indicated on the side bar should be multiplied by 10^{-2}.

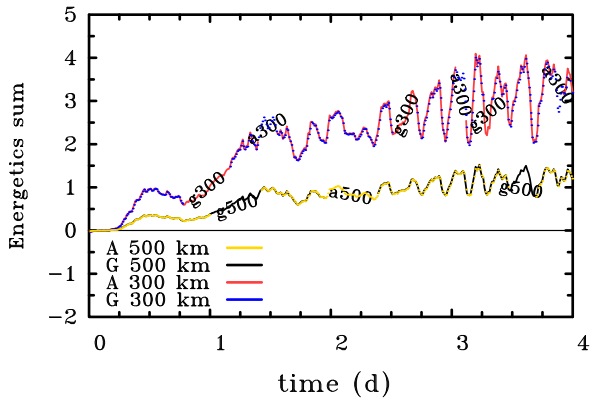

Figure 7. Sum of the terms for Gill's and Anthes' formulation excluding the dissipation term for cylinders of radius $R = 300$ km and 500 km. Values on the ordinate have been multiplied by 10^3 for plotting purposes. The two curves for each value of R lie essentially on top of each other.

is led to the paradox that "surface friction is responsible for a net increase in kinetic energy and without friction the hurricane could not exist." The resolution of this paradox would appear to be Anthes' de-emphasis of the role of the classical mechanism for spin up in the kinetic energy budget.

The results of our study, especially the noted cancellation of relatively large generation and consumption contributions to the term $\overline{[-\mathbf{u_h} \cdot \nabla_h p']}$ points to limitations in the utility of a global kinetic energy budget in revealing the underlying dynamics of tropical cyclone intensification. An alternative approach would be to examine the energetics of individual air parcels as they move around some hypothetical circuit (see Emanuel (2004) and references), but this approach relies on assumptions about the circuits traversed, circuits that may or may not be realizable in reality.

5. Conclusions

We have re-examined the traditional theory for kinetic energy generation in a tropical cyclone used by Palmén and Jordan (1955), Palmén and Riehl (1957), Frank (1977), Hogsett and Zhang (2009) and succinctly summarized in the review article by Anthes (1974). We have compared this with an alternative interpretation of global kinetic energy generation in geophysical flows inspired by Gill (1982), noting that such interpretations are non-unique.

We have shown that the *net* rate of production of kinetic energy is a comparatively small difference between the generation in regions of inflow and the magnitude of the consumption in regions of outflow, so much so, that this difference is comparable in magnitude with the rate of generation by the net vertical perturbation pressure gradient force. The latter effect was not contained in Anthes' original formulation, which was based only on the horizontal momentum equations.

We pointed out that the kinetic energy generation term in Anthes' formulation involving the radial pressure gradient does not appear in Gill's formulation of the kinetic energy equation or our modification thereof. It is replaced by a term comprising the global integral of the rate of working by perturbation pressure ($\overline{[p'\nabla_h \cdot \mathbf{u_h}]}$) as the flow expands in the horizontal. However, this generation term is largely

compensated in the modified Gill formulation by the boundary flux of mechanical energy (F_{KEG}). The fact that the boundary flux of kinetic energy in the Anthes formulation (F_{KEA}) is typically negligible, as well as the difficulty in anticipating the structure of the term $\overline{[p'\nabla_h \cdot \mathbf{u_h}]}$ in a tropical cyclone are factors weighing in favour of using Anthes' formulation when applied to the generation of kinetic energy in a tropical cyclone. However, in the light of the large cancellation of positive and negative values in the radial pressure-work term, the contribution from the rate of working of the net vertical force is non-negligible in comparison and should be included in any global kinetic energy budget.

While global energetics provide a constraint on flow evolution, we have shown in the context of the kinetic energy equation that they conceal important aspects of energy generation and consumption. This finding highlights the limitations of a global kinetic energy budget in revealing the underlying dynamics of tropical cyclones.

6. Acknowledgements

We thank Drs. Chris Landsea, Anastassia Makarieva and an anonymous reviewer for their perceptive comments on the original manuscript. GK and RKS acknowledge financial support for tropical cyclone research from the Office of Naval Research Global under Grant No. N62909-15-1-N021. MTM acknowledges the support of NSF grant AGS-1313948, NOAA HFIP grant N0017315WR00048, NASA grant NNG11PK021, ONR grant N0001417WX00336, and the U. S. Naval Postgraduate School.

7. Appendix: Calculation of the net vertical force, P

The net vertical force per unit mass, P, defined in Equation (4) and used to construct Figures 5(e) and 5(f) was first calculated on the stretched model grid at the levels where thermodynamic quantities are defined. The vertical perturbation pressure gradient was determined by fitting a quadratic function to three successive levels z_{i-1}, z_i and z_{i+1} at which the perturbation pressure has values p'_{i-1}, p'_i and p'_{i+1}, respectively. Then

$$\left(\frac{\partial p'}{\partial z}\right)_i = \frac{(p'_{i+1}-p'_i)dz_i^2 - (p'_{i-1}-p'_i)dz_{i+1}^2}{dz_{i+1}dz_i(z_{i+1}-z_{i-1})} \qquad (16)$$

where $dz_i = z_i - z_{i-1}$.

8. References

Anthes RA. 1974. The dynamics and energetics of mature tropical cyclones. *Rev. Geophys. Space Phys*,**12**: 495-522

Bryan GH, Fritsch JM. 2002. A benchmark simulation for moist nonhydrostatic numerical models. *Mon. Weather Rev.*, bf 130: 29172928.

Črnivec N, Smith RK, Kilroy G. 2016. Dependence of tropical cyclone intensification rate on sea surface temperature. *Q. J. R. Meteorol. Soc.*, **142**: 1618-1627.

DiMego GJ, Bosart LF. 1982. The transformation of tropical storm Agnes into an extratropical cyclone. Part II: Moisture, vorticity and kinetic energy budgets. *Mon. Weather Rev.*, bf 110: 412-433.

Dunion JP. 2011. Rewriting the climatology of the tropical North Atlantic and Carribean sea atmosphere. *J. Clim*, **24**: 893908.

Emanuel K. 2004. Tropical cyclone energetics and structure. In *Atmospheric turbulence and mesoscale meteorology*, E. Fedorovich, R. Rotunno and B. Stevens, editors, Cambridge University Press, pp280.

Frank WM. 1977. The structure and energetics of the tropical cyclone ll. Dynamics and energetics. *Mon. Weather Rev.*, **105**: 1136-1160.

Gill AE. 1982. *Atmosphere-Ocean Dynamics*. New York: Academic. 4th ed., 662pp

Hogsett W, Zhang D-L. 2009. Numerical simulation of Hurricane Bonnie (1998). Part III: Energetics. *J. Atmos. Sci.*, **66**: 2678-2696.

Kilroy G, Smith RK, Montgomery MT. 2016. Why do model tropical cyclones grow progressively in size and decay in intensity after reaching maturity? *J. Atmos. Sci.*, **73**: 487-503.

Kurihara Y. 1975. 1975: Budget analysis of a tropical cyclone simulated in an axisymmetric numerical model. *J. Atmos. Sci.*, , **32**: 25-59.

McWilliams JC. 2011. *Fundamentals of geophysical fluid dynamics*. Cambridge University Press, 283pp.

Mapes BE, Zuidema P. 1996: Radiative-dynamical consequences of dry tongues in the tropical troposphere. *J. Atmos. Sci.*, **53**: 620-638.

Montgomery MT, Smith RK. 2017a: Recent developments in the fluid dynamics of tropical cyclones. *Annu. Rev. Fluid Mech.*, **49**: 1-33, doi:10.1146/annurev-fluid-010816-060022.

Montgomery MT, Smith RK. 2017b: On the applicability of linear, axisymmetric dynamics in intensifying and mature tropical cyclones. *Fluids*, **2**: 69. doi:10.3390/fluids2040069.

Ooyama K. 1969: Numerical simulation of the life-cycle of tropical cyclones. *J. Atmos. Sci.*, **26**: 3-40.

Palmén E, Jordan CL. 1955. Note on the release of kinetic energy in tropical cyclones. *Tellus*, **7**: 186-189.

Palmén E, Riehl H. 1957. Budget of angular momentum and energy in tropical storms. *J. Meteor.*, **14**: 150-159.

Peixoto JP, Oort AH. 1992 *Physics of climate*. American Institute of Physics, New York, p 520.

Smith RK. 2006. Accurate determination of a balanced axisymmetric vortex. *Tellus*, **58A**: 98-103.

Smith RK, Vogl S, 2008: A simple model of the hurricane boundary layer revisited. *Q. J. R. Meteorol. Soc.*, **134**: 337-351.

Smith RK, Montgomery MT, 2016: The efficiency of diabatic heating and tropical cyclone intensification. *Q. J. R. Meteorol. Soc.*, **142**: 2081-2086.

Smith RK Montgomery MT Nguyen SV. 2009: Tropical cyclone spin up revisited. *Q. J. R. Meteorol. Soc.*, **135**: 1321-1335.

Tuleya RE, Kurihra Y. 1975. The energy and angular momentum budgets of a three-dimensional tropical cyclone model. *J. Atmos. Sci.*, **32**: 287-301.

Wang Y, Cui X, Li, X, Zhang W, Huang Y. 2016. Kinetic energy budget during the genesis period of Tropical Cyclone Durian (2001) in the South China Sea. *Mon. Weather Rev.*, **144**: 2831-854.

Zhang JA Rogers RF Nolan DS and Marks FD 2011: On the characteristic height scales of the hurricane boundary layer. *Mon. Weather Rev.*, **139**: 2523-2535.

Quarterly Journal of the Royal Meteorological Society *Q. J. R. Meteorol. Soc.* **144: 1–9 (2018)**

The generation of kinetic energy in tropical cyclones revisited

Roger K. Smith[a]*, Michael T. Montgomery[b] and Gerard Kilroy[a]
[a] *Meteorological Institute, Ludwig Maximilians University of Munich, Munich, Germany*
[b] *Dept. of Meteorology, Naval Postgraduate School, Monterey, CA*
*Correspondence to: Prof. Roger K. Smith, Meteorological Institute, Ludwig-Maximilians University of Munich, Theresienstr. 37, 80333 Munich, Germany. E-mail: roger.smith@lmu.de

Many previous diagnoses of the global kinetic energy for a tropical cyclone have given prominence to a global integral of a pressure-work term in the generation of kinetic energy. However, in his erudite textbook of atmospheric and oceanic dynamics, Gill (1982) derives a form of the kinetic energy equation in which there is no such explicit source term. In this paper we revisit the interpretations of the generation of kinetic energy given previously in the light of Gill's analysis and compare the various interpretations, which are non-unique.
Further, even though global energetics provide a constraint on the flow evolution, in the context of the kinetic energy equation, they conceal important aspects of energy generation and consumption, a finding that highlights the limitations of a global kinetic energy budget in revealing the underlying dynamics of tropical cyclones.

Key Words: Tropical cyclone, hurricane, typhoon, spin-up, energetics

Received May 17, 2018; Revised ; Accepted

Citation: . . .

1. Introduction

In a classical review paper, Anthes (1974, section DI) summarized the global energetics of tropical cyclones, based in part on the work of Palmén and Jordan (1955) and Palmén and Riehl (1957). In this review he argues that the kinetic energy is dominated by the horizontal velocity components and he derives an expression for the rate-of-generation of kinetic energy, showing that "The important source of kinetic energy production in the hurricane is the radial flow toward lower pressure in the inflow layer, represented by $u\partial p/\partial r$." (Here u is the radial velocity component, r is the radius and p is the pressure). In a similar vein, Palmén and Riehl *op. cit.* note that "the generation depends on the vertical correlation between radial flow component and pressure gradient which, for production of kinetic energy, must be positive, i.e., the strongest inflow must occur at the strongest inward directed pressure gradient. They conclude that "kinetic energy production within the cyclone can take place only if the cyclone is of the warm core type." Anthes goes on to argue that "This inflow is a result of surface friction, which reduces the tangential wind speed and thereby destroys the gradient balance, so that the inward pressure gradient force exceeds the Coriolis and centripetal forces. In the warm core low the maximum pressure gradient ($\partial p/\partial r < 0$)[1] occurs just above the surface layer, at which the inflow ($u < 0$) is maximum in magnitude. In the outflow layer, where the radial flow is reversed, the pressure gradient is much weaker. The result is a net production of kinetic energy, dominated by the contribution from the inflow region."

The foregoing interpretations seem at odds with the kinetic energy equation in flux form presented by Gill (1982) in which the term $-u\partial p/\partial r$ does not appear. Nevertheless, in the context of tropical cyclones, subsequent work has built on the formulation by Palmén and Riehl as reviewed by Anthes (e.g. Kurihara 1975, Tuleya and Kurihara 1975, Frank 1977, DiMego and Bosart 1982, Hogsett and Zhang 2009, Wang *et al.* 2016). The generation of kinetic energy in the context of the global climate is discussed by Peixoto and Oort (1992, section 13.2).

The purpose of this paper is to reconcile the different interpretations of kinetic energy generation and to calculate the various terms in the kinetic energy budget from an

[1] Presumably Anthes meant $\partial p/\partial r > 0$.

idealized high-resolution numerical simulation of a tropical cyclone.

2. Kinetic energy equations

In its most basic form, the momentum equation may be written as

$$\frac{\partial \mathbf{u}}{\partial t} + \mathbf{u}\cdot\nabla\mathbf{u} + \mathbf{f}\wedge\mathbf{u} = -\frac{1}{\rho}\nabla p - g\mathbf{k} - \mathbf{F} \qquad (1)$$

where $\mathbf{u}$ is the three dimensional velocity vector, p is the pressure, ρ is the density, $\mathbf{F}$ is the frictional force opposing the motion, $\mathbf{f} = f\mathbf{k}$, f is the Coriolis parameter ($2\Omega\sin\phi$, where ϕ is latitude and Ω is the earth's rotation rate), g is the acceleration due to gravity, and $\mathbf{k}$ is the unit vector in the vertical direction (here and below, all vector quantities are in bold type). For simplicity, an f-plane is assumed (f = constant) and the Coriolis terms proportional to the cosine of the latitude have been neglected as is customary for geophysical flow analyses off of the equator (e.g., McWilliams 2011).

The kinetic energy equation is obtained by taking the scalar product Equation (1) with $\mathbf{u}$ using the identity $\mathbf{u}\cdot\nabla\mathbf{u} = \nabla(\frac{1}{2}\mathbf{u^2}) + \omega\wedge\mathbf{u}$, where $\omega = \nabla\wedge\mathbf{u}$ is the vorticity vector. This procedure gives:

$$\frac{\partial}{\partial t}(\tfrac{1}{2}\mathbf{u^2}) + \mathbf{u}\cdot\nabla(\tfrac{1}{2}\mathbf{u^2}) = -\frac{1}{\rho}\mathbf{u}\cdot\nabla p - gw - \mathbf{u}\cdot\mathbf{F}, \quad (2)$$

where $w = \mathbf{k}\cdot\mathbf{u}$ is the vertical component of velocity. Note that the Coriolis force ($-\mathbf{f}\wedge\mathbf{u}$) does not appear in the energy equation because it is orthogonal to $\mathbf{u}$.

An alternative form of the energy equation is obtained by removing some hydrostatically-balanced reference pressure, $p_{ref}(z)$, from (1), where $dp_{ref}/dz = -g\rho_{ref}$ defines a reference density, ρ_{ref}, that is a function of altitude z. Then, with the substitution $p = p_{ref}(z) + p'$ and $\rho = \rho_{ref}(z) + \rho'$, the first two terms on the right-hand-side of Equation (1), $-(1/\rho)\nabla p - g\mathbf{k}$, become $-(1/\rho)\nabla p' + b\mathbf{k}$, where $b = -g(\rho - \rho_{ref})/\rho$ is the buoyancy force of an air parcel per unit mass. Then, Equation (2) becomes

$$\frac{\partial}{\partial t}(\tfrac{1}{2}\mathbf{u^2}) + \mathbf{u}\cdot\nabla(\tfrac{1}{2}\mathbf{u^2}) = -\frac{1}{\rho}\mathbf{u_h}\cdot\nabla_h p' + Pw - \mathbf{u}\cdot\mathbf{F}, \quad (3)$$

where $\mathbf{u_h}$ is the horizontal velocity vector, ∇_h is the horizontal gradient operator and

$$P = -\frac{1}{\rho}\frac{\partial p}{\partial z} - g = -\frac{1}{\rho}\frac{\partial p'}{\partial z} + b \qquad (4)$$

is the net vertical perturbation gradient force per unit mass. Despite the explicit appearance of p' in the first term on the right-hand-side, all the terms in Equation (3) are independent of the reference pressure $p_{ref}(z)$, since, in particular, $\mathbf{u_h}\cdot\nabla_h p_{ref}(z) = 0$. For simplicity, we take $p_{ref}(z)$ and $\rho_{ref}(z)$ to be the ambient pressure and density, respectively, assuming that these are in hydrostatic equilibrium. Then p' vanishes at large distances from the vortex axis.

We examine now the different forms of Equation (3) derived by Anthes (1974), Gill (1982), and others beginning with a slight modification of Gill's formulation.

2.1. *Modified Gill's formulation*

In essence, Gill's formulation of the kinetic energy equation is as follows. Using the result that for any scalar field, γ,

$$\rho\frac{D\gamma}{Dt} = \frac{\partial}{\partial t}(\rho\gamma) + \nabla\cdot(\rho\gamma\mathbf{u}), \qquad (5)$$

where $D/Dt = \partial/\partial t + \mathbf{u}\cdot\nabla$ is the material derivative (see Gill 1982, Equation 4.3.6)[2], the material form of Equation (3) times ρ may be written in flux form as

$$\frac{\partial}{\partial t}(\tfrac{1}{2}\rho\mathbf{u^2}) + \nabla\cdot\mathbf{F_{KE}} = p'\nabla_h\cdot\mathbf{u_h} + \rho Pw + \frac{\partial(p'w)}{\partial z} - \rho\mathbf{u}\cdot\mathbf{F}, \qquad (6)$$

where

$$\mathbf{F_{KE}} = (p' + \tfrac{1}{2}\rho\mathbf{u^2})\mathbf{u}, \qquad (7)$$

is the *mechanical energy flux density vector* (Gill, 1982, cf. Equation 4.6.4).

The global kinetic energy budget can be obtained by integrating Equation (6) over a cylindrical volume of space, V, of radius R and height H centred on the storm and using the boundary conditions that $u = 0$ at $r = 0$, and $w = 0$ at $z = 0$ and $z = H$. Here, we use a cylindrical coordinate system (r, λ, z) centred on the vortex, where r is the radius, λ is the azimuth and z is the height. We denote an integral of the quantity χ over the volume V by

$$\overline{[\chi]} = \frac{1}{\pi R^2 H}\int_0^R r dr \int_0^{2\pi} d\lambda \int_0^H \chi dz$$

Then (6) becomes

MODIFIED GILL'S FORM

$$\frac{d}{dt}\overline{[\tfrac{1}{2}\rho\mathbf{u^2}]} = \overline{[p'\nabla_h\cdot\mathbf{u_h}]} + \overline{[\rho Pw]} - F_{KEG} - D, \qquad (8)$$

where

$$F_{KEG} = \frac{1}{\pi R^2 H}\int_0^{2\pi} d\lambda \int_0^H \left[u(p' + \tfrac{1}{2}\rho\mathbf{u^2})\right]_{r=R} dz, \qquad (9)$$

is the *flux of mechanical energy* through the side boundary $r = R$, and for a Newtonian fluid with dynamic viscosity coefficient μ,

$$D = \overline{[\mu\Phi_\nu]}, \qquad (10)$$

where, in cylindrical coordinates,

$$\Phi_\nu = 2\left[\left(\frac{\partial u}{\partial r}\right)^2 + \left(\frac{1}{r}\frac{\partial v}{\partial\lambda} + \frac{u}{r}\right)^2 + \left(\frac{\partial w}{\partial z}\right)^2\right] + \left[r\frac{\partial}{\partial r}\left(\frac{v}{r}\right) + \frac{1}{r}\frac{\partial u}{\partial\lambda}\right]^2 + \left[\frac{1}{r}\frac{\partial w}{\partial\lambda} + \frac{\partial v}{\partial z}\right]^2 + \left[\frac{\partial u}{\partial z} + \frac{\partial w}{\partial r}\right]^2 - \frac{2}{3}(\nabla\cdot\mathbf{u})^2 \qquad (11)$$

[2] If the density refers to that of a moist air parcel consisting of dry air, water vapour and liquid water, the density is conserved only if the liquid water component is suspended in the parcel. In the presence of precipitation, there will be a small source or sink of density associated with the flux divergence of falling precipitation. In what follows, we will ignore the effects of this source/sink term in the kinetic energy budget.

is the dissipation function[3]. Here, v is the tangential wind component.

Since $\nabla_h \cdot \mathbf{u_h}$ is the fractional change in the horizontal area of an air parcel per unit time, the first term on the right-hand-side of Equation (8) is the cumulative effect of the kinetic energy generated locally when an air parcel with positive perturbation pressure expands in the horizontal or one with a negative perturbation pressure contracts in the horizontal. The second term on the right-hand-side of this equation represents the rate of kinetic energy production by air rising in the presence of a positive net vertical perturbation pressure gradient force ($P > 0$) and air sinking in the presence of a negative net vertical perturbation pressure gradient force ($P < 0$). In Gill's original formulation, the net vertical perturbation pressure gradient force term in Equation (8) is replaced by a buoyancy force, which, by itself, is a non-unique force, and the second term on the right-hand-side is replaced by $\nabla \cdot \mathbf{u}$, which is the fractional change in volume of an air parcel. Note that, in Gill's formulation, there is no term corresponding with $u\partial p/\partial r$ (or equivalently $u\partial p'/\partial r$) in Anthes' formulation of the problem, which a number of authors have argued is the key term in generating kinetic energy.

2.2. *Generalized Anthes' formulation*

As noted above, Anthes reasonably supposes that the vertical velocity makes only a small contribution to the global kinetic energy and his derivation of the kinetic energy equation is based on the horizontal momentum equations only and the neglect of the contribution from $\frac{1}{2}w^2$ in the kinetic energy. Nevertheless, Anthes retains the vertical velocity component in the advection term $\mathbf{u} \cdot \nabla \mathbf{u}$ in Equation (1) and $\mathbf{u} \cdot \nabla(\frac{1}{2}\mathbf{u^2})$ in Equation (2). A slightly generalized form of Anthes' equation follows directly from ρ times Equation (3), which in flux form analogous to (6) is

$$\frac{\partial}{\partial t}(\tfrac{1}{2}\rho\mathbf{u^2}) + \nabla \cdot \mathbf{F_{KEA}} = -\mathbf{u_h} \cdot \nabla_h p' + \rho P w - \rho \mathbf{u} \cdot \mathbf{F}, \qquad (12)$$

where

$$\mathbf{F_{KEA}} = (\tfrac{1}{2}\rho\mathbf{u^2})\mathbf{u}. \qquad (13)$$

Again integrating over the cylinder, Equation (12) becomes

GENERALIZED ANTHES' FORM

$$\frac{d}{dt}\overline{[\tfrac{1}{2}\rho\mathbf{u^2}]} = -\overline{[\mathbf{u_h} \cdot \nabla_h p']} + \overline{[\rho P w]} - F_{KEA} - D, \qquad (14)$$

[3]Equation (8) is, in essence, the kinetic energy equation for the Reynolds averaged flow in which the quantity μ is a turbulent eddy counterpart. In this case, we are presuming that a K-theory closure is adequate so that the Reynolds averaged equations look essentially like the Newtonian fluid formulation. Further, in the mechanical energy flux through the side boundary in Equation (9) we have neglected the eddy diffusive radial flux of kinetic energy. Relative to the advective flux of kinetic energy, the diffusive flux scales as the inverse Reynolds number of the flow, which is always small compared to unity outside of the surface layer. This conclusion is based on recently obtained estimates of the turbulent eddy diffusivity observed in major hurricanes on the order of $50 - 100$ m^{2}s^{-1} (Zhang *et al.* 2011).

where

$$F_{KEA} = \frac{1}{\pi R^2 H}\int_0^{2\pi} d\lambda \int_0^H \left[u(\tfrac{1}{2}\rho\mathbf{u^2})\right]_{r=R} dz. \qquad (15)$$

Equation (14) is a generalization of Anthes' formulation to include the three-dimensional wind vector in the definition of kinetic energy and the rate of working of the net vertical perturbation gradient force per unit volume, $\overline{[\rho P w]}$, which is a non-hydrostatic effect. As in Anthes' original form, the pressure-work term, $-\overline{[\mathbf{u_h} \cdot \nabla_h p']}$, appears explicitly in the global form of the kinetic energy equation. For an axisymmetric flow, this term is simply $\overline{[-u\partial p/\partial r]}$ and, at first sight, one might question its prominence as a source of kinetic energy, since $\partial p/\partial r$ is *not* the only radial force acting on fluid parcels en route to the storm core. Above the frictional boundary layer, the radial pressure gradient is closely balanced by the sum of the centrifugal force and the radial component of the Coriolis force. Moreover, this source term does not appear in Gill's formulation (cf. Eq. (8)), although it is replaced by the term $\overline{[p'\nabla_h \cdot \mathbf{u_h}]}$ and the boundary flux terms are different. Even so, one should bear in mind that even in the axisymmetric case, $\overline{[-u\partial p/\partial r]}$ is generating *not only a radial contribution to the kinetic energy, but also an azimuthal contribution* through the action of the generalized Coriolis force $(f + v/r)u$. The generation of this azimuthal contribution is implicit in the kinetic energy equation as the generalized Coriolis force does no work, but it does convert radial momentum to tangential momentum.

3. Kinetic energy budget for an idealized simulation

We examine now the generation terms in the two forms of the kinetic energy equation for the case of an idealized tropical cyclone simulation. We begin with a brief description of the numerical model and go on to present the results.

3.1. *The numerical model*

The numerical model used for this study is Bryan's three-dimensional, nondydrostatic cloud model (CM1), version 16 (Bryan and Fritsch, 2002). The simulations relate to the prototype problem for tropical cyclone intensification, which considers the evolution of an initially axisymmetric, cloud-free, warm-cored, baroclinic vortex in a quiescent environment on an f-plane. The initial vortex is in thermal wind balance. A latitude of 20^{o}N and a constant sea surface temperature of 28^{o}C are assumed. The model configuration is more or less the same as described in section 2 of Črnivec *et al.* (2016). The differences are that, following the work of Mapes and Zuidema (1996), a more realistic time scale for Newtonian relaxation to the temperature field (10 days) is applied here instead of the previous default value in CM1 (12 h). Further, an open boundary condition is taken at lateral boundaries instead of rigid walls and the Dunion moist tropical sounding is used as the environmental sounding (Dunion 2011).

The initial tangential wind speed has a maximum of 15 m s^{-1} at the surface at a radius of 100 km. The tangential wind speed decreases sinusoidally with height, becoming zero at a height of 20 km. Above this height, up

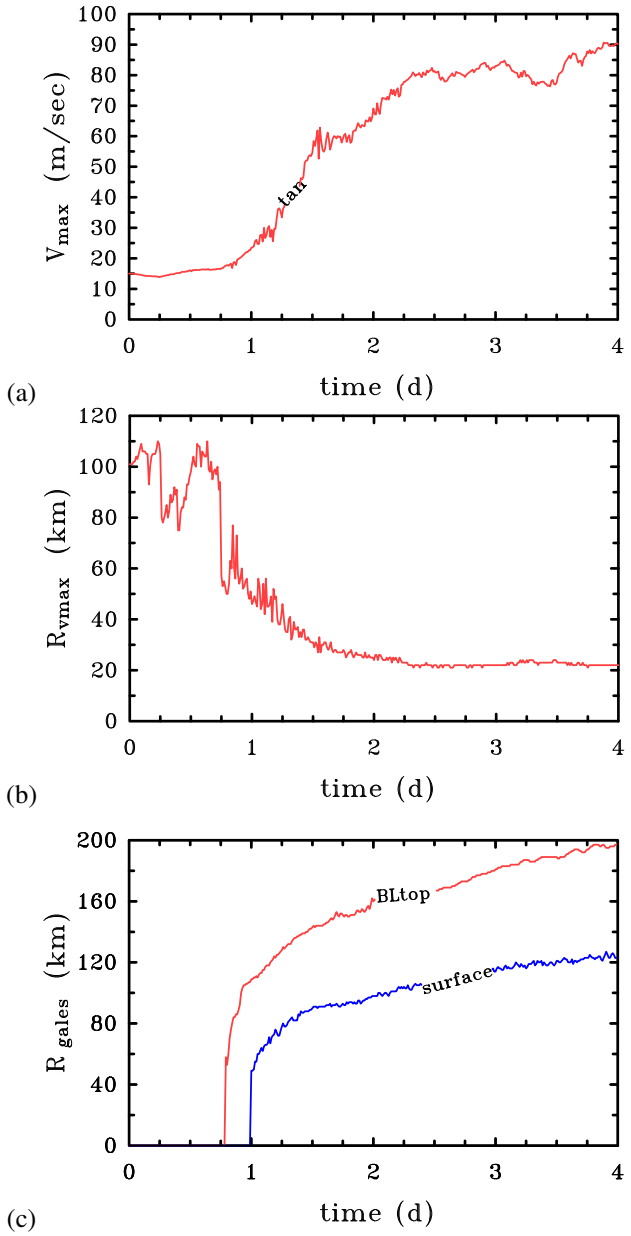

Figure 1. Time series of (a) maximum azimuthally-averaged tangential wind speed (V_{max}). Panel (b) shows the radius R_{vmax} at which the maximum tangential wind speed occurs (V_{max}). Panel (c) shows the radius at which gale force winds occurs (R_{gales}), where R_{gales} calculated at a height of 1 km, and corresponds to the radius of 17 m s^{-1} total winds outside the eyewall.

to 25 km, the tangential wind is set to zero. The balanced pressure, density and temperature fields consistent with this prescribed tangential wind distribution are obtained using the method described by Smith (2006). The calculations are carried out for a period of 4 days with data output every 15 min.

3.2. *A few details of the simulation*

Figure 1 summarizes the vortex evolution in the simulation. Panel (a) shows time series of the maximum azimuthally-averaged tangential wind speed, V_{max}, and panel (b) shows the radius R_{vmax} at which V_{max} occurs. Typically, V_{max} is located a few hundred meters above the surface, within a shallow inflow layer. The evolution is broadly similar to that described in Kilroy *et al.* (2016), who used a different numerical model and a much coarser horizontal resolution (horizontal grid spacing 5 km compared with 1 km used here). In brief, after a gestation for about a day during which deep convection becomes established inside R_{vmax}, the vortex undergoes a rapid intensification phase lasting about 36 h, before reaching a quasi-steady state. Initially R_{vmax} is located at a radius of 100 km, but contracts to a little more than 20 km after about $2\frac{1}{4}$ days. The most rapid contraction occurs during the rapid intensification phase as absolute angular momentum surfaces are drawn inwards quickly within and above the boundary layer.

Figure 1(c) shows the outermost radius of gale-force winds, R_{gales}, defined here as the radius of 17 m s^{-1} azimuthally-averaged tangential winds at a height of 1 km, which is approximately at the top of the frictional boundary layer. Shown also is R_{galesF}, defined as the (outer) radius at which the total wind speed at any grid point at a height of 10 m is 17 m s^{-1}. Both quantities serve as a measure of the vortex size, R_{galesF} being closest to the quantity used by forecasters[4], but R_{gales} being a preferred measure from a theoretical viewpoint (Kilroy *et al.* 2016). The evolution of storm size based on R_{galesF} is similar to that based on R_{gales}, although R_{gales} always exceeds the value of R_{galesF}. After 4 days, R_{gales} exceeds R_{galesF} by about 80 km.

Figure 2 shows vertical cross sections of the azimuthally-averaged, 3 h time averaged, radial and tangential velocity components, the vertical velocity component, and the M-surfaces during the intensification phase of the vortex. The time averages are centred on 36 h during the period of rapid intensification and at 60 h near the end of this period. The basic features of the flow are qualitatively similar at both times, but all three velocity components strengthen over the period, the M-surfaces moving inwards in the lower troposphere and outwards in the upper troposphere. The flow structure is similar to that which has been described in many previous studies (see e.g. the recent review by Montgomery and Smith 2017a and refs.) with a layer of strong shallow inflow marking the frictional boundary layer, a layer of weaker inflow in the lower troposphere, a region of strong outflow in the upper troposphere and a layer of enhanced inflow below the outflow. The maximum tangential wind speed occurs within, but near the top of the frictional boundary layer[5]. Much of the ascent occurs in an annular region on the order of 50-60 km in radius. The region inside this annulus shows mostly descent.

3.3. *Kinetic energy evolution*

Figure 3 shows time series of the domain-averaged kinetic energy per unit mass, $\overline{\left[\frac{1}{2}\rho\mathbf{u^2}\right]}$, for domain radii 300 km and 500 km and a domain height of 20 km. As anticipated by Anthes (1974), this quantity is dominated by the horizontal velocity components: in fact, the curves for $\overline{\left[\frac{1}{2}\rho\mathbf{u^2}\right]}$ and $\overline{\left[\frac{1}{2}\rho\mathbf{u_h^2}\right]}$ essentially overlap. It follows that the contribution of the vertical velocity to the global kinetic energy is

[4]Based on the wind speed in a particular sector and not azimuthally averaged.

[5]At 60 h, the tangential wind field exhibits a second local maximum in the eyewall. This is a transient feature that is presumably associated with a centrifugal wave near the base of the eyewall (e.g. Montgomery and Smith 2017, p550) excited by an elevated pulse of boundary layer outflow shortly before. This feature is not seen at 48 h or 72 h and its presence doesn't alter the findings concerning the kinetic energy budget.

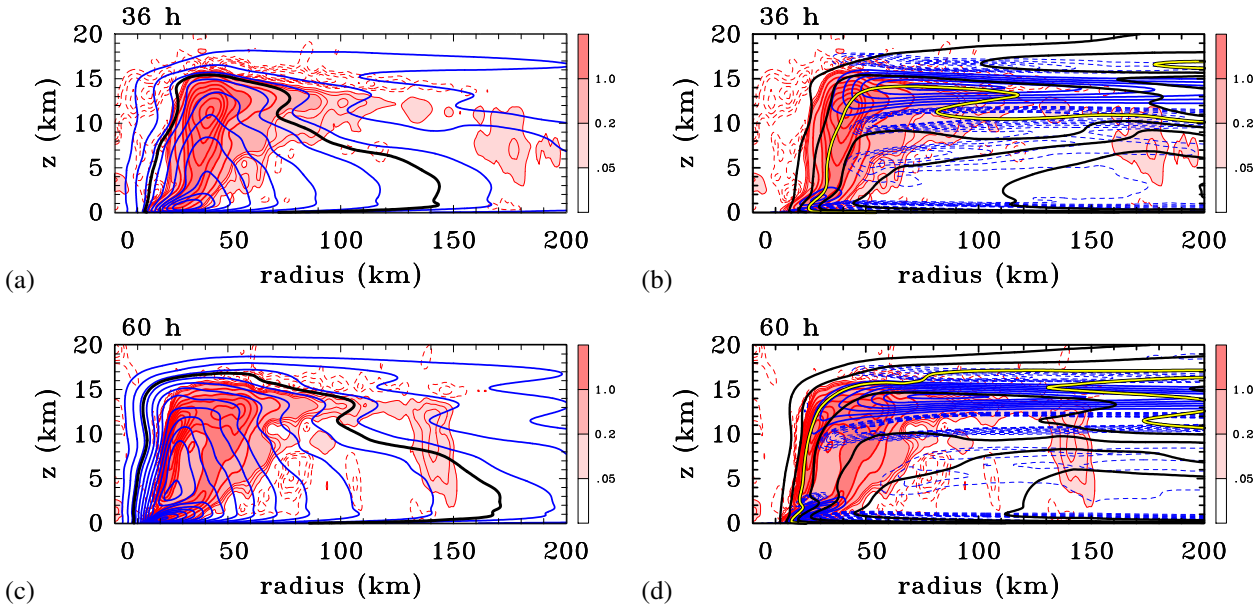

Figure 2. Left panels: Vertical cross sections of the azimuthally-averaged, 3 hour time averaged tangential velocity component (blue contours) centred at 36 h and 60 h. Superimposed are contours and shading of the averaged vertical velocity. Contour intervals are as follows. Tangential velocity: blue contours every 5 m s^{-1}, with a thick black contour highlighting the 17 m s^{-1} contour. Vertical velocity: thin red contours every 0.05 m s^{-1} to 0.2 m s^{-1}, thick red contour interval 0.5 m s^{-1}, thin dashed red contours indicate subsidence at intervals of 0.02 m s^{-1}. Right Panels: Vertical cross sections of the azimuthally-averaged, 3 hour time averaged radial velocity component together with the averaged vertical velocity centred at the same times. Contour intervals are as follows. Radial velocity: thick blue contours 4 m s^{-1}, dashed negative, thin blue dashed contours every 0.5 m s^{-1} down to -3.5 m s^{-1}. Absolute angular momentum: thick black contours every 2×10^5 m^2 s^{-1}, with the 6×10^5 m^2 s^{-1} contour highlighted in yellow.

negligible. Notable features of the curves for both domain sizes are the slight decrease during the first 12 h on account of surface friction, followed by a rapid increase as the vortex intensifies. As time proceeds, the rate of increase progressively declines.

3.4. *Kinetic energy generation: Anthes' formulation*

Figure 4 shows time series of the principal terms in the generalized Anthes formulation (the right-hand-side of Equation (14)), excluding only the global dissipation term since the focus of the paper is on kinetic energy generation. For both domain radii, 300 km (Fig. 4(a)) and 500 km (Fig. 4(a)), both the terms $\overline{[-\mathbf{u_h} \cdot \nabla_h p']}$ and $\overline{[\rho P w]}$ are positive[6], but, perhaps surprisingly, the former term is not appreciably larger than the latter, even beyond 2 days when the differences are largest. The boundary flux term F_{KEA} is virtually zero throughout the calculation. For the larger domain size (R = 500 km), the temporal behaviour of the various terms is similar, but, as expected, the magnitudes of the respective terms are appreciably smaller (Fig. 4(b)), since the largest contributions to the averages are from well inside a 300 km radius (note the different scales on the ordinate in Figs. 4(a) and 4(b)).

The finding that the two terms $\overline{[-\mathbf{u_h} \cdot \nabla_h p']}$ and $\overline{[\rho P w]}$ are not appreciably different in magnitude is at first sight surprising since, as shown in Figure 3, the contribution of the vertical velocity to the total kinetic energy is negligible. Moreover, the $\overline{[\rho P w]}$ term does not appear in Anthes' original formulation because the formulation was based on the horizontal momentum equations only. An explanation of this result is suggested by an examination of the radial-height structure of the azimuthally-averaged generation term before completing the columnar average, i.e. $< -\mathbf{u_h} \cdot \nabla_h p' >$, where the angle brackets denote an azimuthal average. The structure of this average together with those of the other generation term, $< \rho P w >$, at 36 h and 60 h, is shown in Figure 5. At both times, the Anthes generation term $< -\mathbf{u_h} \cdot \nabla_h p' >$ shows coherent regions of large kinetic energy generation and of large kinetic energy destruction. The main region of generation in panels (a) and (b) is at low levels, below about 2 km, where the strongest inflow occurs and where the inward directed radial pressure gradient force is particularly strong (panels (c) and (d) of Figure 5). There is a second region of generation in an annular column, mostly on the outer side of the eyewall updraught below about 9 km at 36 h and below about 12 km at 60 h. The generation terms in panels (a) and (b) are similar in structure and magnitude to that shown by Kurihara (1975, Figure 42, upper right) for a lower resolution axisymmetric simuulation.

Since the radial pressure gradient is positive at all heights [panels (c) and (d) of Figure 5], these generation regions must be ones in which there is generally inflow[7]. For the same reason, where there is outflow, there is kinetic energy removal as seen in the two principal coherent regions in panels (a) and (b) where $< -\mathbf{u_h} \cdot \nabla_h p' ><< 0$. It follows that the computed value of $\overline{[-\mathbf{u_h} \cdot \nabla_h p']}$ is the remainder resulting from the cancellation of two comparatively large contributions from $< \mathbf{u_h} \cdot \nabla_h p' >$ of opposite sign, namely $< -\mathbf{u_h} \cdot \nabla_h p' >_+$ and $< -\mathbf{u_h} \cdot \nabla_h p' >_-$, the former being the sum of all positive values of $-\mathbf{u_h} \cdot \nabla_h p'$ and the latter $< -\mathbf{u_h} \cdot \nabla_h p' >_-$ to be the sum

[6]The finite difference form of the vertical perturbation pressure gradient in calculating the term $\overline{[\rho P w]}$ is detailed in the appendix.

[7]Note that eddy effects are included in all generation terms.

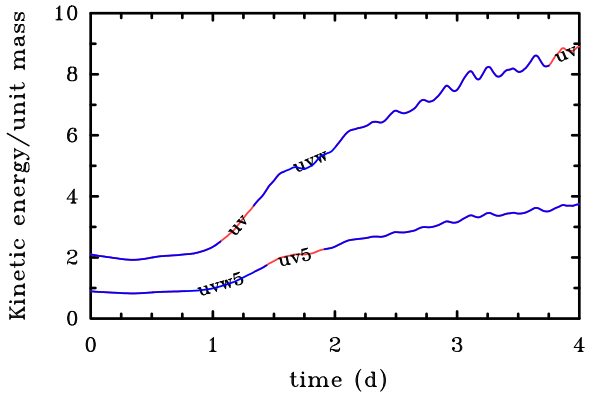

Figure 3. Time series of the left-hand-side of Equation 14, $\overline{[\frac{1}{2}\rho \mathbf{u^2}]}$ (curves labelled uvw) compared to $\overline{[\frac{1}{2}\rho \mathbf{u_h^2}]}$ (curves labelled uv) for cylinders of 300 km and 500 km. The curves for each cylinder size lie essentially on top of each other so that only a single curve is evident. The curves for the 500 km domain are labelled with a '5'.

of all negative values. This large cancellation is evident in the time series shown in Figure 4.

In summary, a substantial fraction of the kinetic energy that is generated is removed in regions where there is outflow and the residual is relatively small, comparable, indeed, with the kinetic energy generated by the rate-of-working of the net vertical perturbation pressure gradient force (buoyancy plus perturbation pressure gradient), principally in the region of diabatically-forced ascent. The structure of the net vertical perturbation pressure gradient force at 36 h and 60 h is shown in panels (e) and (f) of Figure 5. As expected, this force is concentrated in an annular region overlapping the region of diabatic heating.

3.5. *Kinetic energy generation (Gill's formulation)*

Figure 6 shows time series of the principal terms in the modified Gill formulation (the right-hand-side of Equation (8)), excluding again the global dissipation term. In this formulation, the term $\overline{[p'\nabla_h \cdot \mathbf{u_h}]}$ is positive with mean amplitude and fluctuations about this mean increasing with time during the 4 day calculation [Fig. 6(b)]. For the first day, the term is a little less than the $\overline{[\rho P w]}$ term, but thereafter becomes progressively larger. The increasing energy source represented by the sum of the two foregoing terms is opposed, in part, by the net outward flux of mechanical energy through the radial boundary, F_{KEG}.

Panels (c) and (d) of Figure 6 show the structure of the term $< p'\nabla_h \cdot \mathbf{u_h} >$, again 36 h and 60 h. The radial and vertical integral of this term form the cylindrical average $\overline{[p'\nabla_h \cdot \mathbf{u_h}]}$ in the modified Gill's formulation of the energy equation. The qualitative radius-height structure of $< p'\nabla_h \cdot \mathbf{u_h} >$ at the two times shown is less easy to infer from the solutions in Figure 2. Moreover, as shown in Figure 6, there is significant cancellation between the term $\overline{[p'\nabla_h \cdot \mathbf{u_h}]}$ and the boundary flux term in Gill's formulation [Equation (8)]. For this reason, the Anthes' formulation of the energy equation would seem to be preferable to Gill's formulation, even though both formulations are correct and give the same tendency of kinetic energy over the control volume of integration (see next subsection).

3.6. *Total kinetic energy generation*

A check on the foregoing calculations is provided by calculating the total tendency of kinetic energy generation, which is the sum of all the terms on the right-hand-side of Equations (8) or (14). This sum should be the same for each formulation. That this is the case is verified in Figure 7, which shows the sum for each domain size. As expected, the curves for the two formulations are coincident.

4. Discussion

Anthes' statement noted in the Introduction that "the important source of kinetic energy production in the hurricane is the radial flow toward lower pressure in the inflow layer, represented by $-u\partial p/\partial r$" may seem at first sight problematic because, above the boundary layer, the radial pressure gradient is very closely in balance with sum of centrifugal and Coriolis forces. Thus the energy source associated with $-u\partial p/\partial r$ might appear, at least at first sight, to be a gross overestimate. However, the kinetic energy equation doesn't recognize the balance constraint and, in this equation, the radial pressure gradient acts to generate not only kinetic energy of radial motion, but also that of tangential motion through the action of the generalized Coriolis force $(f + v/r)u$, a term that appears in the tangential momentum equation in cylindrical coordinates. This is despite the fact that the generalized Coriolis force does not appear explicitly in the kinetic energy equation.

As noted also in the Introduction, Anthes recognized that much of the inflow into the storm is " ... a result of surface friction, which reduces the tangential wind speed and thereby destroys the gradient balance, so that the inward pressure gradient force exceeds the Coriolis and centripetal[8] forces" and he pointed out that "In the warm core low the maximum pressure gradient ($-\partial p/\partial r < 0$ [sign corrected: our insertion]) occurs at the lowest level, at which the inflow ($u < 0$) is maximum. In the outflow layer, where the radial flow is reversed, the pressure gradient is much weaker. The result is a net production of kinetic energy, dominated by the contribution from the inflow region". While this view is broadly supported by the calculations presented herein, the calculations provide a sharper view of the *net* production of kinetic energy indicating a region of significant kinetic energy generation accompanying inflow *throughout* the lower troposphere above the boundary layer as well as significant regions where kinetic energy is consumed as air flows outwards, against the radial pressure gradient, above the boundary layer. Indeed, the generation above the boundary layer is a manifestation of spin up by the classical mechanism articulated by Ooyama (1969), while the generation within the boundary layer, highlighted by Anthes, is a manifestation of the nonlinear boundary layer spin up mechanism articulated by Smith and Vogl (2008), Smith *et al.* (2009), Smith and Montgomery (2016) and Montgomery and Smith (2017b).

Anthes argues that the boundary layer " ... must be responsible for a net gain of kinetic energy" even though "a substantial dissipation of kinetic energy in the hurricane occurs in the boundary layer through turbulent diffusion and ultimate loss of energy to the sea surface". As a result, he

[8]Presumably, Anthes means the centrifugal force.

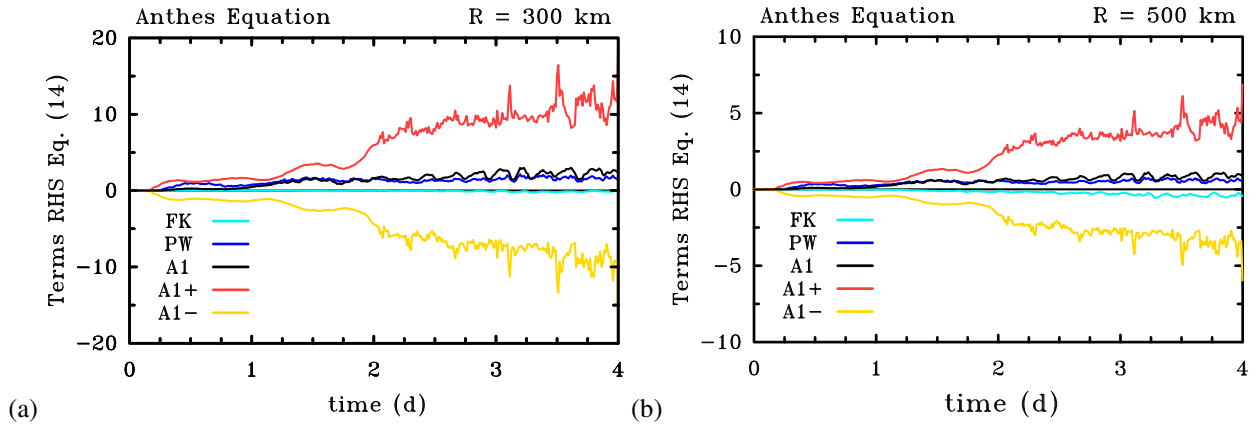

Figure 4. Time series of the kinetic energy tendency terms on the right-hand-side of Equation (14), the Anthes' formulation, averaged over a cylinder of size (a) 300 km and (b) 500 km. Units on the ordinate are 10^{-3} W m^{-3}. The dissipation term is not shown. A1 stands for $\overline{[-\mathbf{u_h} \cdot \nabla_h p']}$, FK for F_{KEA} and PW for $\overline{[\rho P w]}$. A1+ and A1- stand for the contributions to A1 from regions where the argument $-\mathbf{u_h} \cdot \nabla_h p'$ is positive and negative, respectively.

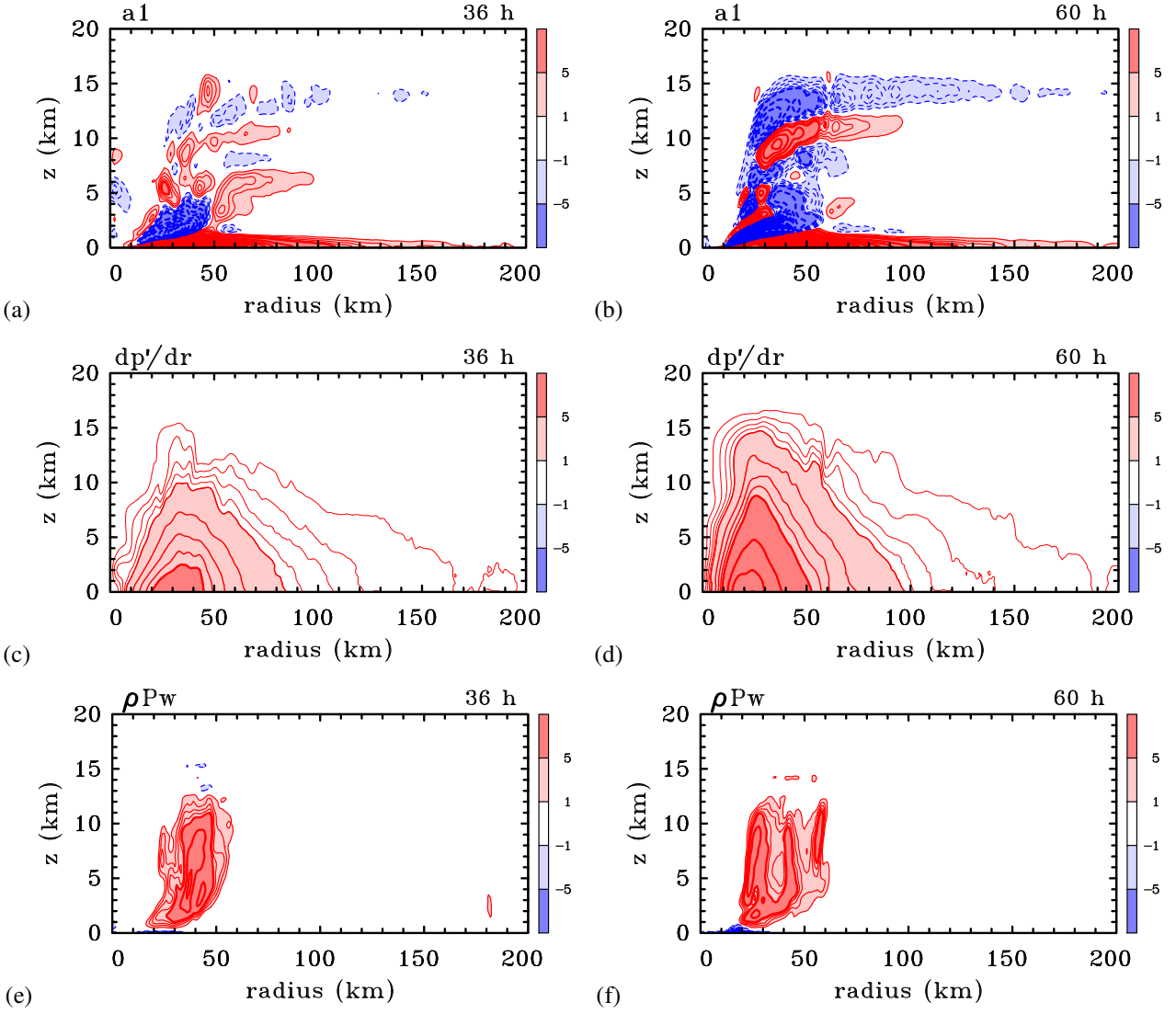

Figure 5. Radius-height cross sections of azimuthally-averaged quantities in Equation (14), before performing the columnar average: $< -\mathbf{u_h} \cdot \nabla_h p' >$ (panels (a), (b)); and $< \rho P w >$ (panels (e), (f)), at 36 h (left panels) and 60 h (right panels). Panels (c) and (d) show similar cross sections of $< \partial p'/\partial r >$ at these times. Contour intervals are as follows. Panels (a), (b), (e) and (f): thick contours 5×10^{-2} W m^{-3}: thin contours 1×10^{-2} W m^{-3}. Solid red contours positive, dashed blue contours negative. Panels (c) and (d): thin contours 0.2×10^{-2} Pa m^{-1} to 0.8×10^{-2} Pa m^{-1}; medium thick contours 1.0×10^{-2} Pa m^{-1} to 5.0×10^{-2} Pa m^{-1}; thick contours every 5.0×10^{-2} Pa m^{-1}. Numbers indicated on the side bar should be multiplied by 10^{-2}.

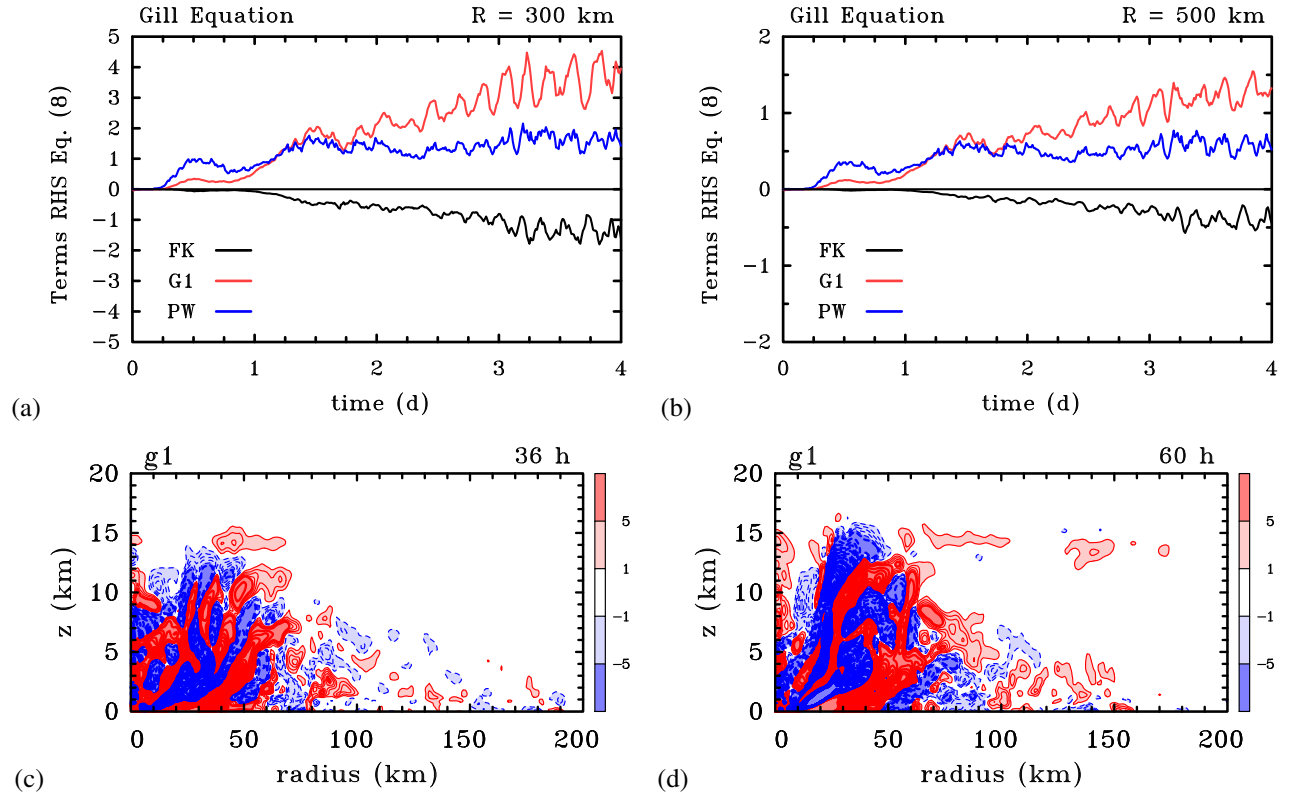

Figure 6. Time series of the kinetic energy tendency terms: $\overline{[p'\nabla_h \cdot \mathbf{u_h}]}$ (denoted by G1); $\overline{[\rho Pw]}$ (denoted PW) and F_{KEG} (denoted FK) in the modified Gill formulation [Equation (8) averaged over a cylinder of size (a) 300 km and (b) 500 km. Units on the ordinate are 10^{-3} W m^{-3}. Panels (c) and (d) show the azimuthally averaged terms $< p'\nabla_h \cdot \mathbf{u_h} >$ in Equation (8) at 36 h and 60 h, respectively. Contour intervals are: thick contours 5×10^{-2} W m^{-3}: thin contours 1×10^{-2} W m^{-3}. Solid red contours positive, dashed blue contours negative. Numbers indicated on the side bar should be multiplied by 10^{-2}.

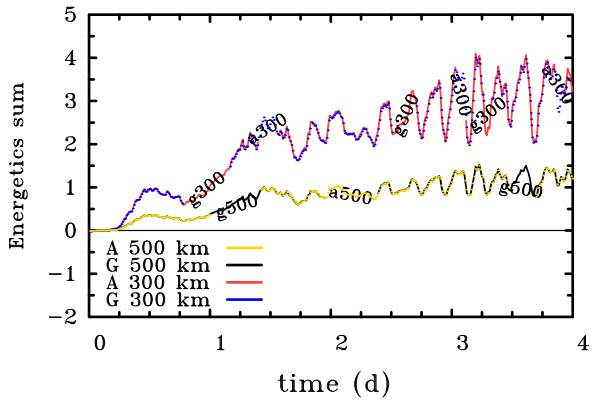

Figure 7. Sum of the terms for Gill's and Anthes' formulation excluding the dissipation term for cylinders of radius $R = 300$ km and 500 km. Values on the ordinate have been multiplied by 10^3 for plotting purposes. The two curves for each value of R lie essentially on top of each other.

is led to the paradox that "surface friction is responsible for a net increase in kinetic energy and without friction the hurricane could not exist." The resolution of this paradox would appear to be Anthes' de-emphasis of the role of the classical mechanism for spin up in the kinetic energy budget.

The results of our study, especially the noted cancellation of relatively large generation and consumption contributions to the term $\overline{[-\mathbf{u_h} \cdot \nabla_h p']}$ points to limitations in the utility of a global kinetic energy budget in revealing the underlying dynamics of tropical cyclone intensification. An alternative approach would be to examine the energetics of individual air parcels as they move around some hypothetical circuit (see Emanuel (2004) and references), but this approach relies on assumptions about the circuits traversed, circuits that may or may not be realizable in reality.

5. Conclusions

We have re-examined the traditional theory for kinetic energy generation in a tropical cyclone used by Palmén and Jordan (1955), Palmén and Riehl (1957), Frank (1977), Hogsett and Zhang (2009) and succinctly summarized in the review article by Anthes (1974). We have compared this with an alternative interpretation of global kinetic energy generation in geophysical flows inspired by Gill (1982), noting that such interpretations are non-unique.

We have shown that the *net* rate of production of kinetic energy is a comparatively small difference between the generation in regions of inflow and the magnitude of the consumption in regions of outflow, so much so, that this difference is comparable in magnitude with the rate of generation by the net vertical perturbation pressure gradient force. The latter effect was not contained in Anthes' original formulation, which was based only on the horizontal momentum equations.

We pointed out that the kinetic energy generation term in Anthes' formulation involving the radial pressure gradient does not appear in Gill's formulation of the kinetic energy equation or our modification thereof. It is replaced by a term comprising the global integral of the rate of working by perturbation pressure ($\overline{[p'\nabla_h \cdot \mathbf{u_h}]}$) as the flow expands in the horizontal. However, this generation term is largely

compensated in the modified Gill formulation by the boundary flux of mechanical energy (F_{KEG}). The fact that the boundary flux of kinetic energy in the Anthes formulation (F_{KEA}) is typically negligible, as well as the difficulty in anticipating the structure of the term $\overline{[p'\nabla_h \cdot \mathbf{u_h}]}$ in a tropical cyclone are factors weighing in favour of using Anthes' formulation when applied to the generation of kinetic energy in a tropical cyclone. However, in the light of the large cancellation of positive and negative values in the radial pressure-work term, the contribution from the rate of working of the net vertical force is non-negligible in comparison and should be included in any global kinetic energy budget.

While global energetics provide a constraint on flow evolution, we have shown in the context of the kinetic energy equation that they conceal important aspects of energy generation and consumption. This finding highlights the limitations of a global kinetic energy budget in revealing the underlying dynamics of tropical cyclones.

6. Acknowledgements

We thank Drs. Chris Landsea, Anastassia Makarieva and an anonymous reviewer for their perceptive comments on the original manuscript. GK and RKS acknowledge financial support for tropical cyclone research from the Office of Naval Research Global under Grant No. N62909-15-1-N021. MTM acknowledges the support of NSF grant AGS-1313948, NOAA HFIP grant N0017315WR00048, NASA grant NNG11PK021, ONR grant N0001417WX00336, and the U. S. Naval Postgraduate School.

7. Appendix: Calculation of the net vertical force, P

The net vertical force per unit mass, P, defined in Equation (4) and used to construct Figures 5(e) and 5(f) was first calculated on the stretched model grid at the levels where thermodynamic quantities are defined. The vertical perturbation pressure gradient was determined by fitting a quadratic function to three successive levels z_{i-1}, z_i and z_{i+1} at which the perturbation pressure has values p'_{i-1}, p'_i and p'_{i+1}, respectively. Then

$$\left(\frac{\partial p'}{\partial z}\right)_i = \frac{(p'_{i+1}-p'_i)dz_i^2 - (p'_{i-1}-p'_i)dz_{i+1}^2}{dz_{i+1}dz_i(z_{i+1}-z_{i-1})} \qquad (16)$$

where $dz_i = z_i - z_{i-1}$.

8. References

Anthes RA. 1974. The dynamics and energetics of mature tropical cyclones. *Rev. Geophys. Space Phys*,**12**: 495-522

Bryan GH, Fritsch JM. 2002. A benchmark simulation for moist nonhydrostatic numerical models. *Mon. Weather Rev.*, bf 130: 29172928.

Črnivec N, Smith RK, Kilroy G. 2016. Dependence of tropical cyclone intensification rate on sea surface temperature. *Q. J. R. Meteorol. Soc.*, **142**: 1618-1627.

DiMego GJ, Bosart LF. 1982. The transformation of tropical storm Agnes into an extratropical cyclone. Part II: Moisture, vorticity and kinetic energy budgets. *Mon. Weather Rev.*, bf 110: 412-433.

Dunion JP. 2011. Rewriting the climatology of the tropical North Atlantic and Carribean sea atmosphere. *J. Clim*, **24**: 893908.

Emanuel K. 2004. Tropical cyclone energetics and structure. In *Atmospheric turbulence and mesoscale meteorology*, E. Fedorovich, R. Rotunno and B. Stevens, editors, Cambridge University Press, pp280.

Frank WM. 1977. The structure and energetics of the tropical cyclone ll. Dynamics and energetics. *Mon. Weather Rev.*, **105**: 1136-1160.

Gill AE. 1982. *Atmosphere-Ocean Dynamics*. New York: Academic. 4th ed., 662pp

Hogsett W, Zhang D-L. 2009. Numerical simulation of Hurricane Bonnie (1998). Part III: Energetics. *J. Atmos. Sci.*, **66**: 2678-2696.

Kilroy G, Smith RK, Montgomery MT. 2016. Why do model tropical cyclones grow progressively in size and decay in intensity after reaching maturity? *J. Atmos. Sci.*, **73**: 487-503.

Kurihara Y. 1975. 1975: Budget analysis of a tropical cyclone simulated in an axisymmetric numerical model. *J. Atmos. Sci.*, , **32**: 25-59.

McWilliams JC. 2011. *Fundamentals of geophysical fluid dynamics*. Cambridge University Press, 283pp.

Mapes BE, Zuidema P. 1996: Radiative-dynamical consequences of dry tongues in the tropical troposphere. *J. Atmos. Sci.*, **53**: 620-638.

Montgomery MT, Smith RK. 2017a: Recent developments in the fluid dynamics of tropical cyclones. *Annu. Rev. Fluid Mech.*, **49**: 1-33, doi:10.1146/annurev-fluid-010816-060022.

Montgomery MT, Smith RK. 2017b: On the applicability of linear, axisymmetric dynamics in intensifying and mature tropical cyclones. *Fluids*, **2**: 69. doi:10.3390/fluids2040069.

Ooyama K. 1969: Numerical simulation of the life-cycle of tropical cyclones. *J. Atmos. Sci.*, **26**: 3-40.

Palmén E, Jordan CL. 1955. Note on the release of kinetic energy in tropical cyclones. *Tellus*, **7**: 186-189.

Palmén E, Riehl H. 1957. Budget of angular momentum and energy in tropical storms. *J. Meteor.*, **14**: 150-159.

Peixoto JP, Oort AH. 1992 *Physics of climate*. American Institute of Physics, New York, p 520.

Smith RK. 2006. Accurate determination of a balanced axisymmetric vortex. *Tellus*, **58A**: 98-103.

Smith RK, Vogl S, 2008: A simple model of the hurricane boundary layer revisited. *Q. J. R. Meteorol. Soc.*, **134**: 337-351.

Smith RK, Montgomery MT, 2016: The efficiency of diabatic heating and tropical cyclone intensification. *Q. J. R. Meteorol. Soc.*, **142**: 2081-2086.

Smith RK Montgomery MT Nguyen SV. 2009: Tropical cyclone spin up revisited. *Q. J. R. Meteorol. Soc.*, **135**: 1321-1335.

Tuleya RE, Kurihra Y. 1975. The energy and angular momentum budgets of a three-dimensional tropical cyclone model. *J. Atmos. Sci.*, **32**: 287-301.

Wang Y, Cui X, Li, X, Zhang W, Huang Y. 2016. Kinetic energy budget during the genesis period of Tropical Cyclone Durian (2001) in the South China Sea. *Mon. Weather Rev.*, **144**: 2831-854.

Zhang JA Rogers RF Nolan DS and Marks FD 2011: On the characteristic height scales of the hurricane boundary layer. *Mon. Weather Rev.*, **139**: 2523-2535.

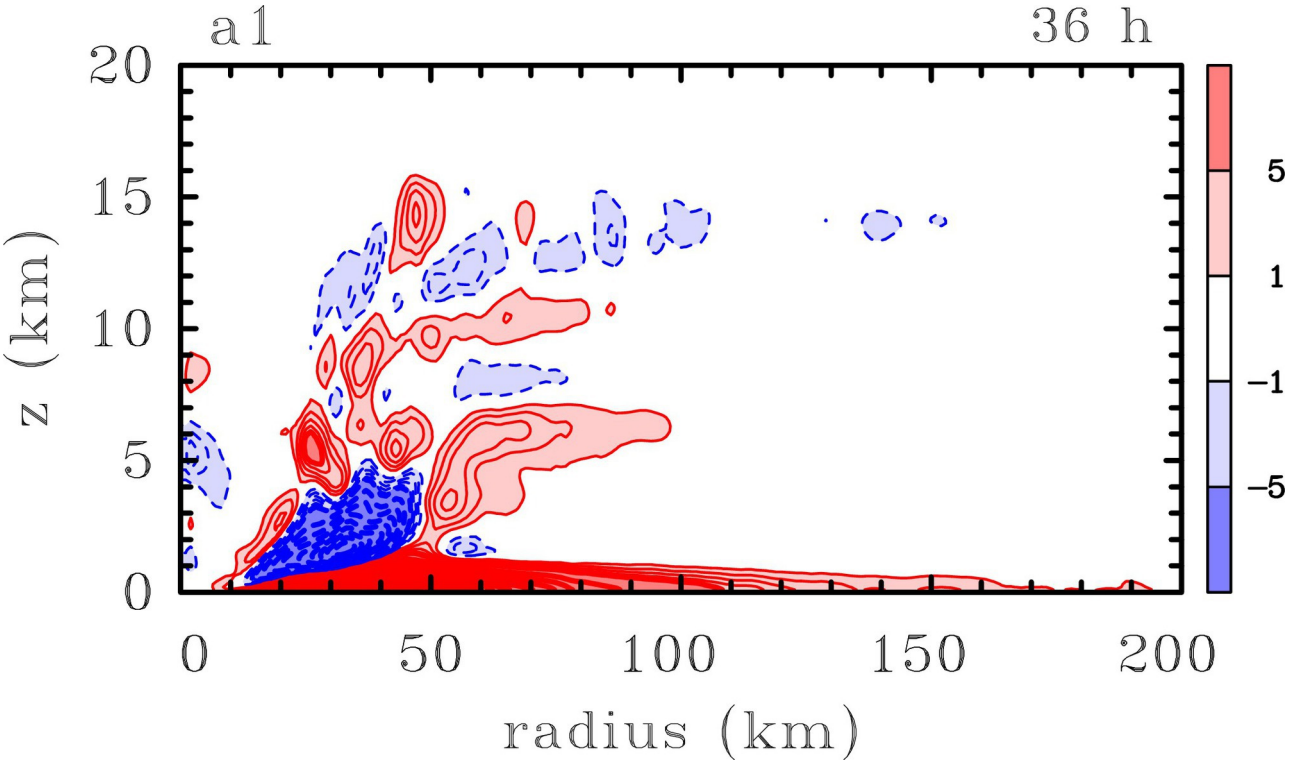

n3_eterms_a1_36h.eps

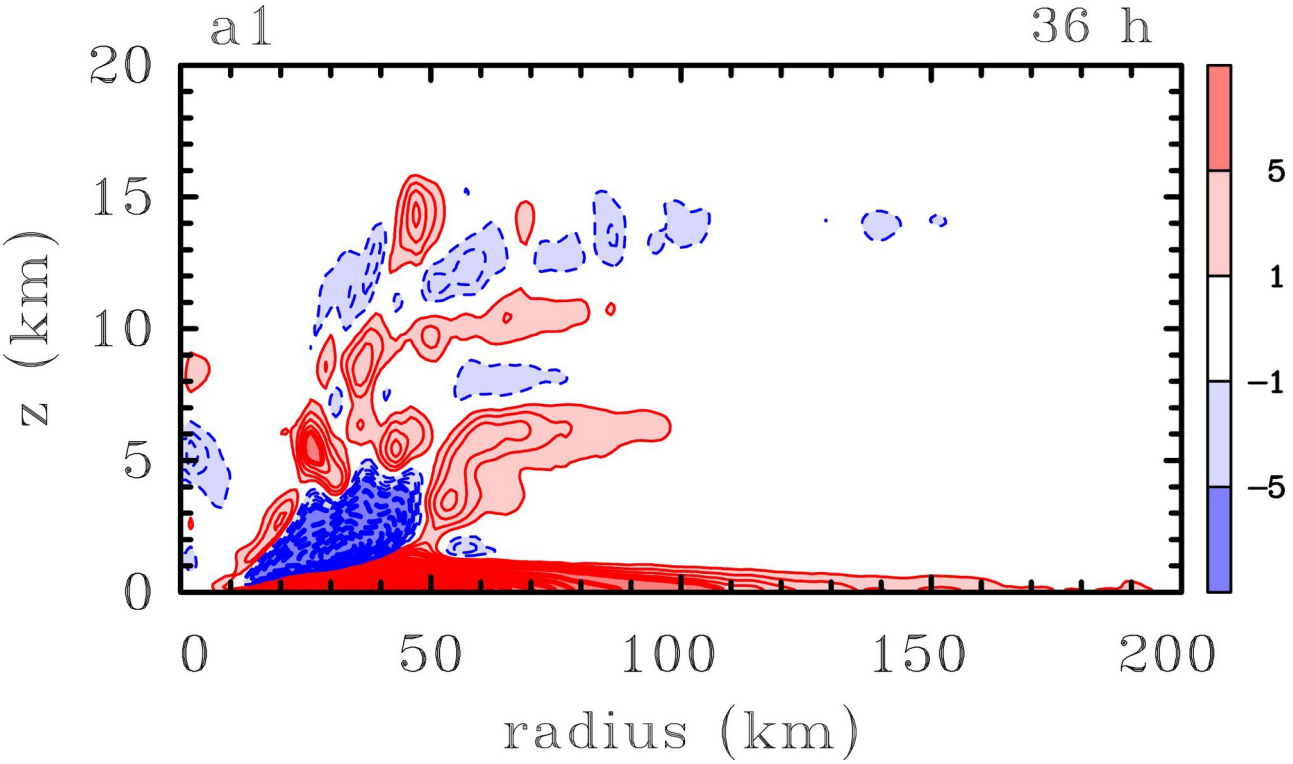

n3_eterms_a1_36h.eps

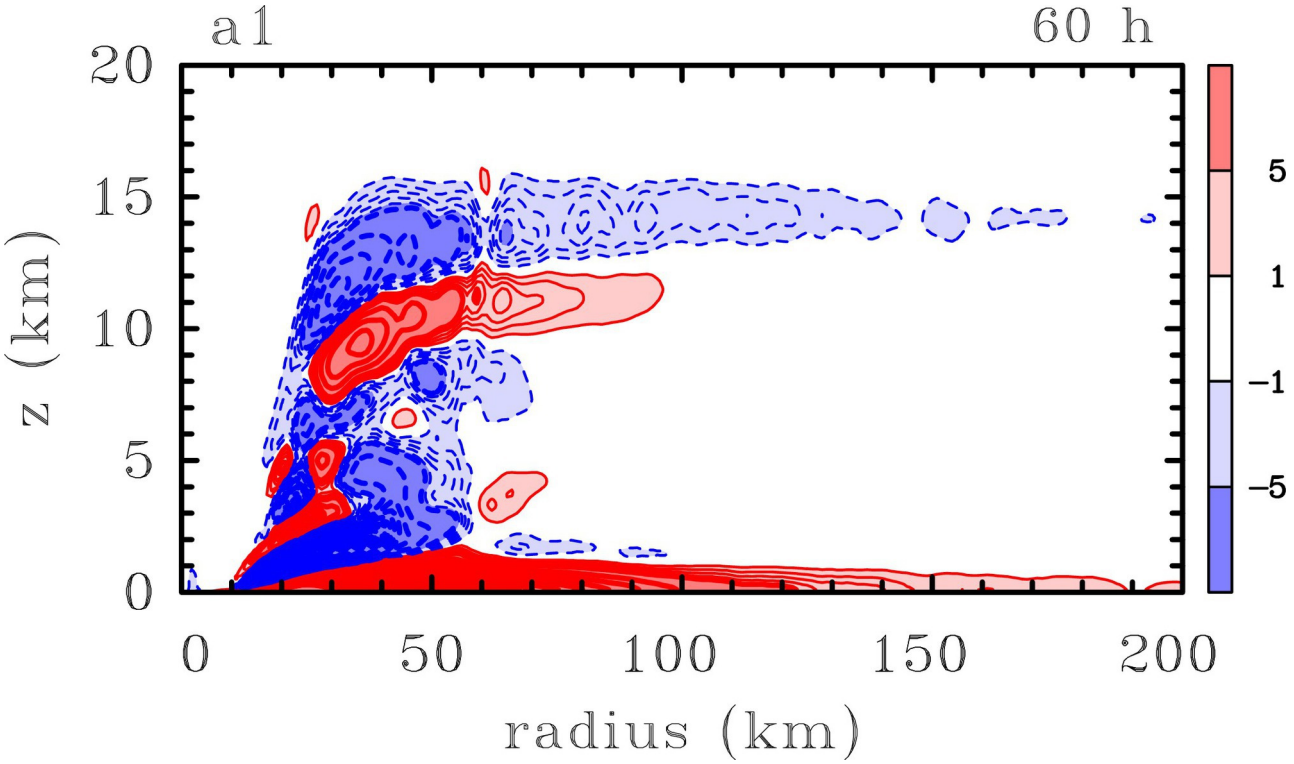

n3_eterms_a1_60h.eps

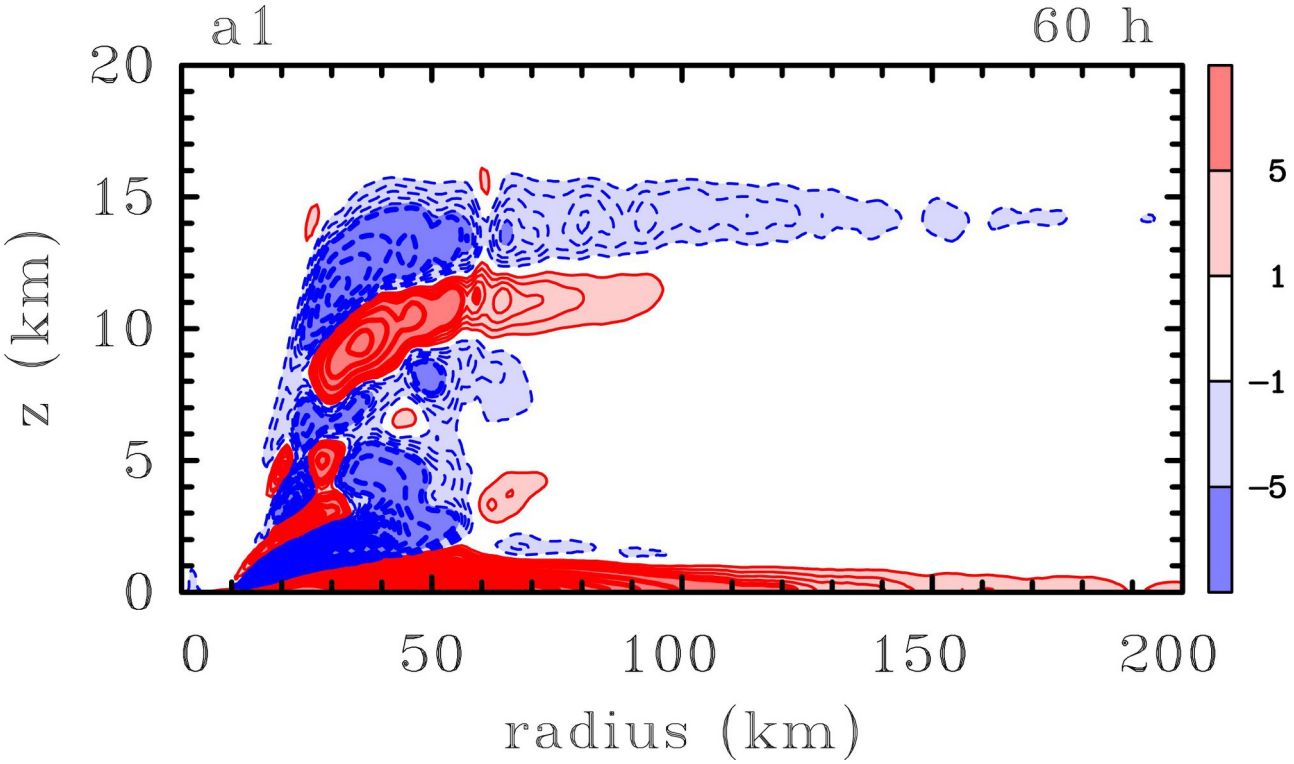

n3_eterms_a1_60h.eps

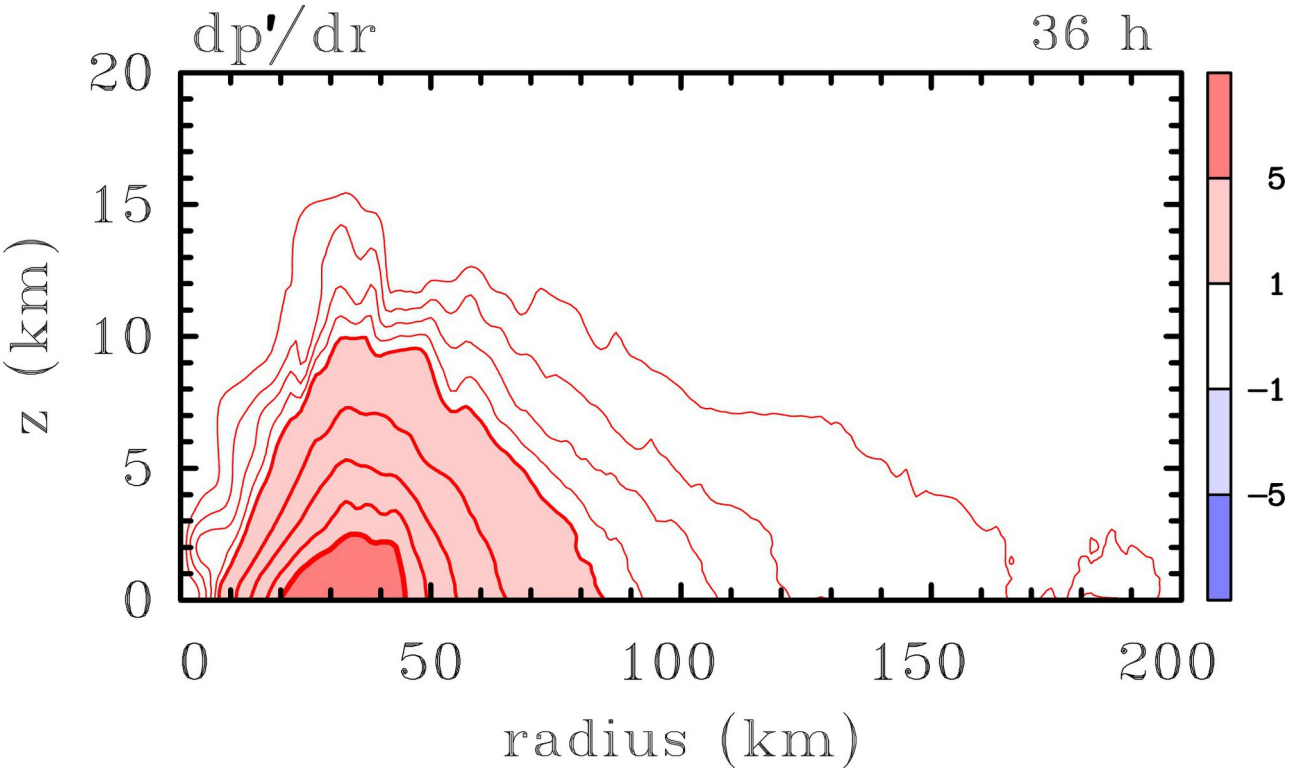

n3_eterms_dpdr_36h.eps

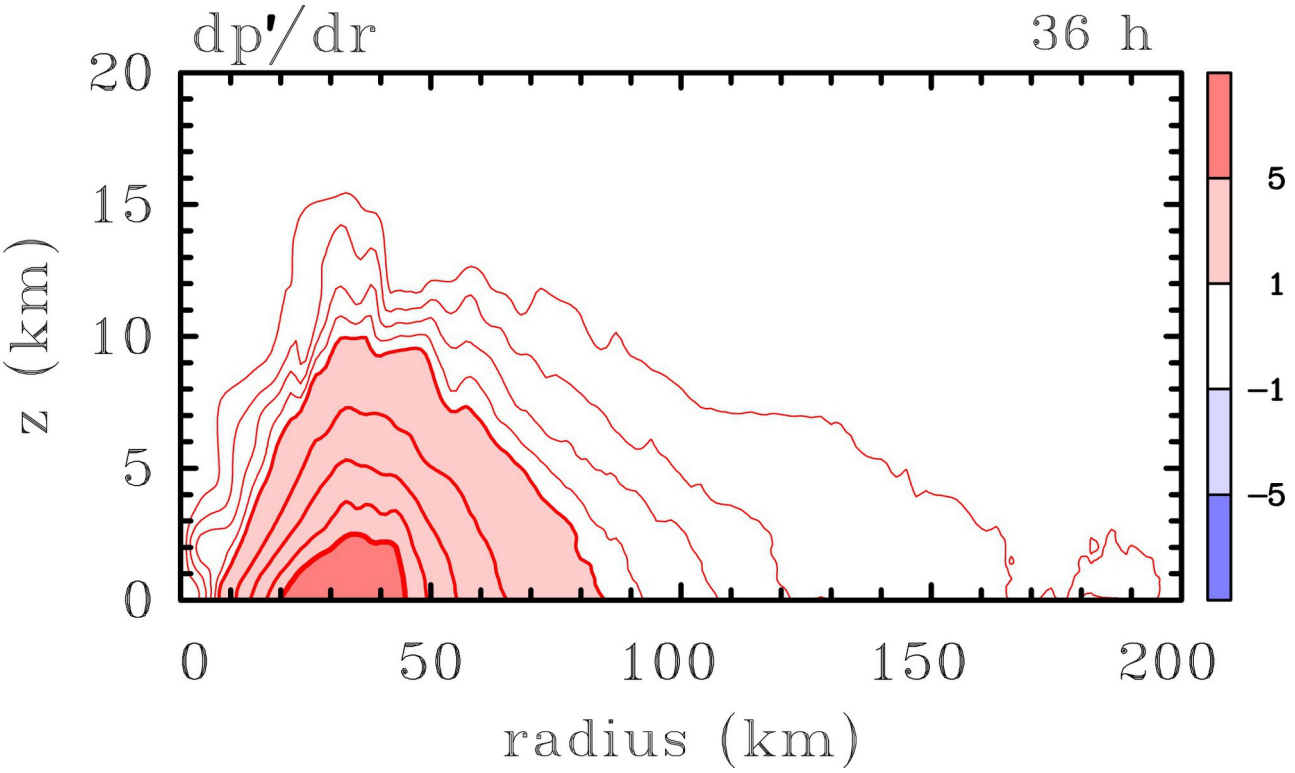

n3_eterms_dpdr_36h.eps

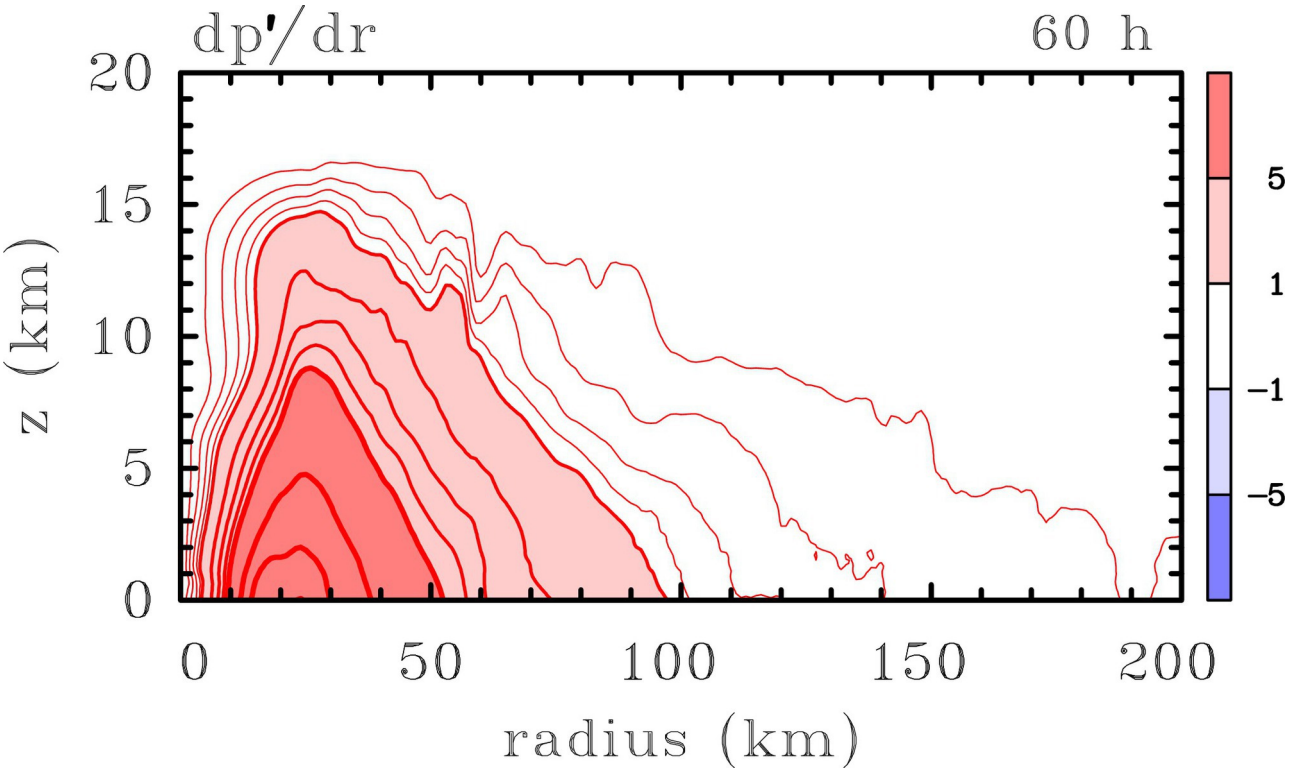

n3_eterms_dpdr_60h.eps

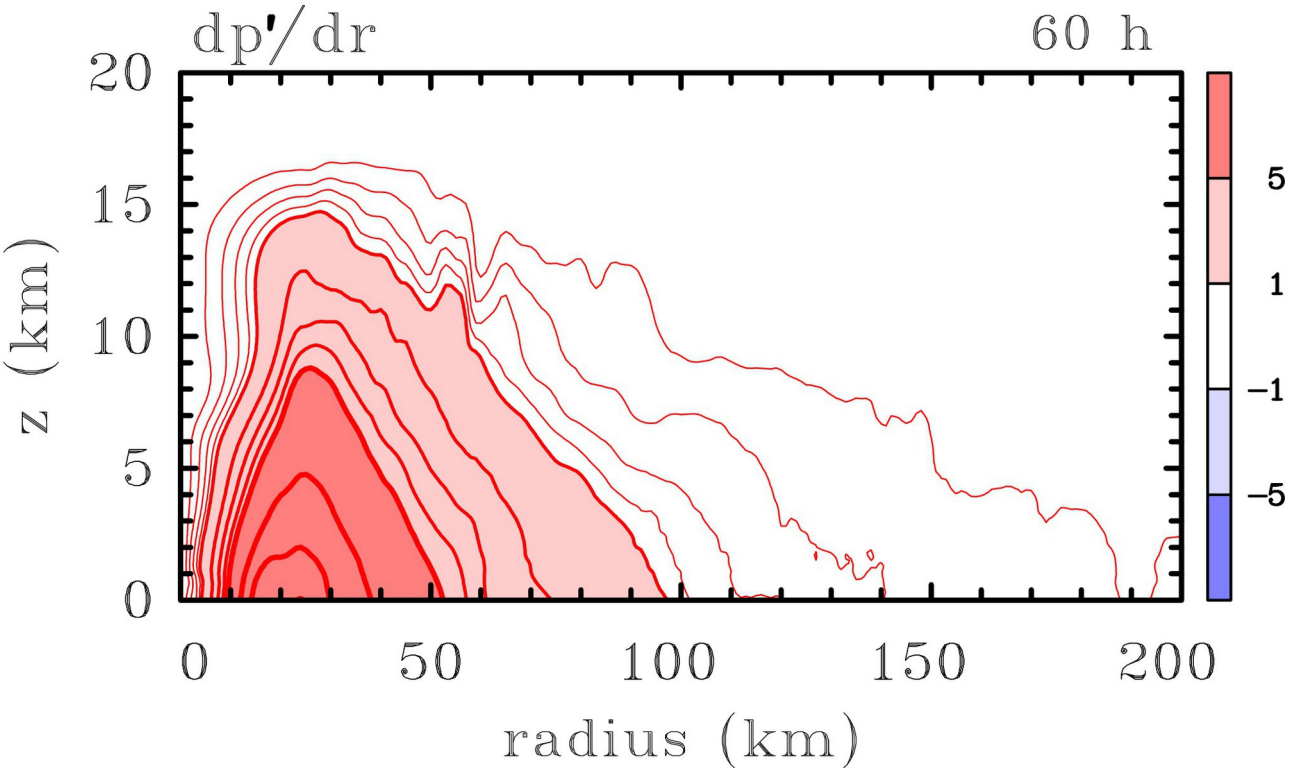

n3_eterms_dpdr_60h.eps

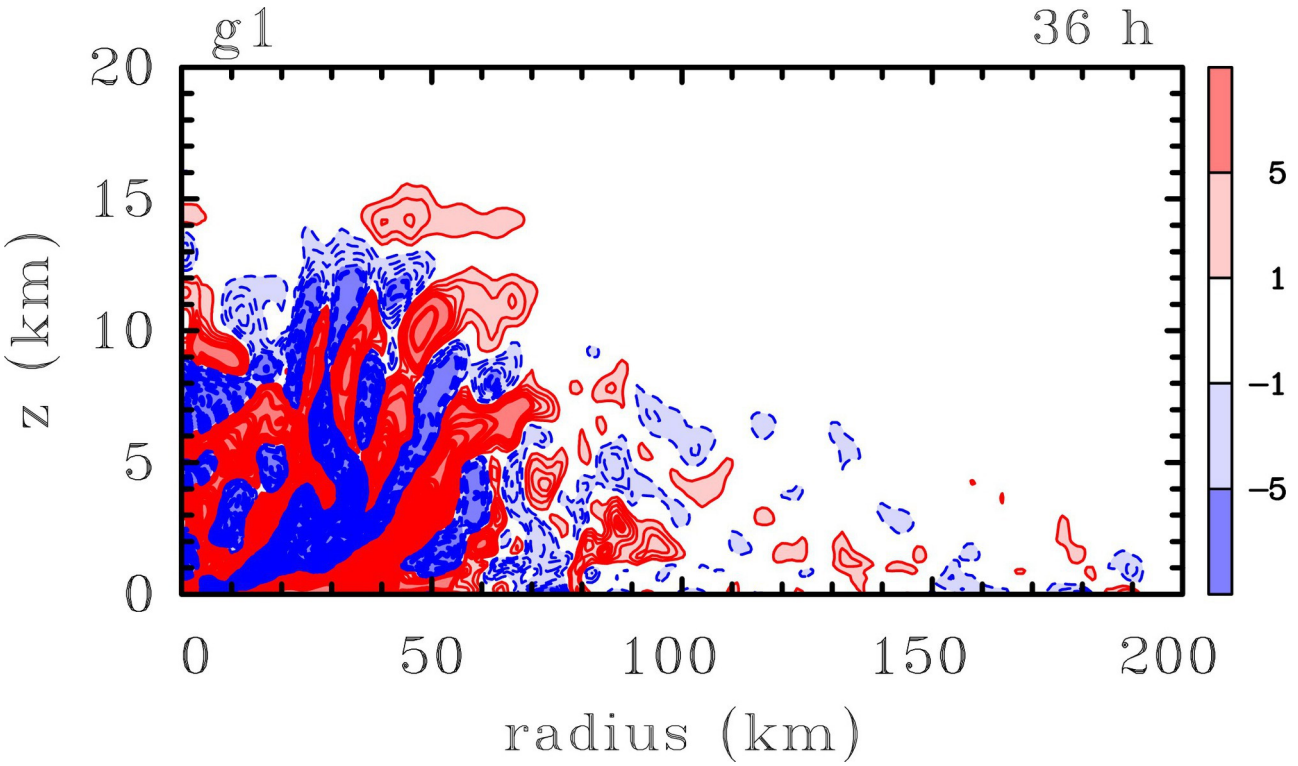

n3_eterms_g1_36h.eps

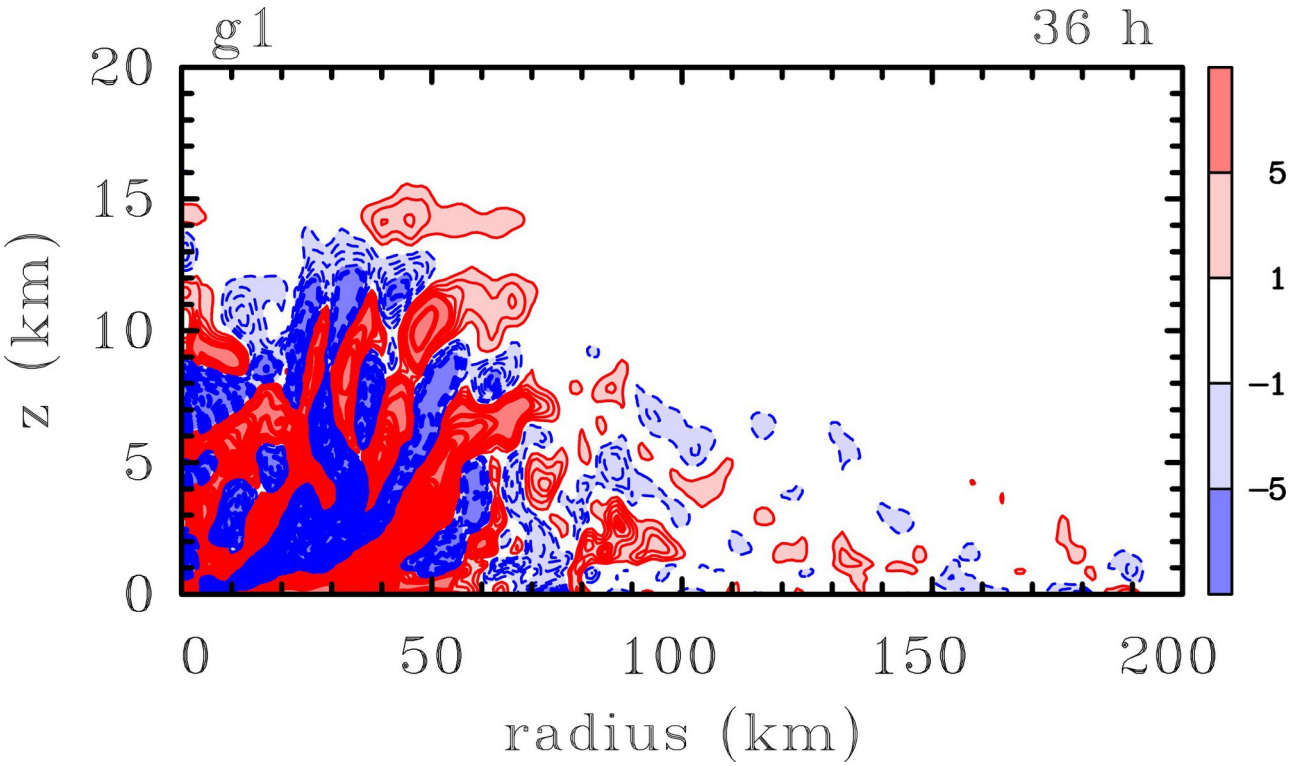

n3_eterms_g1_36h.eps

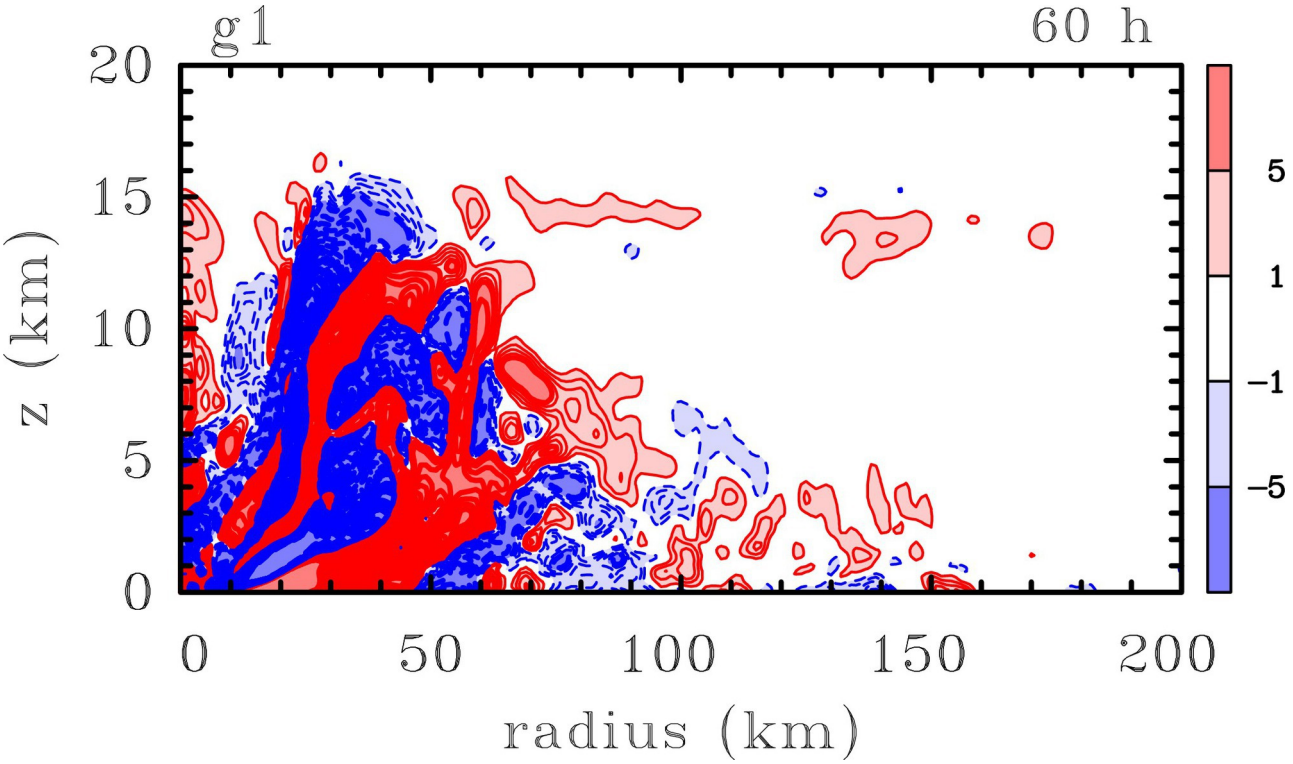

n3_eterms_g1_60h.eps

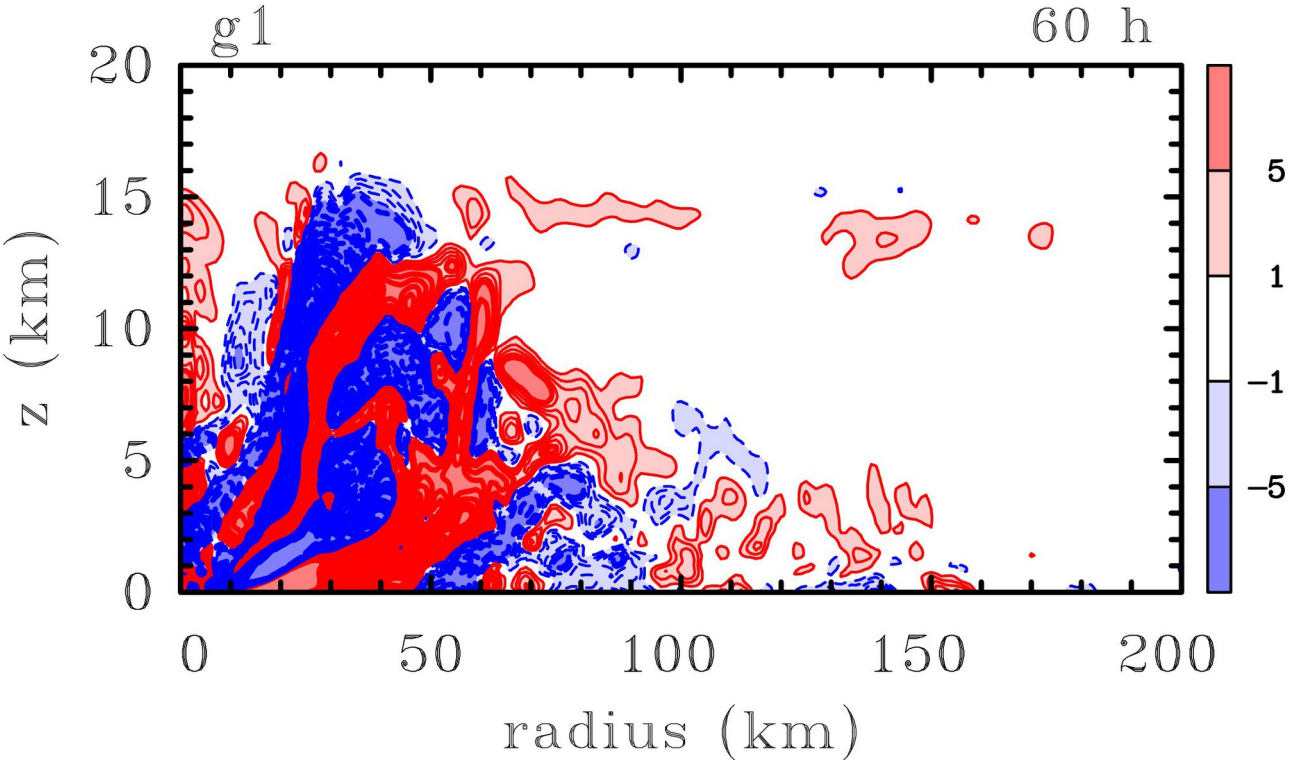

n3_eterms_g1_60h.eps

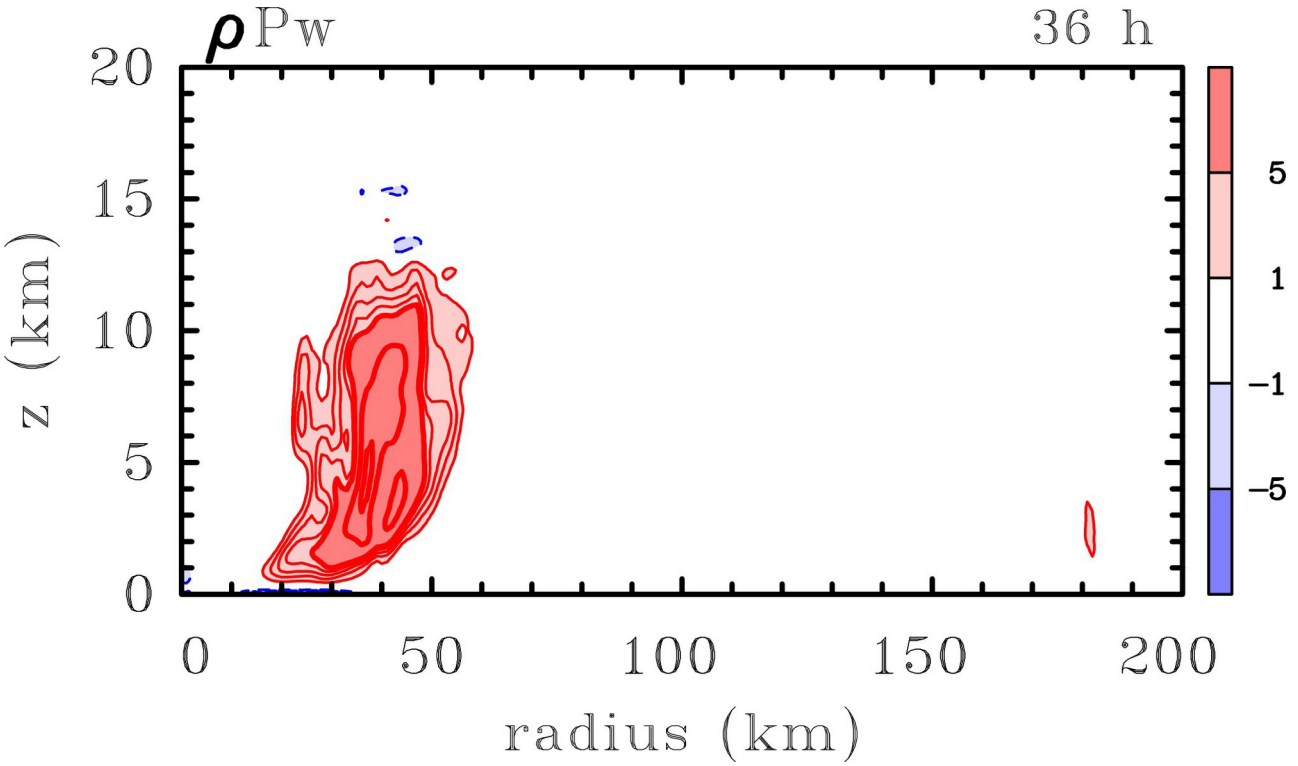

n3_eterms_pw_36h.eps

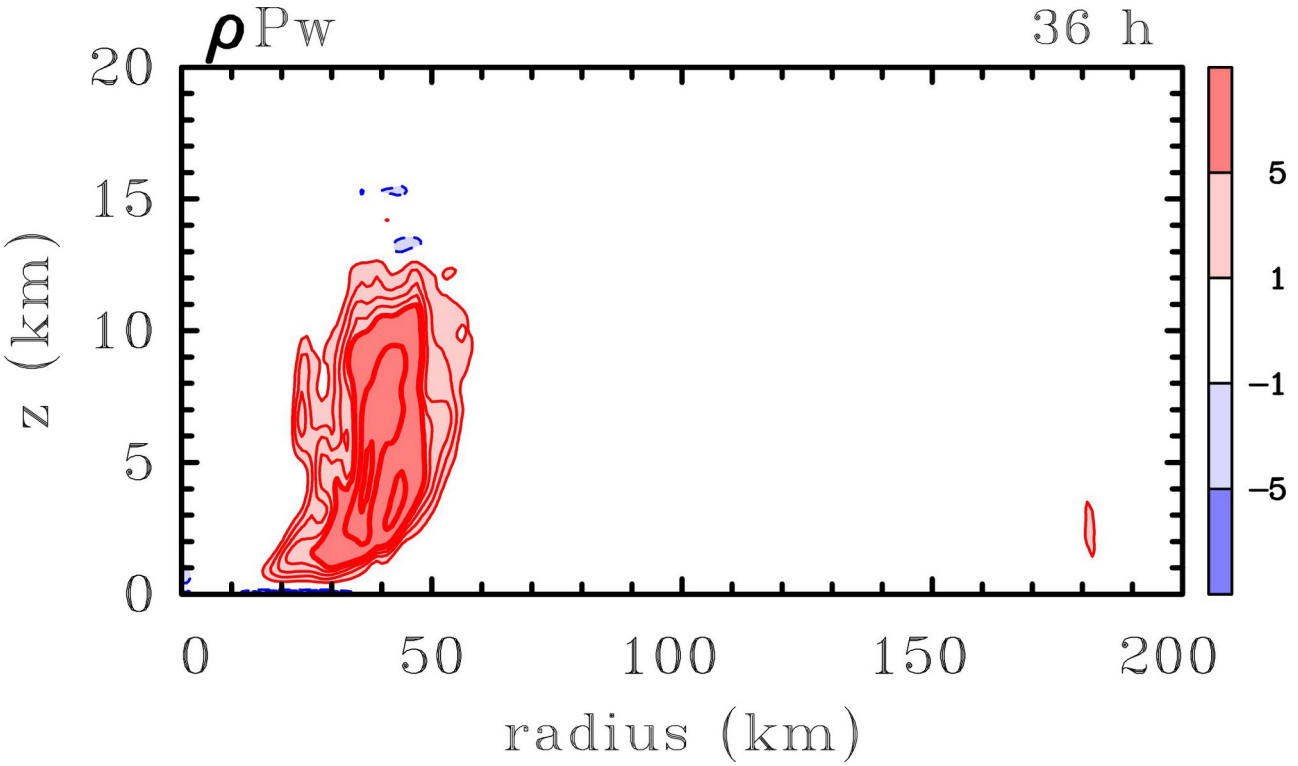

n3_eterms_pw_36h.eps

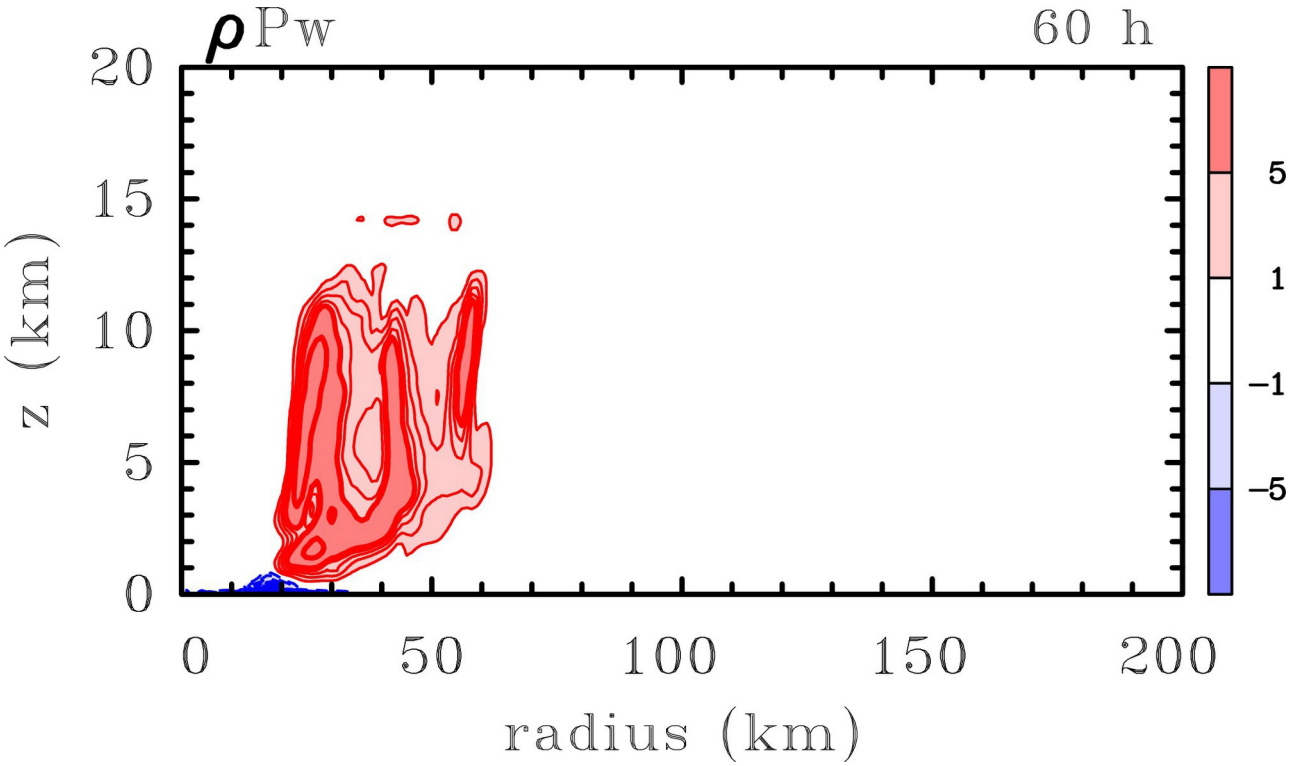

n3_eterms_pw_60h.eps

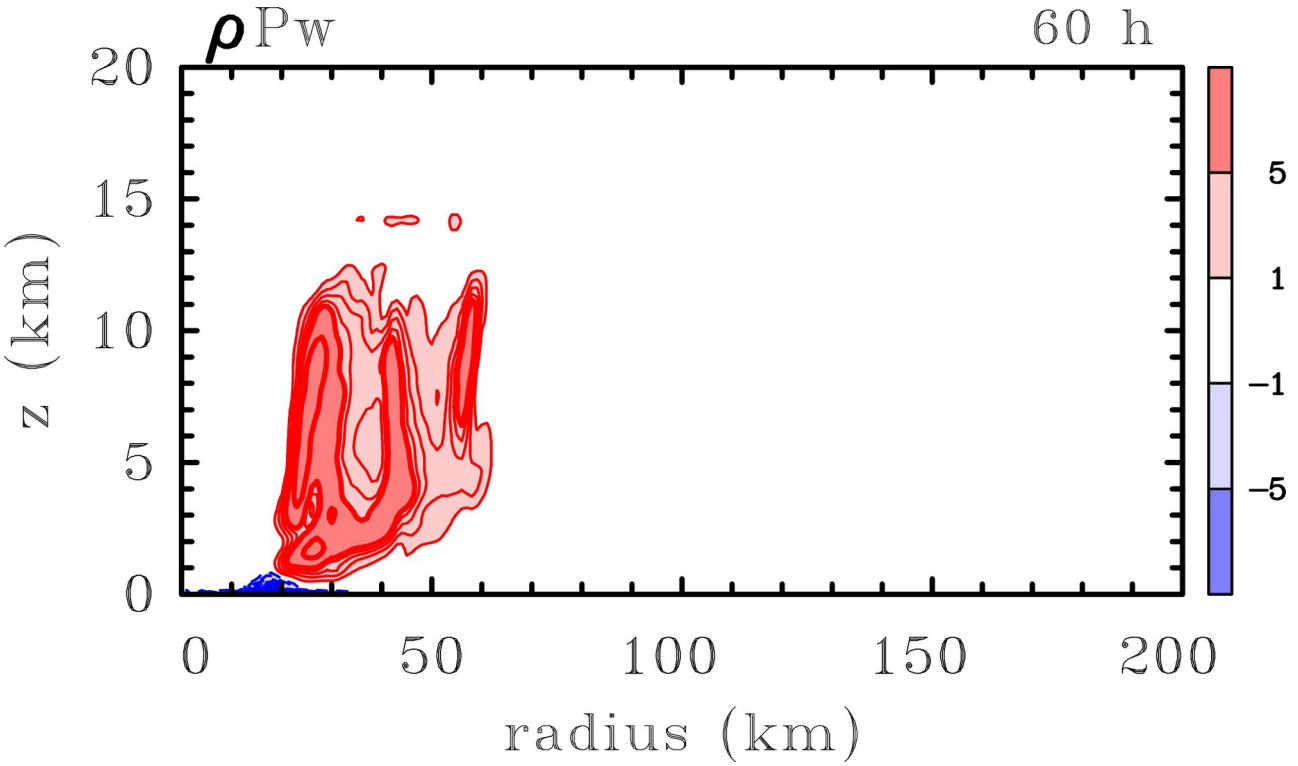

n3_eterms_pw_60h.eps

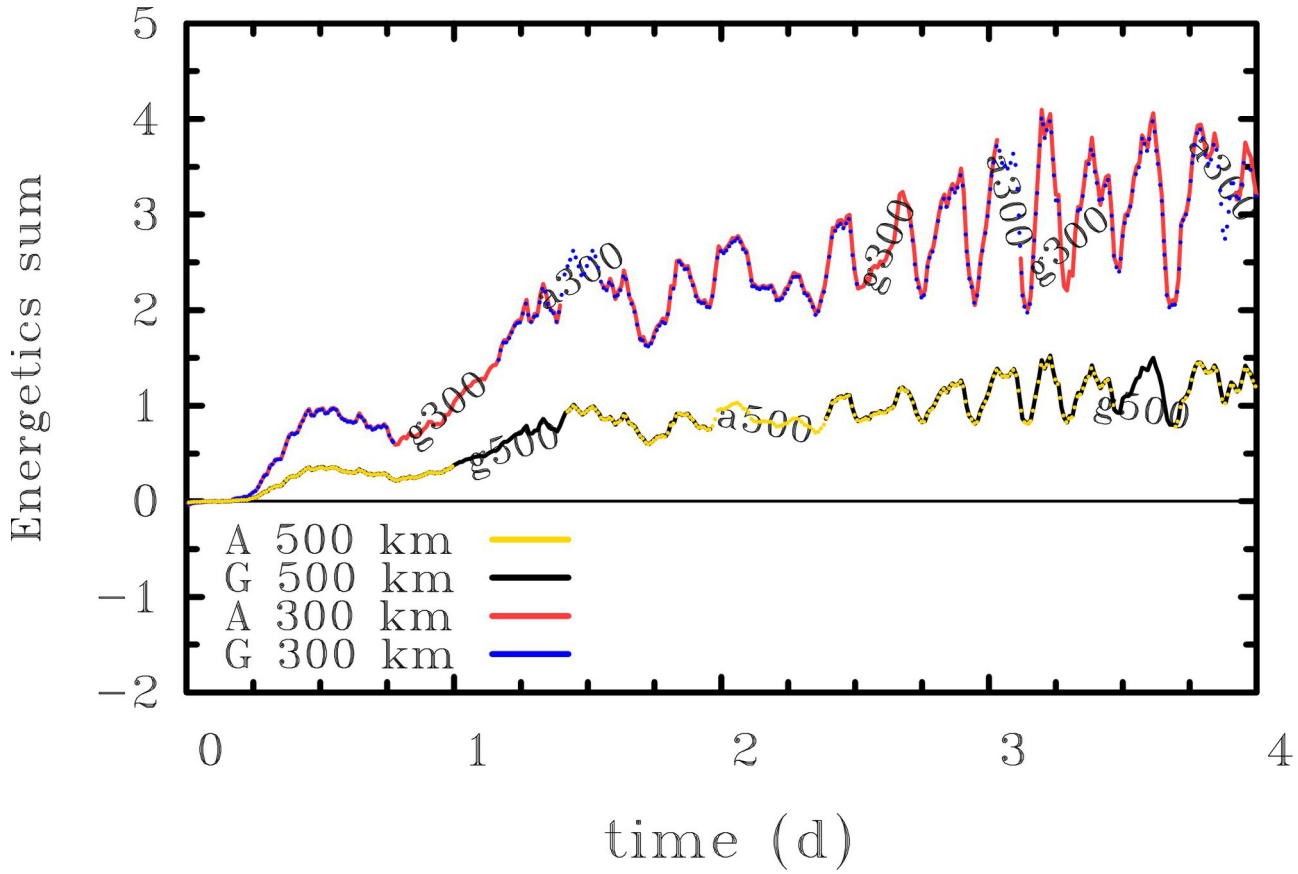

plot_energetics_sum.eps

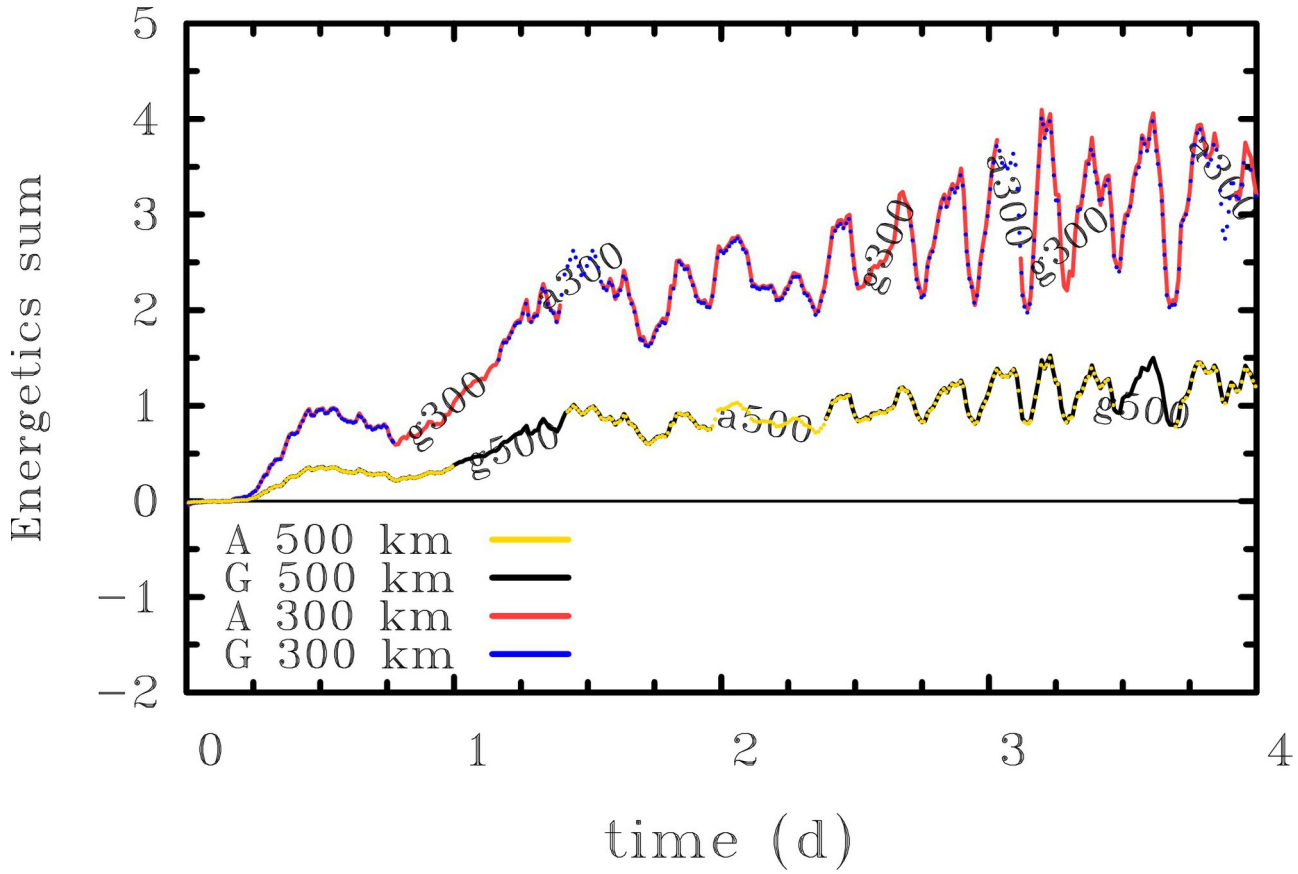

plot_energetics_sum.eps

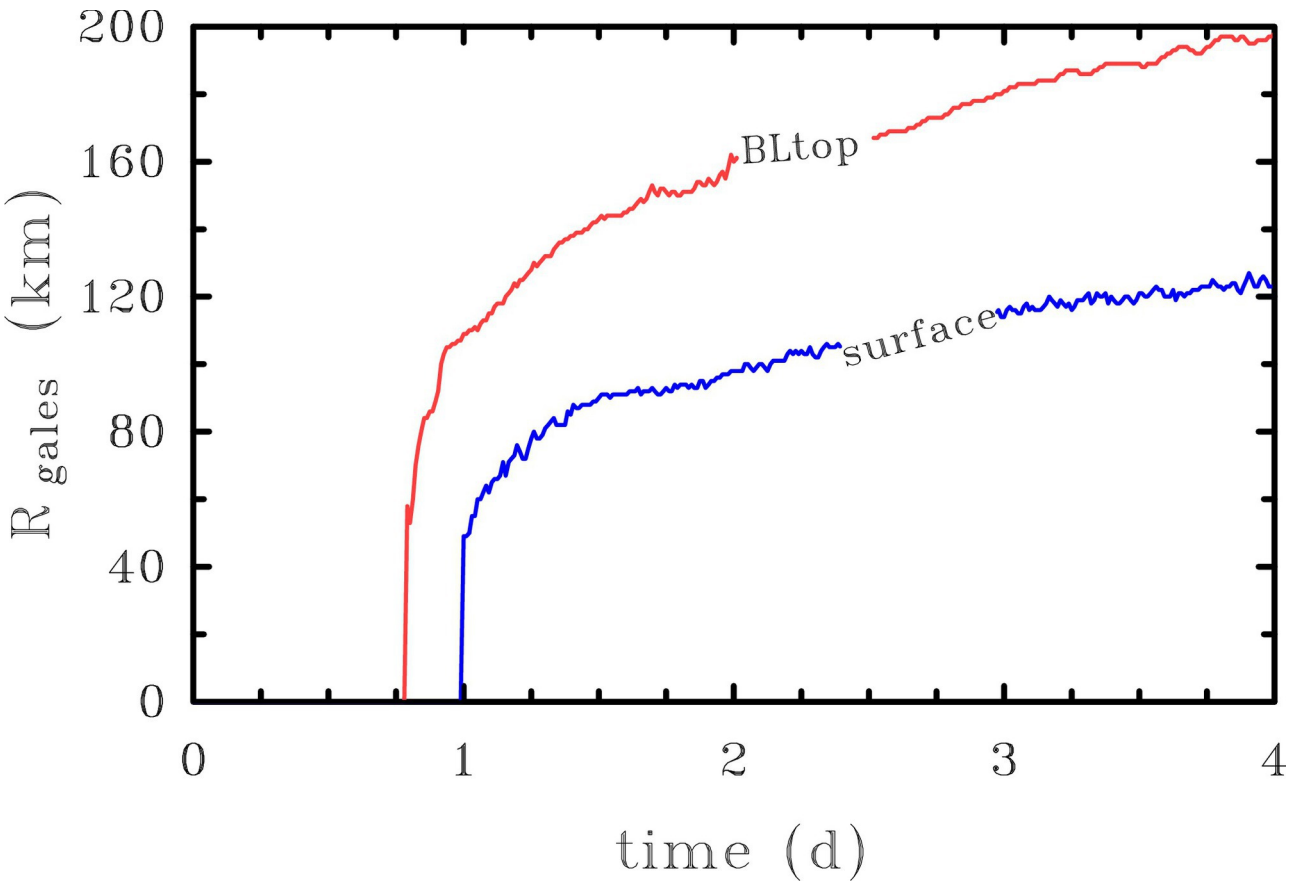

plot_rgales.eps

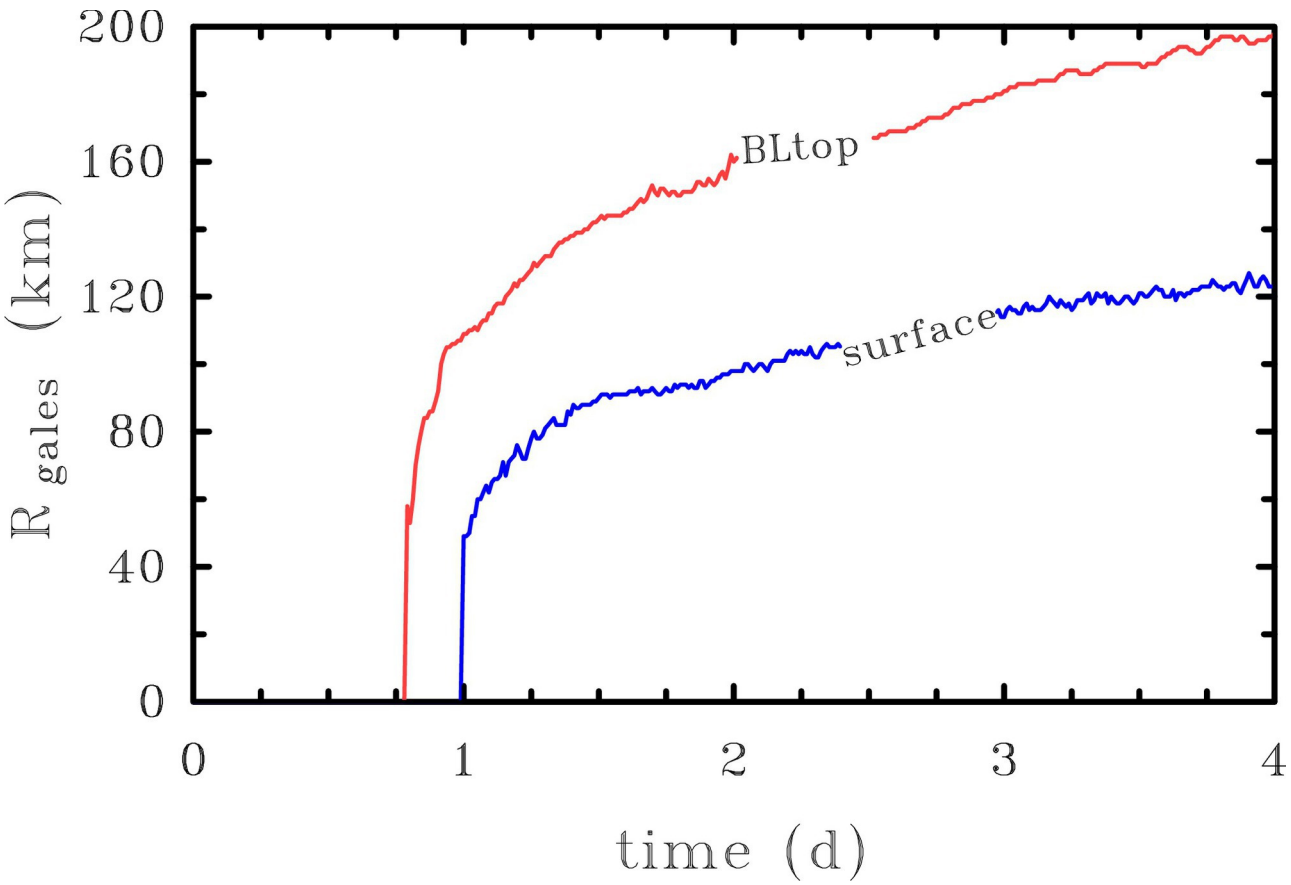

plot_rgales.eps

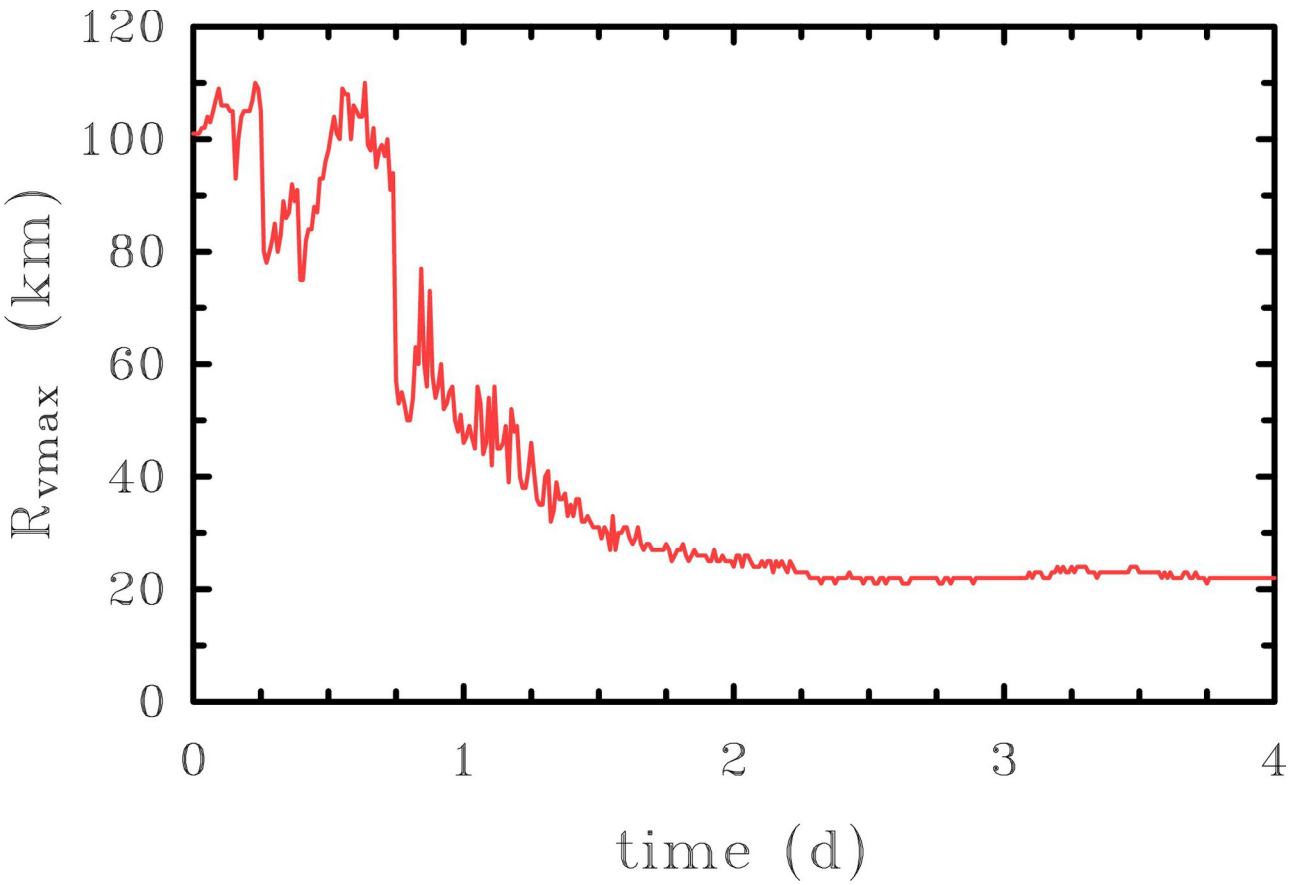

plot_rvmax.eps

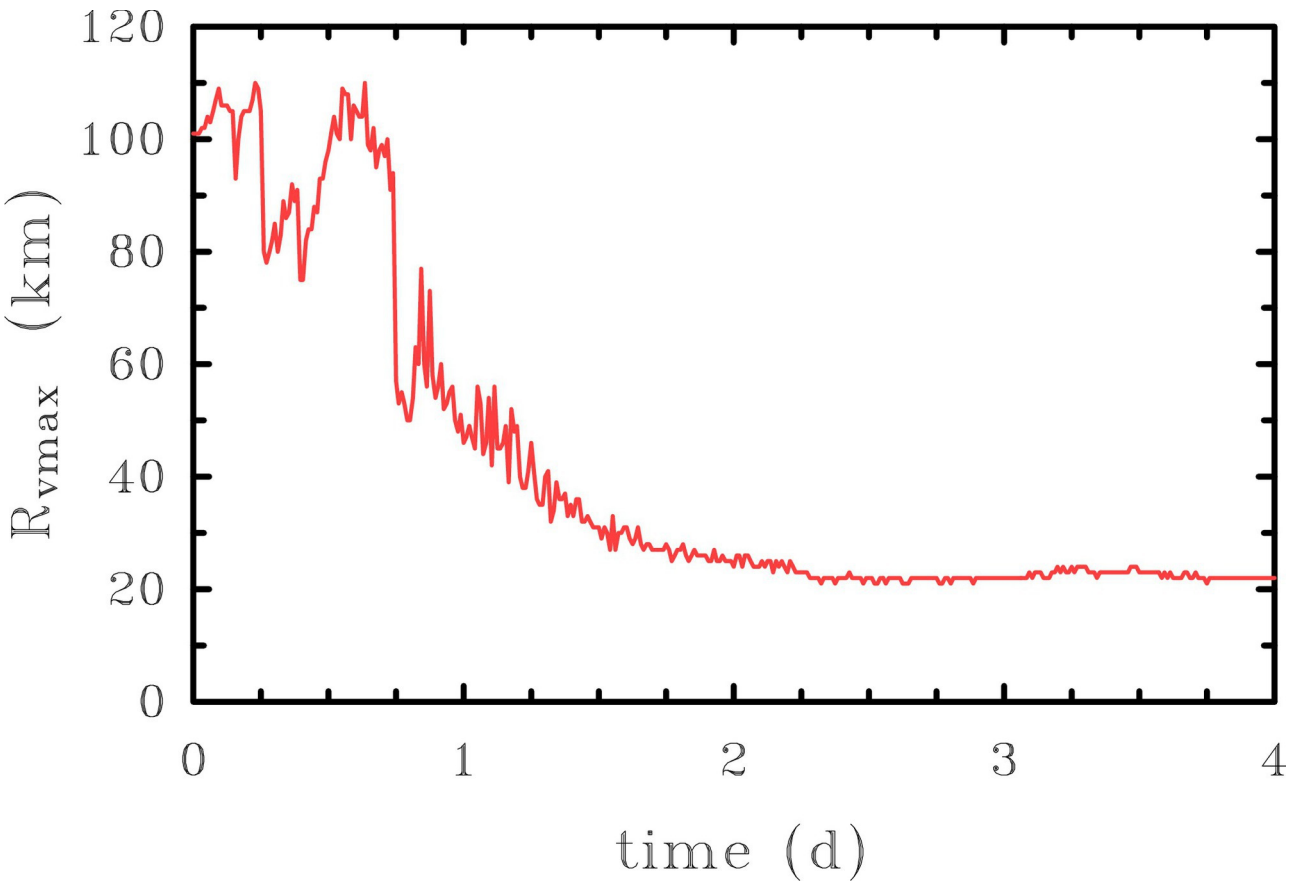

plot_rvmax.eps

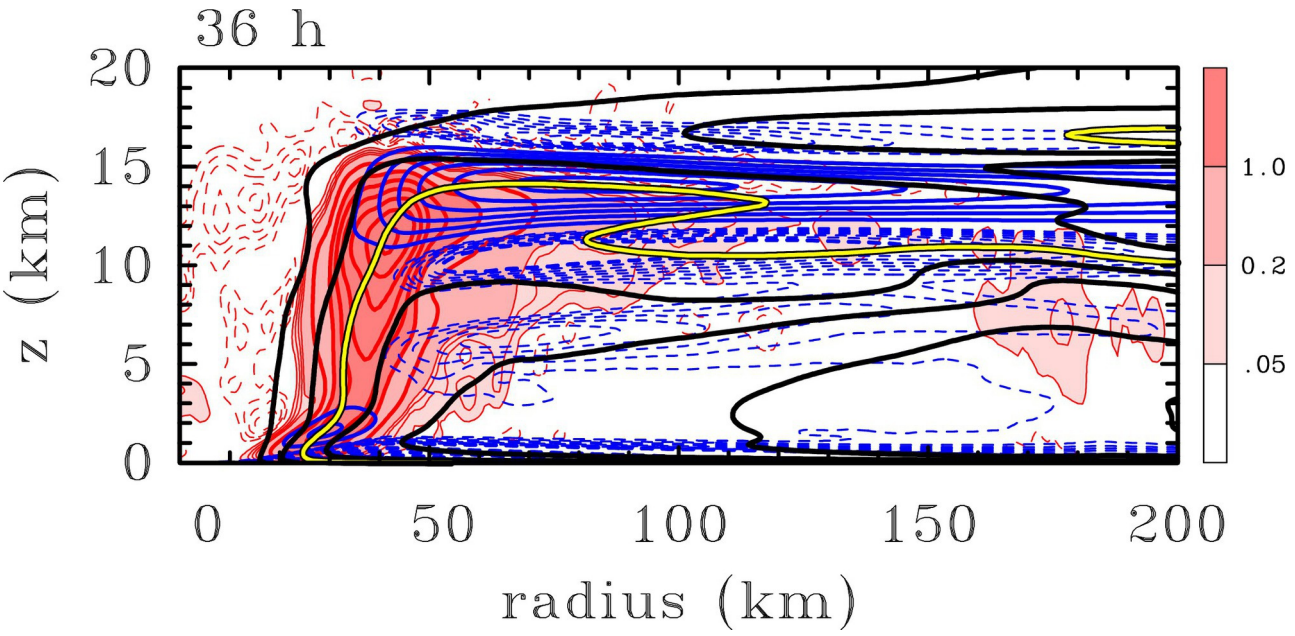

plot_u_thetadot_3h_mean_hr_n3_36h.eps

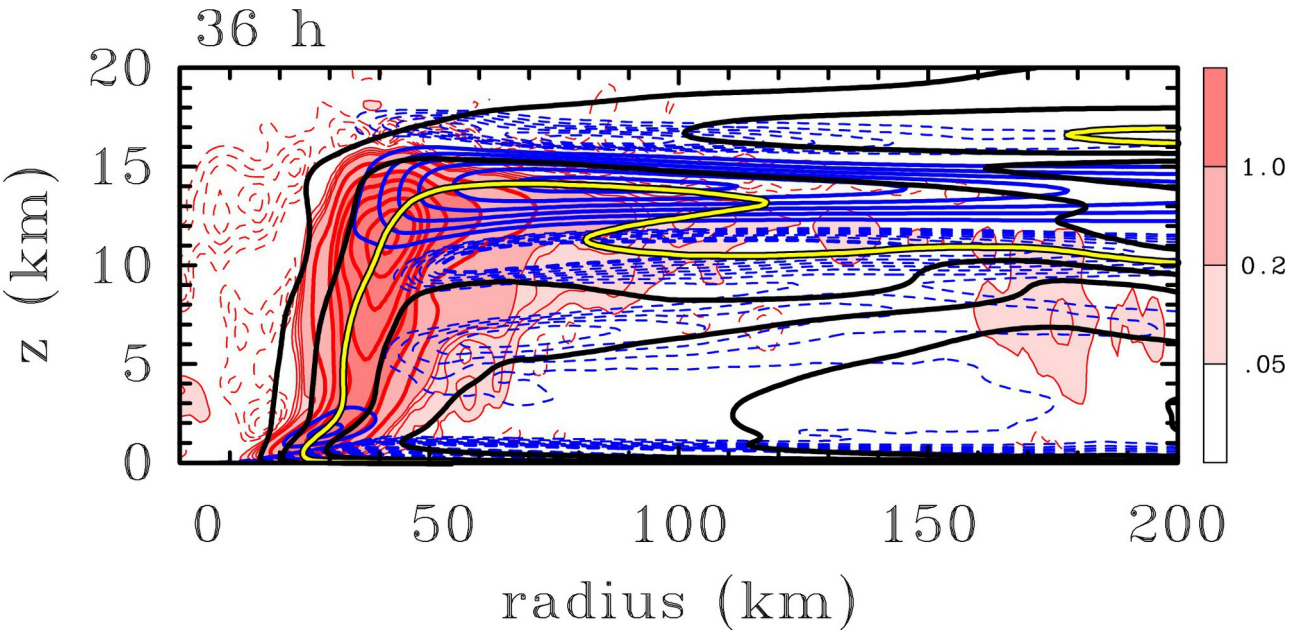

plot_u_thetadot_3h_mean_hr_n3_36h.eps

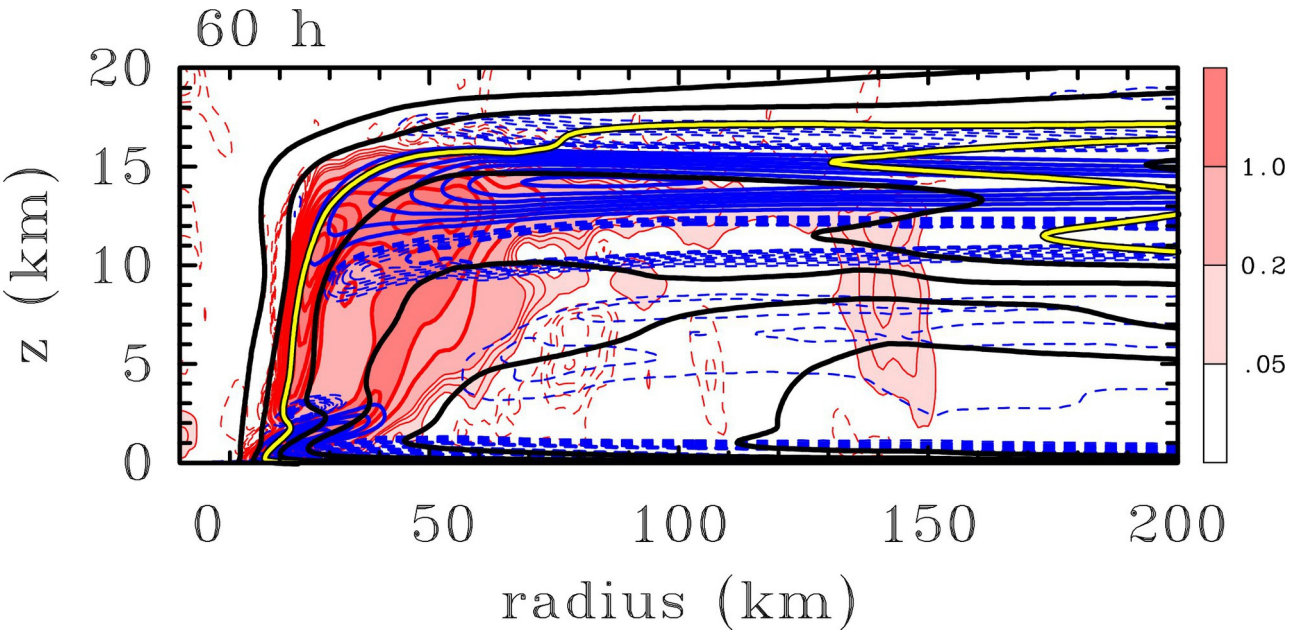

plot_u_thetadot_3h_mean_hr_n3_60h.eps

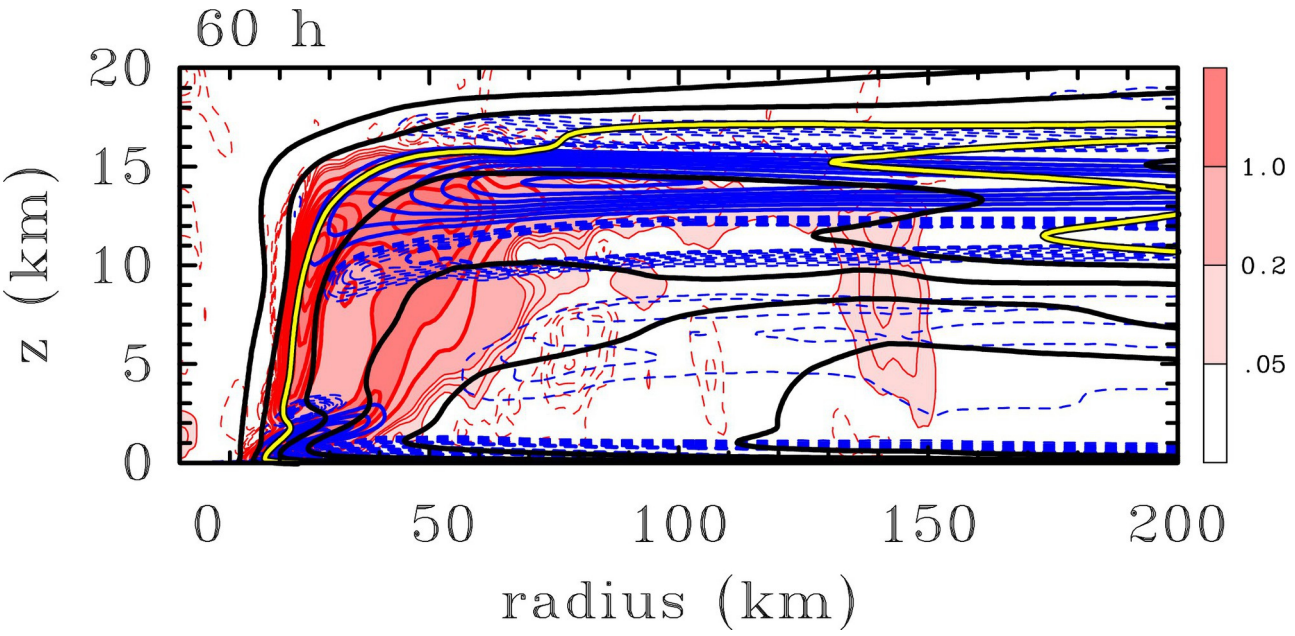

plot_u_thetadot_3h_mean_hr_n3_60h.eps

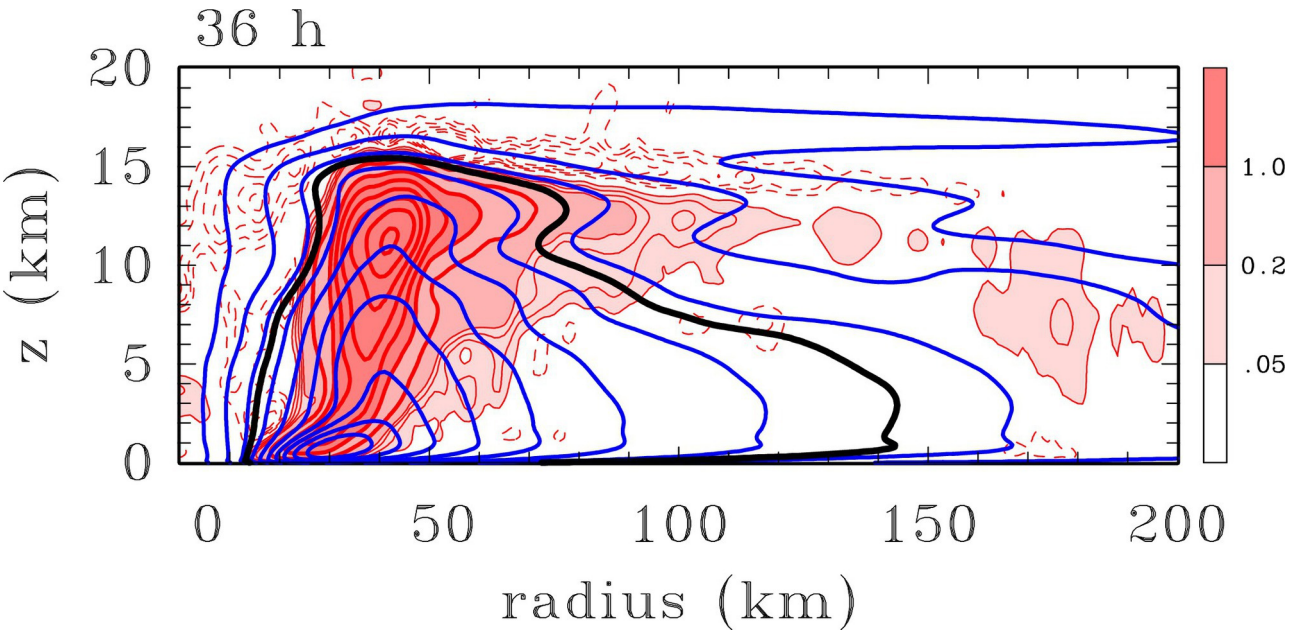

plot_v_thetadot_3h_mean_hr_n3_36h.eps

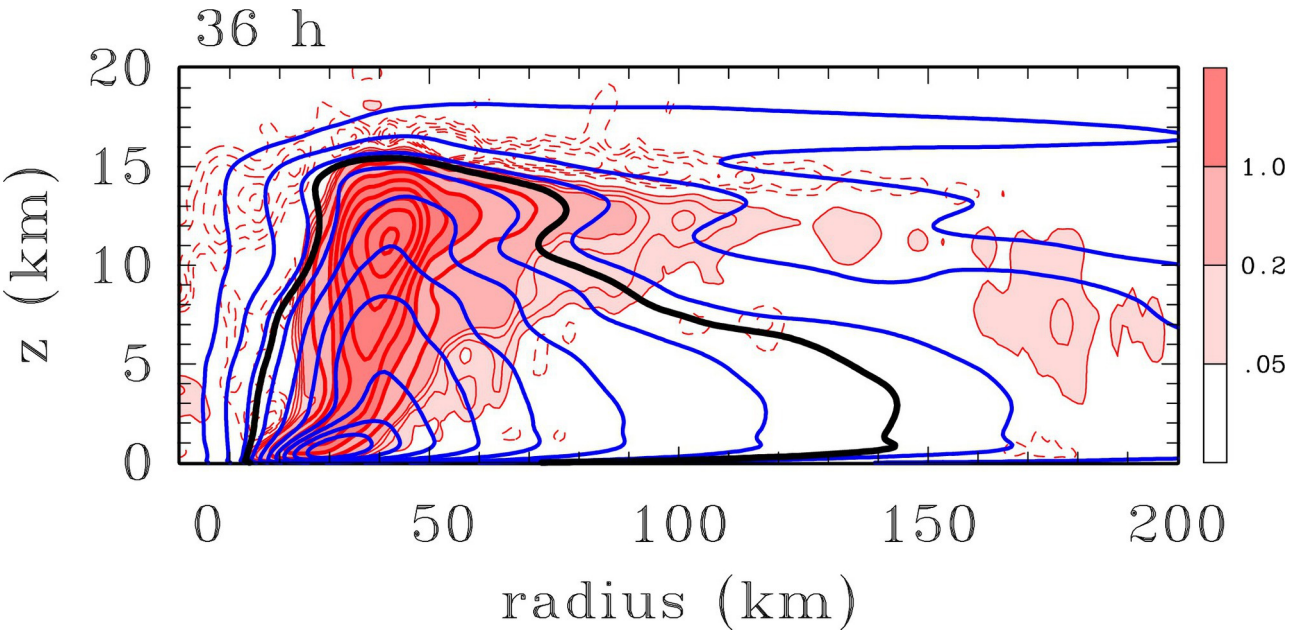

plot_v_thetadot_3h_mean_hr_n3_36h.eps

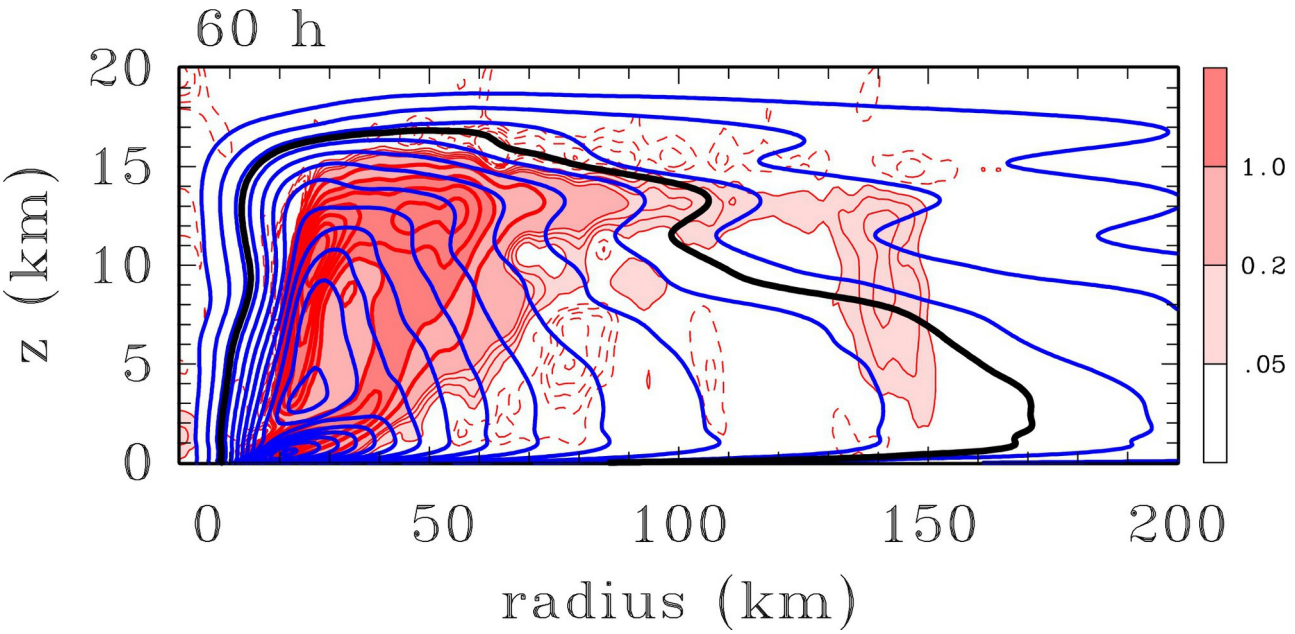

plot_v_thetadot_3h_mean_hr_n3_60h.eps

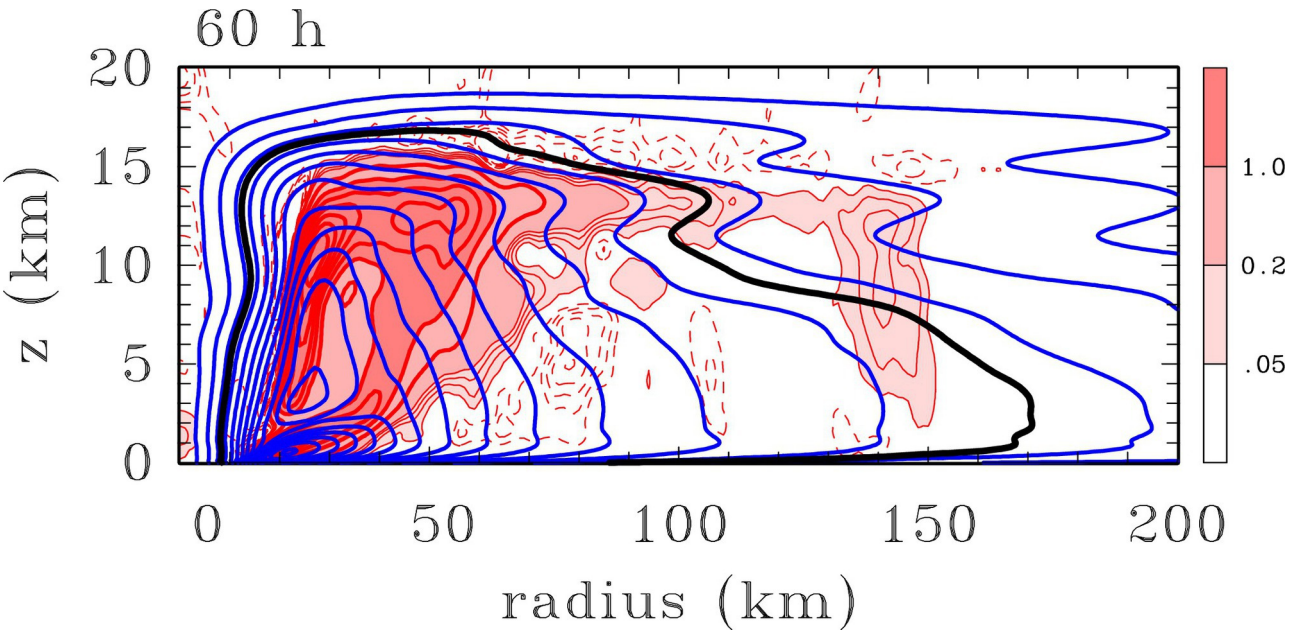

plot_v_thetadot_3h_mean_hr_n3_60h.eps

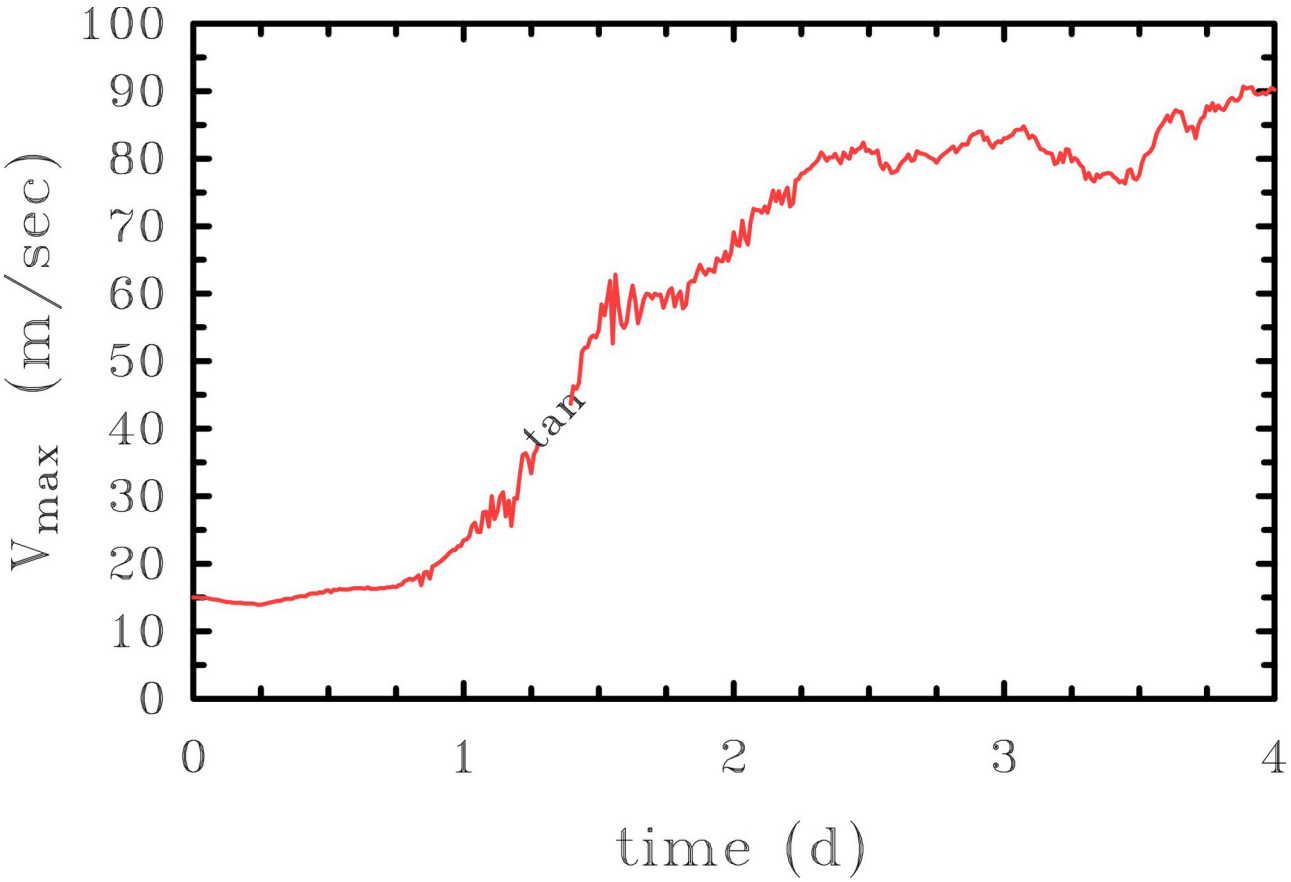

plot_vmax.eps

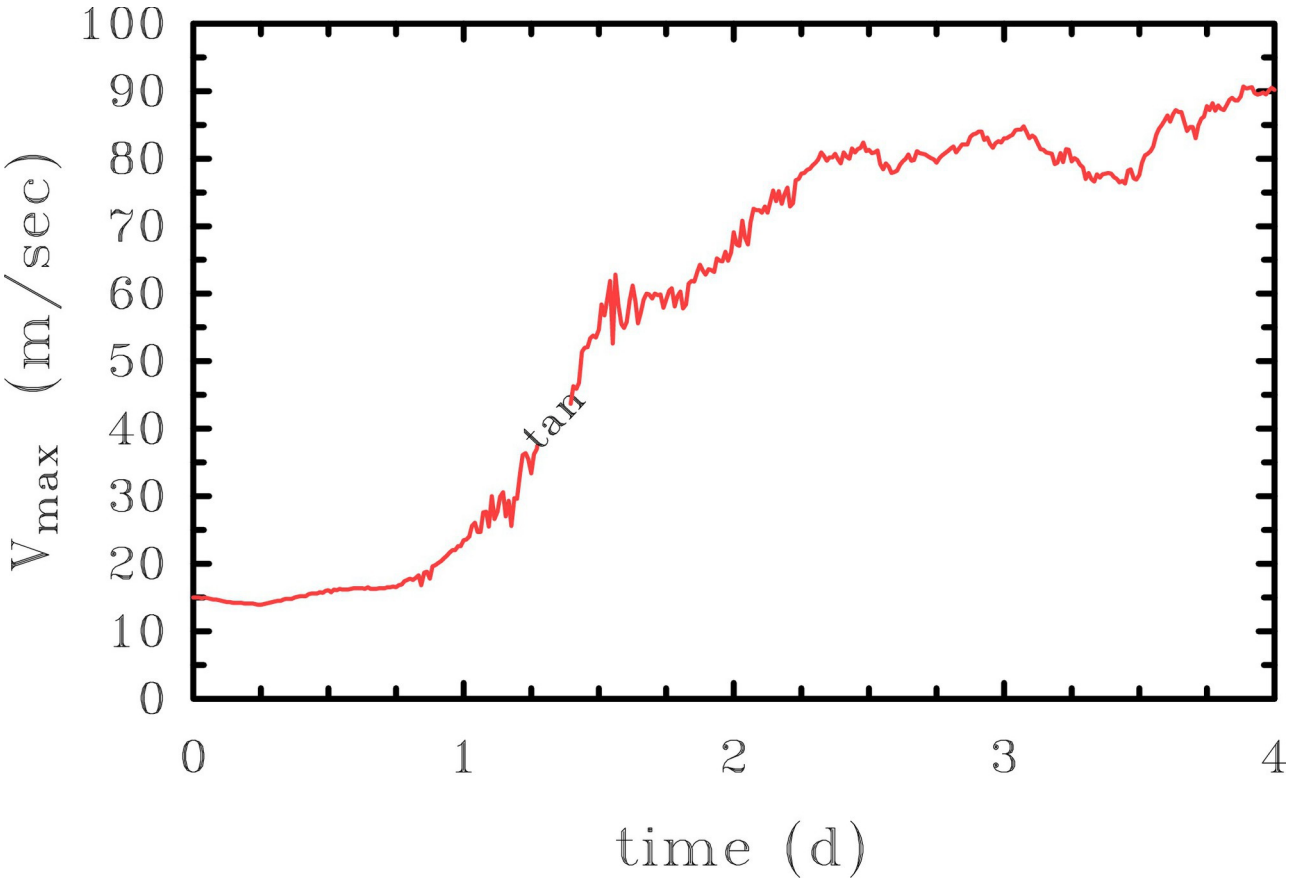

plot_vmax.eps

a Meteorological Institute, Ludwig Maximilians University of Munich, Munich, Germany
b Dept. of Meteorology, Naval Postgraduate School, Monterey, CA
Prof. Roger K. Smith, Meteorological Institute, Ludwig-Maximilians University of Munich, Theresienstr. 37, 80333 Munich, Germany. E-mail: roger.smith@lmu.de

Many previous diagnoses of the global kinetic energy for a tropical cyclone have given prominence to a global integral of a pressure-work term in the generation of kinetic energy. However, in his erudite textbook of atmospheric and oceanic dynamics, Gill (1982) derives a form of the kinetic energy equation in which there is no such explicit source term. In this paper we revisit the interpretations of the generation of kinetic energy given previously in the light of Gill's analysis and compare the various interpretations, which are non-unique.

Further, even though global energetics provide a constraint on the flow evolution, in the context of the kinetic energy equation, they conceal important aspects of energy generation and consumption, a finding that highlights the limitations of a global kinetic energy budget in revealing the underlying dynamics of tropical cyclones.

Tropical cyclone, hurricane, typhoon, spin-up, energetics Fri Jun 29 09:18:27 2018

The generation of kinetic energy in tropical cyclones revisited

Roger K. Smitha, Michael T. Montgomeryb and Gerard Kilroya

Fri Jun 29 09:18:26 2018

1 Introduction

In a classical review paper, Anthes (1974, section DI) summarized the global energetics of tropical cyclones, based in part on the work of Palmén and Jordan (1955) and Palmén and Riehl (1957). In this review he argues that the kinetic energy is dominated by the horizontal velocity components and he derives an expression for the rate-of-generation of kinetic energy, showing that "The important source of kinetic energy production in the hurricane is the radial flow toward lower pressure in the inflow layer, represented by $u\,\partial p/\partial r$." (Here u is the radial velocity component, r is the radius and p is the pressure). In a similar vein, Palmén and Riehl

op. cit. note that "the generation depends on the vertical correlation between radial flow component and pressure gradient which, for production of kinetic energy, must be positive, i.e., the strongest inflow must occur at the strongest inward directed pressure gradient. They conclude that "kinetic energy production within the cyclone can take place only if the cyclone is of the warm core type." Anthes goes on to argue that "This inflow is a result of surface friction, which reduces the tangential wind speed and thereby destroys the gradient balance, so that the inward pressure gradient force exceeds the Coriolis and centripetal forces. In the warm core low the maximum pressure gradient ($\partial p/\partial r < 0$)[1] occurs just above the surface layer, at which the inflow ($u < 0$) is maximum in magnitude. In the outflow layer, where the radial flow is reversed, the pressure gradient is much weaker. The result is a net production of kinetic energy, dominated by the contribution from the inflow region."

The foregoing interpretations seem at odds with the kinetic energy equation in flux form presented by Gill (1982) in which the term $-u\,\partial p/\partial r$ does not appear. Nevertheless, in the context of tropical cyclones, subsequent work has built on the formulation by Palmén and Riehl as reviewed by Anthes (e.g. Kurihara 1975, Tuleya and Kurihara 1975, Frank 1977, DiMego and Bosart 1982, Hogsett and Zhang 2009, Wang *et al.* 2016). The generation of kinetic energy in the context of the global climate is discussed by Peixoto and Oort (1992, section 13.2).

The purpose of this paper is to reconcile the different interpretations of kinetic energy generation and to calculate the various terms in the kinetic energy budget from an idealized high-resolution numerical simulation of a tropical cyclone.

2 Kinetic energy equations

In its most basic form, the momentum equation may be written as

$$\frac{\partial \mathbf{u}}{\partial t} + \mathbf{u}\cdot\nabla\mathbf{u} + \mathbf{f}\wedge\mathbf{u} = -\frac{1}{\rho}\nabla p - g\mathbf{k} - \mathbf{F} \qquad (1)$$

where $\mathbf{u}$ is the three dimensional velocity vector, p is the pressure, ρ is the density, $\mathbf{F}$ is the frictional force opposing the motion, $\mathbf{f} = f\mathbf{k}$, f is the Coriolis parameter ($2\Omega\sin\phi$, where ϕ is latitude and Ω is the earth's rotation rate), g is the acceleration due to gravity, and $\mathbf{k}$ is the unit vector in the vertical direction (here and below, all vector quantities are in bold type). For simplicity, an f-plane is assumed (f = constant) and the Coriolis terms proportional to the cosine of the latitude have been neglected as is customary for geophysical flow analyses off of the equator (e.g., McWilliams 2011).

The kinetic energy equation is obtained by taking the scalar product Equation (1) with $\mathbf{u}$ using the identity $\mathbf{u}\cdot\nabla\mathbf{u} = \nabla(\frac{1}{2}\mathbf{u}^2) + \omega\wedge\mathbf{u}$, where $\omega = \nabla\wedge\mathbf{u}$ is the vorticity vector. This procedure gives:

$$\frac{\partial}{\partial t}(\tfrac{1}{2}\mathbf{u}^2) + \mathbf{u}\cdot\nabla(\tfrac{1}{2}\mathbf{u}^2) = -\frac{1}{\rho}\mathbf{u}\cdot\nabla p - gw - \mathbf{u}\cdot\mathbf{F}, \qquad (2)$$

where $w = \mathbf{k}\cdot\mathbf{u}$ is the vertical component of velocity. Note that the Coriolis force ($-\mathbf{f}\wedge\mathbf{u}$) does not appear in the energy equation because it is orthogonal to $\mathbf{u}$.

An alternative form of the energy equation is obtained by removing some hydrostatically-balanced reference pressure, $p_{ref}(z)$, from (1), where $dp_{ref}/dz = -g\rho_{ref}$

[1] Presumably Anthes meant $\partial p/\partial r > 0$

defines a reference density, ρ_{ref}, that is a function of altitude z. Then, with the substitution $p = p_{ref}(z) + p'$ and $\rho = \rho_{ref}(z) + \rho'$, the first two terms on the right-hand-side of Equation (1), $-(1/\rho)\nabla p - g\mathbf{k}$, become $-(1/\rho)\nabla p' + b\mathbf{k}$, where $b = -g(\rho - \rho_{ref})/\rho$ is the buoyancy force of an air parcel per unit mass. Then, Equation (2) becomes

$$\frac{\partial}{\partial t}\left(\frac{1}{2}\mathbf{u}^2\right) + \mathbf{u}\cdot\nabla\left(\frac{1}{2}\mathbf{u}^2\right) = -\frac{1}{\rho}\mathbf{u_h}\cdot\nabla_h p' + Pw - \mathbf{u}\cdot\mathbf{F}, \tag{3}$$

where $\mathbf{u_h}$ is the horizontal velocity vector, ∇_h is the horizontal gradient operator and

$$P = -\frac{1}{\rho}\frac{\partial p}{\partial z} - g = -\frac{1}{\rho}\frac{\partial p'}{\partial z} + b \tag{4}$$

is the net vertical perturbation gradient force per unit mass. Despite the explicit appearance of p' in the first term on the right-hand-side, all the terms in Equation (3) are independent of the reference pressure $p_{ref}(z)$, since, in particular, $\mathbf{u_h}\cdot\nabla_h p_{ref}(z) = 0$. For simplicity, we take $p_{ref}(z)$ and $\rho_{ref}(z)$ to be the ambient pressure and density, respectively, assuming that these are in hydrostatic equilibrium. Then p' vanishes at large distances from the vortex axis.

We examine now the different forms of Equation (3) derived by Anthes (1974), Gill (1982), and others beginning with a slight modification of Gill's formulation.

2.1 Modified Gill's formulation

In essence, Gill's formulation of the kinetic energy equation is as follows. Using the result that for any scalar field, γ,

$$\rho\frac{D\gamma}{Dt} = \frac{\partial}{\partial t}(\rho\gamma) + \nabla\cdot(\rho\gamma\mathbf{u}), \tag{5}$$

where $D/Dt = \partial/\partial t + \mathbf{u}\cdot\nabla$ is the material derivative (see Gill 1982, Equation 4.3.6)[2], the material form of Equation (3) times ρ may be written in flux form as

$$\frac{\partial}{\partial t}\left(\frac{1}{2}\rho\mathbf{u}^2\right) + \nabla\cdot\mathbf{F_{KE}} = p'\nabla_h\cdot\mathbf{u_h} + \rho Pw + \frac{\partial(p'w)}{\partial z} - \rho\mathbf{u}\cdot\mathbf{F}, \tag{6}$$

where

$$\mathbf{F_{KE}} = \left(p' + \frac{1}{2}\rho\mathbf{u}^2\right)\mathbf{u}, \tag{7}$$

is the *mechanical energy flux density vector* (Gill, 1982, cf. Equation 4.6.4).

The global kinetic energy budget can be obtained by integrating Equation (6) over a cylindrical volume of space, V, of radius R and height H centred on the storm and using the boundary conditions that $u = 0$ at $r = 0$, and $w = 0$ at $z = 0$ and $z = H$. Here, we use a cylindrical coordinate system (r, λ, z) centred on the vortex, where r is the radius, λ is the azimuth and z is the height. We denote an integral of the quantity χ over the volume V by

$$\overline{[\chi]} = \frac{1}{\pi R^2 H}\int_0^R r\,dr \int_0^{2\pi} d\lambda \int_0^H \chi\,dz$$

Then (6) becomes MODIFIED GILL'S FORM

[2] If the density refers to that of a moist air parcel consisting of dry air, water vapour and liquid water, the density is conserved only if the liquid water component is suspended in the parcel. In the presence of precipitation, there will be a small source or sink of density associated with the flux divergence of falling precipitation. In what follows, we will ignore the effects of this source/sink term in the kinetic energy budget.

$$\frac{d}{dt}\overline{\left[\frac{1}{2}\rho\mathbf{u}^2\right]} = \overline{[p'\nabla_h\cdot\mathbf{u_h}]} + \overline{[\rho Pw]} - F_{KEG} - D, \tag{8}$$

where

$$F_{KEG} = \frac{1}{\pi R^2 H}\int_0^{2\pi} d\lambda \int_0^H \left[u(p' + \frac{1}{2}\rho\mathbf{u}^2)\right]_{r=R} dz, \tag{9}$$

is the *flux of mechanical energy* through the side boundary $r = R$, and for a Newtonian fluid with dynamic viscosity coefficient μ,

$$D = \overline{[\mu\Phi_v]}, \tag{10}$$

where, in cylindrical coordinates,

$$\begin{aligned}\Phi_v = 2&\left[\left(\frac{\partial u}{\partial r}\right)^2 + \left(\frac{1}{r}\frac{\partial v}{\partial\lambda} + \frac{u}{r}\right)^2 + \left(\frac{\partial w}{\partial z}\right)^2\right]\\ &+ \left[r\frac{\partial}{\partial r}\left(\frac{v}{r}\right) + \frac{1}{r}\frac{\partial u}{\partial\lambda}\right]^2 + \left[\frac{1}{r}\frac{\partial w}{\partial\lambda} + \frac{\partial v}{\partial z}\right]^2\\ &+ \left[\frac{\partial u}{\partial z} + \frac{\partial w}{\partial r}\right]^2 - \frac{2}{3}(\nabla\cdot\mathbf{u})^2\end{aligned} \tag{11}$$

is the dissipation function[3]. Here, v is the tangential wind component.

Since $\nabla_h\cdot\mathbf{u_h}$ is the fractional change in the horizontal area of an air parcel per unit time, the first term on the right-hand-side of Equation (8) is the cumulative effect of the kinetic energy generated locally when an air parcel with positive perturbation pressure expands in the horizontal or one with a negative perturbation pressure contracts in the horizontal. The second term on the right-hand-side of this equation represents the rate of kinetic energy production by air rising in the presence of a positive net vertical perturbation pressure gradient force ($P > 0$) and air sinking in the presence of a negative net vertical perturbation pressure gradient force ($P < 0$). In Gill's original formulation, the net vertical perturbation pressure gradient force term in Equation (8) is replaced by a buoyancy force, which, by itself, is a non-unique force, and the second term on the right-hand-side is replaced by $\nabla\cdot\mathbf{u}$, which is the fractional change in volume of an air parcel. Note that, in Gill's formulation, there is no term corresponding with $u\,\partial p/\partial r$ (or equivalently $u\,\partial p'/\partial r$) in Anthes' formulation of the problem, which a number of authors have argued is the key term in generating kinetic energy.

2.2 Generalized Anthes' formulation

As noted above, Anthes reasonably supposes that the vertical velocity makes only a small contribution to the global kinetic energy and his derivation of the kinetic energy equation is based on the horizontal momentum equations only and the neglect of the contribution from $\frac{1}{2}w^2$ in the kinetic energy. Nevertheless, Anthes retains the vertical velocity component in the advection term $\mathbf{u}\cdot\nabla\mathbf{u}$ in Equation (1) and $\mathbf{u}\cdot\nabla(\frac{1}{2}\mathbf{u}^2)$ in Equation (2). A slightly generalized form of Anthes' equation follows directly from ρ times Equation (3), which in flux form

[3] Equation (8) is, in essence, the kinetic energy equation for the Reynolds averaged flow in which the quantity μ is a turbulent eddy counterpart. In this case, we are presuming that a K-theory closure is adequate so that the Reynolds averaged equations look essentially like the Newtonian fluid formulation. Further, in the mechanical energy flux through the side boundary in Equation (9) we have neglected the eddy diffusive radial flux of kinetic energy. Relative to the advective flux of kinetic energy, the diffusive flux scales as the inverse Reynolds number of the flow, which is always small compared to unity outside of the surface layer. This conclusion is based on recently obtained estimates of the turbulent eddy diffusivity observed in major hurricanes on the order of $50 - 100\,\mathrm{m^2\,s^{-1}}$ (Zhang *et al*. 2011).

analogous to (6) is

$$\frac{\partial}{\partial t}\left(\frac{1}{2}\rho\mathbf{u}^2\right) + \nabla\cdot\mathbf{F}_{\mathbf{KEA}} = -\mathbf{u_h}\cdot\nabla_h p' + \rho P w - \rho\mathbf{u}\cdot\mathbf{F}, \tag{12}$$

where

$$\mathbf{F}_{\mathbf{KEA}} = \left(\frac{1}{2}\rho\mathbf{u}^2\right)\mathbf{u}. \tag{13}$$

Again integrating over the cylinder, Equation (12) becomes GENERALIZED ANTHES' FORM

$$\frac{d}{dt}\overline{\left[\frac{1}{2}\rho\mathbf{u}^2\right]} = -\overline{[\mathbf{u_h}\cdot\nabla_h p']} + \overline{[\rho P w]} - F_{KEA} - D, \tag{14}$$

where

$$F_{KEA} = \frac{1}{\pi R^2 H}\int_0^{2\pi} d\lambda \int_0^H \left[u\left(\frac{1}{2}\rho\mathbf{u}^2\right)\right]_{r=R} dz. \tag{15}$$

Equation (14) is a generalization of Anthes' formulation to include the three-dimensional wind vector in the definition of kinetic energy and the rate of working of the net vertical perturbation gradient force per unit volume, $\overline{[\rho P w]}$, which is a non-hydrostatic effect. As in Anthes' original form, the pressure-work term, $-\overline{[\mathbf{u_h}\cdot\nabla_h p']}$, appears explicitly in the global form of the kinetic energy equation. For an axisymmetric flow, this term is simply $\overline{[-u\,\partial p/\partial r]}$ and, at first sight, one might question its prominence as a source of kinetic energy, since $\partial p/\partial r$ is *not* the only radial force acting on fluid parcels en route to the storm core. Above the frictional boundary layer, the radial pressure gradient is closely balanced by the sum of the centrifugal force and the radial component of the Coriolis force. Moreover, this source term does not appear in Gill's formulation (cf. Eq. (8)), although it is replaced by the term $\overline{[p'\nabla_h\cdot\mathbf{u_h}]}$ and the boundary flux terms are different. Even so, one should bear in mind that even in the axisymmetric case, $\overline{[-u\,\partial p/\partial r]}$ is generating *not only a radial contribution to the kinetic energy, but also an azimuthal contribution* through the action of the generalized Coriolis force $(f+v/r)u$. The generation of this azimuthal contribution is implicit in the kinetic energy equation as the generalized Coriolis force does no work, but it does convert radial momentum to tangential momentum.

3 Kinetic energy budget for an idealized simulation

We examine now the generation terms in the two forms of the kinetic energy equation for the case of an idealized tropical cyclone simulation. We begin with a brief description of the numerical model and go on to present the results.

3.1 The numerical model

The numerical model used for this study is Bryan's three-dimensional, nondydrostatic cloud model (CM1), version 16 (Bryan and Fritsch, 2002). The simulations relate to the prototype problem for tropical cyclone intensification, which considers the evolution of an initially axisymmetric, cloud-free, warm-cored, baroclinic vortex in a quiescent environment on an f-plane. The initial vortex is in thermal wind balance. A latitude of 20 ^{o}N and a constant sea surface temperature of 28 ^{o}C are assumed. The model configuration is more or less the same as

described in section 2 of Črnivec *et al.* (2016). The differences are that, following the work of Mapes and Zuidema (1996), a more realistic time scale for Newtonian relaxation to the temperature field (10 days) is applied here instead of the previous default value in CM1 (12 h). Further, an open boundary condition is taken at lateral boundaries instead of rigid walls and the Dunion moist tropical sounding is used as the environmental sounding (Dunion 2011).

The initial tangential wind speed has a maximum of 15 m s $^{-1}$ at the surface at a radius of 100 km. The tangential wind speed decreases sinusoidally with height, becoming zero at a height of 20 km. Above this height, up to 25 km, the tangential wind is set to zero. The balanced pressure, density and temperature fields consistent with this prescribed tangential wind distribution are obtained using the method described by Smith (2006). The calculations are carried out for a period of 4 days with data output every 15 min.

(a)
(b)
(c)

Figure 1: Time series of (a) maximum azimuthally-averaged tangential wind speed (V_{max}). Panel (b) shows the radius R_{vmax} at which the maximum tangential wind speed occurs (V_{max}). Panel (c) shows the radius at which gale force winds occurs (R_{gales}), where R_{gales} calculated at a height of 1 km, and corresponds to the radius of 17 m s $^{-1}$ total winds outside the eyewall.

3.2 A few details of the simulation

Figure 1 summarizes the vortex evolution in the simulation. Panel (a) shows time series of the maximum azimuthally-averaged tangential wind speed, V_{max}, and panel (b) shows the radius R_{vmax} at which V_{max} occurs. Typically, V_{max} is located a few hundred meters above the surface, within a shallow inflow layer. The evolution is broadly similar to that described in Kilroy *et al.* (2016), who used a different numerical model and a much coarser horizontal resolution (horizontal grid spacing 5 km compared with 1 km used here). In brief, after a gestation for about a day during which deep convection becomes established inside R_{vmax}, the vortex undergoes a rapid intensification phase lasting about 36 h, before reaching a quasi-steady state. Initially R_{vmax} is located at a radius of 100 km, but contracts to a little more than 20 km after about $2\frac{1}{4}$ days. The most rapid contraction occurs during the rapid intensification phase as absolute angular momentum surfaces are drawn inwards quickly within and above the boundary layer.

Figure 1(c) shows the outermost radius of gale-force winds, R_{gales}, defined here as the radius of 17 m s $^{-1}$ azimuthally-averaged tangential winds at a height of 1 km, which is approximately at the top of the frictional boundary layer. Shown also is R_{galesF}, defined as the (outer) radius at which the total wind speed at any grid point at a height of 10 m is 17 m s $^{-1}$. Both quantities serve as a measure of the vortex size, R_{galesF} being closest to the quantity used by forecasters[4], but R_{gales} being a preferred measure from a theoretical viewpoint (Kilroy *et*

[4] Based on the wind speed in a particular sector and not azimuthally averaged.

al. 2016). The evolution of storm size based on R_{galesF} is similar to that based on R_{gales}, although R_{gales} always exceeds the value of R_{galesF}. After 4 days, R_{gales} exceeds R_{galesF} by about 80 km.

Figure 3.2 shows vertical cross sections of the azimuthally-averaged, 3 h time averaged, radial and tangential velocity components, the vertical velocity component, and the M-surfaces during the intensification phase of the vortex. The time averages are centred on 36 h during the period of rapid intensification and at 60 h near the end of this period. The basic features of the flow are qualitatively similar at both times, but all three velocity components strengthen over the period, the M-surfaces moving inwards in the lower troposphere and outwards in the upper troposphere. The flow structure is similar to that which has been described in many previous studies (see e.g. the recent review by Montgomery and Smith 2017a and refs.) with a layer of strong shallow inflow marking the frictional boundary layer, a layer of weaker inflow in the lower troposphere, a region of strong outflow in the upper troposphere and a layer of enhanced inflow below the outflow. The maximum tangential wind speed occurs within, but near the top of the frictional boundary layer[5]. Much of the ascent occurs in an annular region on the order of 50-60 km in radius. The region inside this annulus shows mostly descent.

(a) (b)
(c) (d)

Left panels: Vertical cross sections of the azimuthally-averaged, 3 hour time averaged tangential velocity component (blue contours) centred at 36 h and 60 h. Superimposed are contours and shading of the averaged vertical velocity. Contour intervals are as follows. Tangential velocity: blue contours every 5 m s $^{-1}$, with a thick black contour highlighting the 17 m s $^{-1}$ contour. Vertical velocity: thin red contours every 0.05 m s $^{-1}$ to 0.2 m s $^{-1}$, thick red contour interval 0.5 m s $^{-1}$, thin dashed red contours indicate subsidence at intervals of 0.02 m s $^{-1}$. Right Panels: Vertical cross sections of the azimuthally-averaged, 3 hour time averaged radial velocity component together with the averaged vertical velocity centred at the same times. Contour intervals are as follows. Radial velocity: thick blue contours 4 m s $^{-1}$, dashed negative, thin blue dashed contours every 0.5 m s $^{-1}$ down to -3.5 m s $^{-1}$. Absolute angular momentum: thick black contours every 2×10^5 m ^{2} s $^{-1}$, with the 6×10^5 m ^{2} s $^{-1}$ contour highlighted in yellow.

3.3 Kinetic energy evolution

Figure 2 shows time series of the domain-averaged kinetic energy per unit mass, $\overline{\left[\frac{1}{2}\rho\mathbf{u}^2\right]}$, for domain radii 300 km and 500 km and a domain height of 20 km. As anticipated by Anthes (1974), this quantity is dominated by the horizontal velocity components: in fact, the curves for $\overline{\left[\frac{1}{2}\rho\mathbf{u}^2\right]}$ and $\overline{\left[\frac{1}{2}\rho\mathbf{u}_\mathbf{h}^2\right]}$ essentially overlap. It follows that the contribution of the vertical

[5] At 60 h, the tangential wind field exhibits a second local maximum in the eyewall. This is a transient feature that is presumably associated with a centrifugal wave near the base of the eyewall (e.g. Montgomery and Smith 2017, p550) excited by an elevated pulse of boundary layer outflow shortly before. This feature is not seen at 48 h or 72 h and its presence doesn't alter the findings concerning the kinetic energy budget.

velocity to the global kinetic energy is negligible. Notable features of the curves for both domain sizes are the slight decrease during the first 12 h on account of surface friction, followed by a rapid increase as the vortex intensifies. As time proceeds, the rate of increase progressively declines.

3.4 Kinetic energy generation: Anthes' formulation

Figure 3 shows time series of the principal terms in the generalized Anthes formulation (the right-hand-side of Equation (14)), excluding only the global dissipation term since the focus of the paper is on kinetic energy generation. For both domain radii, 300 km (Fig. 4(a)) and 500 km (Fig. 4(a)), both the terms $\overline{[-\mathbf{u_h} \cdot \nabla_h p']}$ and $\overline{[\rho P w]}$ are positive, but, perhaps surprisingly, the former term is not appreciably larger than the latter, even beyond 2 days when the differences are largest. The boundary flux term F_{KEA} is virtually zero throughout the calculation. For the larger domain size (R = 500 km), the temporal behaviour of the various terms is similar, but, as expected, the magnitudes of the respective terms are appreciably smaller (Fig. 4(b)), since the largest contributions to the averages are from well inside a 300 km radius (note the different scales on the ordinate in Figs. 4(a) and 4(b)).

The finding that the two terms $\overline{[-\mathbf{u_h} \cdot \nabla_h p']}$ and $\overline{[\rho P w]}$ are not appreciably different in magnitude is at first sight surprising since, as shown in Figure 2, the contribution of the vertical velocity to the total kinetic energy is negligible. Moreover, the $\overline{[\rho P w]}$ term does not appear in Anthes' original formulation because the formulation was based on the horizontal momentum equations only. An explanation of this result is suggested by an examination of the radial-height structure of the azimuthally-averaged generation term before completing the columnar average, i.e. $< -\mathbf{u_h} \cdot \nabla_h p' >$, where the angle brackets denote an azimuthal average. The structure of this average together with those of the other generation term, $< \rho P w >$, at 36 h and 60 h, is shown in Figure 4. At both times, the Anthes generation term $< -\mathbf{u_h} \cdot \nabla_h p' >$ shows coherent regions of large kinetic energy generation and of large kinetic energy destruction. The main region of generation in panels (a) and (b) is at low levels, below about 2 km, where the strongest inflow occurs and where the inward directed radial pressure gradient force is particularly strong (panels (c) and (d) of Figure 4). There is a second region of generation in an annular column, mostly on the outer side of the eyewall updraught below about 9 km at 36 h and below about 12 km at 60 h. The generation terms in panels (a) and (b) are similar in structure and magnitude to that shown by Kurihara (1975, Figure 42, upper right) for a lower resolution axisymmetric simuulation.

Figure 2: Time series of the left-hand-side of Equation 14, $\overline{\left[\frac{1}{2}\rho \mathbf{u}^2\right]}$ (curves labelled uvw) compared to $\overline{\left[\frac{1}{2}\rho \mathbf{u_h}^2\right]}$ (curves labelled uv) for cylinders of 300 km and 500 km. The curves for each cylinder size lie essentially on top of each other so that only a single curve is evident. The curves for the 500 km domain are labelled with a '5'.

(a) (b)

Figure 3: Time series of the kinetic energy tendency terms on the right-hand-side of Equation (14), the Anthes' formulation, averaged over a cylinder of size (a) 300 km and (b) 500 km. Units on the ordinate are 10^{-3} W m $^{-3}$. The dissipation term is not shown. A1 stands for $\overline{[-\mathbf{u_h} \cdot \nabla_h p']}$, FK for F_{KEA} and PW for $\overline{[\rho P w]}$. A1+ and A1- stand for the contributions to A1 from regions where the argument $-\mathbf{u_h} \cdot \nabla_h p'$ is positive and negative, respectively.

(a) (b)
(c) (d)
(e) (f)

Figure 4: Radius-height cross sections of azimuthally-averaged quantities in Equation (14), before performing the columnar average: $< -\mathbf{u_h} \cdot \nabla_h p' >$ (panels (a), (b)); and $< \rho P w >$ (panels (e), (f)), at 36 h (left panels) and 60 h (right panels). Panels (c) and (d) show similar cross sections of $< \partial p' / \partial r >$ at these times. Contour intervals are as follows. Panels (a), (b), (e) and (f): thick contours 5×10^{-2} W m $^{-3}$: thin contours 1×10^{-2} W m $^{-3}$. Solid red contours positive, dashed blue contours negative. Panels (c) and (d): thin contours 0.2×10^{-2} Pa m $^{-1}$ to 0.8×10^{-2} Pa m $^{-1}$; medium thick contours 1.0×10^{-2} Pa m $^{-1}$ to 5.0×10^{-2} Pa m $^{-1}$; thick contours every 5.0×10^{-2} Pa m $^{-1}$. Numbers indicated on the side bar should be multiplied by 10^{-2}.

(a) (b)
(c) (d)

Figure 5: Time series of the kinetic energy tendency terms: $\overline{[p' \nabla_h \cdot \mathbf{u_h}]}$ (denoted by G1); $\overline{[\rho P w]}$ (denoted PW) and F_{KEG} (denoted FK) in the modified Gill formulation [Equation (8) averaged over a cylinder of size (a) 300 km and (b) 500 km. Units on the ordinate are 10^{-3} W m $^{-3}$. Panels (c) and (d) show the azimuthally averaged terms $< p' \nabla_h \cdot \mathbf{u_h} >$ in Equation (8) at 36 h and 60 h, respectively. Contour intervals are: thick contours 5×10^{-2} W m $^{-3}$: thin contours 1×10^{-2} W m $^{-3}$. Solid red contours positive, dashed blue contours negative. Numbers indicated on the side bar should be multiplied by 10^{-2}.

Since the radial pressure gradient is positive at all heights [panels (c) and (d) of Figure 4], these generation regions must be ones in which there is generally inflow[6]. For the same reason, where there is outflow, there is kinetic energy removal as seen in the two principal coherent regions in panels (a) and (b) where $< -\mathbf{u_h} \cdot \nabla_h p' >< 0$. It follows that the computed value of $\overline{[-\mathbf{u_h} \cdot \nabla_h p']}$ is the remainder resulting from the cancellation of two comparatively large contributions from $< \mathbf{u_h} \cdot \nabla_h p' >$ of opposite sign, namely $< -\mathbf{u_h} \cdot \nabla_h p' >_+$ and $< -\mathbf{u_h} \cdot \nabla_h p' >_-$, the former being the sum of all positive values of $-\mathbf{u_h} \cdot \nabla_h p'$ and the latter $< -\mathbf{u_h} \cdot \nabla_h p' >_-$ to be the sum of all negative values. This large cancellation is evident in the time series shown in Figure 3.

In summary, a substantial fraction of the kinetic energy that is generated is removed in regions where there is outflow and the residual is relatively small, comparable, indeed, with the

[6] Note that eddy effects are included in all generation terms.

kinetic energy generated by the rate-of-working of the net vertical perturbation pressure gradient force (buoyancy plus perturbation pressure gradient), principally in the region of diabatically-forced ascent. The structure of the net vertical perturbation pressure gradient force at 36 h and 60 h is shown in panels (e) and (f) of Figure 4. As expected, this force is concentrated in an annular region overlapping the region of diabatic heating.

3.5 Kinetic energy generation (Gill's formulation)

Figure 5 shows time series of the principal terms in the modified Gill formulation (the right-hand-side of Equation (8)), excluding again the global dissipation term. In this formulation, the term $\overline{[p'\nabla_h \cdot \mathbf{u_h}]}$ is positive with mean amplitude and fluctuations about this mean increasing with time during the 4 day calculation [Fig. 5(b)]. For the first day, the term is a little less than the $\overline{[\rho P w]}$ term, but thereafter becomes progressively larger. The increasing energy source represented by the sum of the two foregoing terms is opposed, in part, by the net outward flux of mechanical energy through the radial boundary, F_{KEG}.

Panels (c) and (d) of Figure 5 show the structure of the term $< p'\nabla_h \cdot \mathbf{u_h} >$, again 36 h and 60 h. The radial and vertical integral of this term form the cylindrical average $\overline{[p'\nabla_h \cdot \mathbf{u_h}]}$ in the modified Gill's formulation of the energy equation. The qualitative radius-height structure of $< p'\nabla_h \cdot \mathbf{u_h} >$ at the two times shown is less easy to infer from the solutions in Figure 3.2. Moreover, as shown in Figure 5, there is significant cancellation between the term $\overline{[p'\nabla_h \cdot \mathbf{u_h}]}$ and the boundary flux term in Gill's formulation [Equation (8)]. For this reason, the Anthes' formulation of the energy equation would seem to be preferable to Gill's formulation, even though both formulations are correct and give the same tendency of kinetic energy over the control volume of integration (see next subsection).

Figure 6: Sum of the terms for Gill's and Anthes' formulation excluding the dissipation term for cylinders of radius $R = 300$ km and 500 km. Values on the ordinate have been multiplied by 10^3 for plotting purposes. The two curves for each value of R lie essentially on top of each other.

3.6 Total kinetic energy generation

A check on the foregoing calculations is provided by calculating the total tendency of kinetic energy generation, which is the sum of all the terms on the right-hand-side of Equations (8) or (14). This sum should be the same for each formulation. That this is the case is verified in Figure 6, which shows the sum for each domain size. As expected, the curves for the two formulations are coincident.

4 Discussion

Anthes' statement noted in the Introduction that "the important source of kinetic

energy production in the hurricane is the radial flow toward lower pressure in the inflow layer, represented by $-u\,\partial p/\partial r$" may seem at first sight problematic because, above the boundary layer, the radial pressure gradient is very closely in balance with sum of centrifugal and Coriolis forces. Thus the energy source associated with $-u\,\partial p/\partial r$ might appear, at least at first sight, to be a gross overestimate. However, the kinetic energy equation doesn't recognize the balance constraint and, in this equation, the radial pressure gradient acts to generate not only kinetic energy of radial motion, but also that of tangential motion through the action of the generalized Coriolis force $(f+v/r)u$, a term that appears in the tangential momentum equation in cylindrical coordinates. This is despite the fact that the generalized Coriolis force does not appear explicitly in the kinetic energy equation.

As noted also in the Introduction, Anthes recognized that much of the inflow into the storm is " ... a result of surface friction, which reduces the tangential wind speed and thereby destroys the gradient balance, so that the inward pressure gradient force exceeds the Coriolis and centripetal[7] forces" and he pointed out that "In the warm core low the maximum pressure gradient ($-\partial p/\partial r < 0$ [sign corrected: our insertion]) occurs at the lowest level, at which the inflow ($u < 0$) is maximum. In the outflow layer, where the radial flow is reversed, the pressure gradient is much weaker. The result is a net production of kinetic energy, dominated by the contribution from the inflow region". While this view is broadly supported by the calculations presented herein, the calculations provide a sharper view of the *net* production of kinetic energy indicating a region of significant kinetic energy generation accompanying inflow *throughout* the lower troposphere above the boundary layer as well as significant regions where kinetic energy is consumed as air flows outwards, against the radial pressure gradient, above the boundary layer. Indeed, the generation above the boundary layer is a manifestation of spin up by the classical mechanism articulated by Ooyama (1969), while the generation within the boundary layer, highlighted by Anthes, is a manifestation of the nonlinear boundary layer spin up mechanism articulated by Smith and Vogl (2008), Smith *et al.* (2009), Smith and Montgomery (2016) and Montgomery and Smith (2017b).

Anthes argues that the boundary layer " ... must be responsible for a net gain of kinetic energy" even though "a substantial dissipation of kinetic energy in the hurricane occurs in the boundary layer through turbulent diffusion and ultimate loss of energy to the sea surface". As a result, he is led to the paradox that "surface friction is responsible for a net increase in kinetic energy and without friction the hurricane could not exist." The resolution of this paradox would appear to be Anthes' de-emphasis of the role of the classical mechanism for spin up in the kinetic energy budget.

The results of our study, especially the noted cancellation of relatively large generation and consumption contributions to the term $\overline{[-\mathbf{u_h}\cdot\nabla_h p']}$ points to limitations in the utility of a global kinetic energy budget in revealing the underlying dynamics of tropical cyclone intensification. An alternative approach would be to examine the energetics of individual air parcels as they move around some hypothetical circuit (see Emanuel (2004) and references), but this approach relies on assumptions about the circuits traversed, circuits that may or may not be realizable in reality.

[7] Presumably, Anthes means the centrifugal force.

5 Conclusions

We have re-examined the traditional theory for kinetic energy generation in a tropical cyclone used by Palmén and Jordan (1955), Palmén and Riehl (1957), Frank (1977), Hogsett and Zhang (2009) and succinctly summarized in the review article by Anthes (1974). We have compared this with an alternative interpretation of global kinetic energy generation in geophysical flows inspired by Gill (1982), noting that such interpretations are non-unique.

We have shown that the *net* rate of production of kinetic energy is a comparatively small difference between the generation in regions of inflow and the magnitude of the consumption in regions of outflow, so much so, that this difference is comparable in magnitude with the rate of generation by the net vertical perturbation pressure gradient force. The latter effect was not contained in Anthes' original formulation, which was based only on the horizontal momentum equations.

We pointed out that the kinetic energy generation term in Anthes' formulation involving the radial pressure gradient does not appear in Gill's formulation of the kinetic energy equation or our modification thereof. It is replaced by a term comprising the global integral of the rate of working by perturbation pressure ($\overline{[p'\nabla_h \cdot \mathbf{u_h}]}$) as the flow expands in the horizontal. However, this generation term is largely compensated in the modified Gill formulation by the boundary flux of mechanical energy (F_{KEG}). The fact that the boundary flux of kinetic energy in the Anthes formulation (F_{KEA}) is typically negligible, as well as the difficulty in anticipating the structure of the term $\overline{[p'\nabla_h \cdot \mathbf{u_h}]}$ in a tropical cyclone are factors weighing in favour of using Anthes' formulation when applied to the generation of kinetic energy in a tropical cyclone. However, in the light of the large cancellation of positive and negative values in the radial pressure-work term, the contribution from the rate of working of the net vertical force is non-negligible in comparison and should be included in any global kinetic energy budget.

While global energetics provide a constraint on flow evolution, we have shown in the context of the kinetic energy equation that they conceal important aspects of energy generation and consumption. This finding highlights the limitations of a global kinetic energy budget in revealing the underlying dynamics of tropical cyclones.

6 Acknowledgements

We thank Drs. Chris Landsea, Anastassia Makarieva and an anonymous reviewer for their perceptive comments on the original manuscript. GK and RKS acknowledge financial support for tropical cyclone research from the Office of Naval Research Global under Grant No. N62909-15-1-N021. MTM acknowledges the support of NSF grant AGS-1313948, NOAA HFIP grant N0017315WR00048, NASA grant NNG11PK021, ONR grant N0001417WX00336, and the U. S. Naval Postgraduate School.

7 Appendix: Calculation of the net vertical force, P

The net vertical force per unit mass, P, defined in Equation (4) and used to construct Figures 4(e) and 4(f) was first calculated on the stretched model grid at the levels where

thermodynamic quantities are defined. The vertical perturbation pressure gradient was determined by fitting a quadratic function to three successive levels z_{i-1}, z_i and z_{i+1} at which the perturbation pressure has values p'_{i-1}, p'_i and p'_{i+1}, respectively. Then

$$\left(\frac{\partial p'}{\partial z}\right)_i = \frac{(p'_{i+1}-p'_i)dz_i^2-(p'_{i-1}-p'_i)dz_{i+1}^2}{dz_{i+1}dz_i(z_{i+1}-z_{i-1})} \quad (16)$$

where $dz_i = z_i - z_{i-1}$.

References

Anthes RA. 1974. The dynamics and energetics of mature tropical cyclones. *Rev. Geophys. Space Phys*, **12**: 495-522

Bryan GH, Fritsch JM. 2002. A benchmark simulation for moist nonhydrostatic numerical models. *Mon. Weather Rev.*, bf 130: 2917–2928.

Črnivec N, Smith RK, Kilroy G. 2016. Dependence of tropical cyclone intensification rate on sea surface temperature. *Q. J. R. Meteorol. Soc.*, **142**: 1618-1627.

DiMego GJ, Bosart LF. 1982. The transformation of tropical storm Agnes into an extratropical cyclone. Part II: Moisture, vorticity and kinetic energy budgets. *Mon. Weather Rev.*, bf 110: 412-433.

Dunion JP. 2011. Rewriting the climatology of the tropical North Atlantic and Carribean sea atmosphere. *J. Clim*, **24**: 893–908.

Emanuel K. 2004. Tropical cyclone energetics and structure. In *Atmospheric turbulence and mesoscale meteorology*, E. Fedorovich, R. Rotunno and B. Stevens, editors, Cambridge University Press, pp280.

Frank WM. 1977. The structure and energetics of the tropical cyclone ll. Dynamics and energetics. *Mon. Weather Rev.*, **105**: 1136-1160.

Gill AE. 1982. *Atmosphere-Ocean Dynamics*. New York: Academic. 4th ed., 662pp

Hogsett W, Zhang D-L. 2009. Numerical simulation of Hurricane Bonnie (1998). Part III: Energetics. *J. Atmos. Sci.*, **66**: 2678-2696.

Kilroy G, Smith RK, Montgomery MT. 2016. Why do model tropical cyclones grow progressively in size and decay in intensity after reaching maturity? *J. Atmos. Sci.*, **73**: 487-503.

Kurihara Y. 1975. 1975: Budget analysis of a tropical cyclone simulated in an axisymmetric numerical model. *J. Atmos. Sci.*, , **32**: 25-59.

McWilliams JC. 2011. *Fundamentals of geophysical fluid dynamics*. Cambridge University Press, 283pp.

Mapes BE, Zuidema P. 1996: Radiative-dynamical consequences of dry tongues in the tropical troposphere. *J. Atmos. Sci.*, **53**: 620-638.

Montgomery MT, Smith RK. 2017a: Recent developments in the fluid dynamics of tropical cyclones. *Annu. Rev. Fluid Mech*., **49**: 1-33, doi:10.1146/annurev-fluid-010816-060022.

Montgomery MT, Smith RK. 2017b: On the applicability of linear, axisymmetric dynamics in intensifying and mature tropical cyclones. *Fluids*, **2**: 69. doi:10.3390/fluids2040069.

Ooyama K. 1969: Numerical simulation of the life-cycle of tropical cyclones. *J. Atmos. Sci.*, **26**: 3-40.

Palmén E, Jordan CL. 1955. Note on the release of kinetic energy in tropical cyclones.

Tellus, **7**: 186-189.

Palmén E, Riehl H. 1957. Budget of angular momentum and energy in tropical storms. *J. Meteor.*, **14**: 150-159.

Peixoto JP, Oort AH. 1992 *Physics of climate*. American Institute of Physics, New York, p 520.

Smith RK. 2006. Accurate determination of a balanced axisymmetric vortex. *Tellus*, **58A**: 98-103.

Smith RK, Vogl S, 2008: A simple model of the hurricane boundary layer revisited. *Q. J. R. Meteorol. Soc*., **134**: 337-351.

Smith RK, Montgomery MT, 2016: The efficiency of diabatic heating and tropical cyclone intensification. *Q. J. R. Meteorol. Soc.*, **142**: 2081-2086.

Smith RK Montgomery MT Nguyen SV. 2009: Tropical cyclone spin up revisited. *Q. J. R. Meteorol. Soc*., **135**: 1321-1335.

Tuleya RE, Kurihra Y. 1975. The energy and angular momentum budgets of a three-dimensional tropical cyclone model. *J. Atmos. Sci.*, **32**: 287-301.

Wang Y, Cui X, Li, X, Zhang W, Huang Y. 2016. Kinetic energy budget during the genesis period of Tropical Cyclone Durian (2001) in the South China Sea. *Mon. Weather Rev.*, **144**: 2831-854.

Zhang JA Rogers RF Nolan DS and Marks FD 2011: On the characteristic height scales of the hurricane boundary layer. *Mon. Weather Rev.*, **139**: 2523-2535.